NOX

GENERAL ELECTRIC

Research Laboratory

FINAL REPORT

LOW-TEMPERATURE BRITTLENESS OF REFRACTORY METALS

H.W. Schadler and J.R. Low, Jr.

Contract No. Nonr-2614(00)

April 1962

Office of Naval Research

62-3-1

SCHENECTADY, NEW YORK

62-GC-206

FINAL REPORT

to

OFFICE OF NAVAL RESEARCH

LOW-TEMPERATURE BRITTLENESS OF REFRACTORY METALS

H.W. Schadler and J.R. Low, Jr.

Contract No. Nonr-2614(00)

Period: August 1958 to March 1962

Research Laboratory
GENERAL ELECTRIC COMPANY
Schenectady, N.Y.

62-GC-206

April 1962

TABLE OF CONTENTS

Table of Contents (continued)

LOW-TEMPERATURE BRITTLENESS OF REFRACTORY METALS

H.W. Schadler and J.R. Low, Jr.

I. INTRODUCTION

Summary Statement

The relation between the macroscopic and microscopic flow characteristic of body-centered cubic metals and the ductile to brittle transition which is characteristic of some of them has been the subject of intense investigation for many years. The importance of this phenomenon to the use of steel as an engineering material has naturally meant that the early work was primarily done on steels. However, as the need for the use of the body-centered cubic refractory metals of Groups VIA and VIIA of the Periodic Table has increased, so has the need to understand the ductile to brittle transition in these materials. Notably important are the metals: Cr, Mo, and W.

Assuming that a sound understanding of the flow behavior of these metals is important to an understanding of the ductile to brittle transition, the work described in this report was undertaken on tungsten. Tungsten was selected for several reasons: first, because being the metal with the highest melting point it represents the last chance of the metallurgist to satisfy the need for a high-temperature material, and second because its high melting point should be an advantage in the preparation of pure material. Third, at the start of this contract a dislocation etch-pitting technique was reported for tungsten and it was felt that the etch-pitting technique would be an advantage in studying the microscopic flow characteristics. The preparation of pure material was felt to be essential to the basic understanding of the flow behavior because purity is known to influence the flow and fracture characteristics of other body-centered cubic metals.

The work has taken on three general aspects: (1) the production of high-purity material, (2) determination of the modes of deformation and the mechanical properties of tungsten single crystals as a function of temperature, and (3) the behavior of individual dislocations. The tungsten was produced in the form of single crystals and purified using the electron bombardment floating zone refining technique developed by Calverly, Davis, and Lever[1]* in 1957. The modes of deformation and mechanical properties were determined at temperatures of from 500° to 20°K using standard techniques and the single crystals. The behavior of individual dislocations was observed with the aid of the etch-pitting technique of Wolff[2] and the technique of Stein and Low[3] for measuring dislocation velocities.

*Numbers refer to references at end of report.

This report is organized about these three general areas and in addition includes two appendices: A, a study of the recrystallization characteristics of cold-worked single crystals, and B, a brief report on crystallography of twins in Mo-35 A/o Re single crystal. As in most scientific investigations, not all of the goals have been reached to date and not all of the questions answered, but it is hoped that this work when coupled with current and subsequent work will add to our understanding of the mechanical behavior of body-centered cubic metals and alloys.

Acknowledgments

The author is happy to acknowledge the financial assistance of the Office of Naval Research and the inspirational assistance which the atmosphere of curiosity prevalent at the General Electric Research Laboratory provides. A list of all the individuals who have offered help and advice would be too long to include, but the author is particularly indebted to V.J. DeCarlo who helped in the growth of the single crystals used in this study.

The financial support has permitted the publication of three technical papers, and two additional papers which will be submitted for publication.

Publications

"Deformation Behavior of Zone Melted Tungsten Single Crystals," Trans. Met. Soc. AIME, 218, 649 (1960).

"Identification of Deformation Twins in Molybdenum - 35 Per Cent Rhenium Alloys," Trans. Met. Soc. AIME, 221, 650 (1961).

"Correlation of Etch Pits and Dislocations in Tungsten Single Crystals," to be published in Direct Observations of Imperfections in Crystals, Interscience Publishers, New York (1962).

"Electron Bombardment Melting of Tungsten," Proceedings of First Symposium on Electron-Beam Melting, March 20, 1959.

Two more papers included in this report will be submitted for publication:

"The Stress-Strain Behavior of Tungsten Single Crystals"

"Dislocation Mobility in Tungsten"

II. GROWTH OF TUNGSTEN SINGLE CRYSTALS BY ELECTRON BOMBARDMENT FLOATING ZONE-REFINING AND PREPARATION OF SPECIMENS

Introduction

At the time of the initiation of this contract the decision was made to adopt a simple and reproducible technique for the production of high-purity tungsten. The technique chosen was the then new electron bombardment floating zone-refining technique developed by Calverly, Davis, and Lever.[1] It offered the advantages of zone refining and the growth of single crystals in a vacuum and free from contact with other metals. At the same time it is relatively simple to build and to operate. This section of the report describes the physical apparatus, the operating characteristics, and the growth conditions used for the tungsten crystals produced. In addition, the structure of the crystals grown is described, and the purity of the crystals is discussed. A description of the procedures used to prepare tensile and bend specimens for testing is included.

Electron Beam Floating Zone-Refining Equipment

The basic concept of electron bombardment floating zone-refining is shown in Fig. 1. Electrons, thermionically emitted from a hot filament, are accelerated by a d-c potential of from 1 to 20 kilovolts to the specimen where they give up their excess kinetic energy as heat. The excess energy is dissipated within a distance equal to the mean free path of the electron in the liquid, and heating of the specimen interior is by conduction. This process requires a vacuum of less than 1 micron and hence affords the possibility of producing purer material than other consolidation techniques. The principal components of the equipment are: (1) the vacuum system, (2) the power supplies for the emitter and the accelerating voltage, and (3) the emitter configuration and the sample holders.

The vacuum system is the standard bell jar type fitted with a liquid nitrogen cold trap and a 200 liter/min oil diffusion pump topped with a water-cooled baffle. The system is equipped with three valves which permit both opening the system to air and rough pumping of the bell jar without turning off the diffusion pump. A ballasted Welch fore pump was used. The system has an ultimate pressure of about 10^{-6} mm of Hg and operates at 10^{-5} mm of Hg when trapped.

In the bell jar are the sample holders and the emitter and focusing shields designed to control the length of the molten zone. In this particular design the sample was held fixed and the emitter was moved vertically along the specimen. Motion was provided by a ball bearing screw thread driven by variable speed motors through a Wilson-type seal mounted in the base plate of the bell jar. Speeds of from 0.1 mm/min to 20 mm/min were available. The emitter used was a 0.015-inch tungsten wire of the General Electric nonsag type with the shape shown in Fig. 2(c). The wire fitted into a 0.018-inch hole in molybdenum cylinders which were held by copper blocks to which flexible power leads were attached. The focusing shields,

shown in Fig. 3, were tantalum sheets held in place by a tungsten cylinder. The drawing in Fig. 3 gives the dimensions of the focusing arrangement used to melt the 1/8-inch-diameter tungsten rods used as the starting material.

To produce single crystals of controlled orientations from a single crystal seed, the goniometer shown in Fig. 4 proved very satisfactory. A crystal of any orientation could be produced from a given seed with this arrangement if several successive rotations were employed. The seeding technique employed was to cut the seed crystal so that its lower surface was parallel to the top of the lower rod. To insure the propagation of the seed crystal and not some stray crystal in the lower polycrystalline rod, the seed crystal was first welded to the lower rod using the electron beam and then the first zone-melting pass was started in the seed crystal itself. Motion of the molten zone was always from top to bottom.

The basic electrical circuit used for zone-melting is illustrated in Fig. 5. The essential features are: the emitter and focusing arrangement already described, the d-c power source, the filament supply, and an emission controller. The d-c supply is a standard filtered 0-5000v, 500 ma supply. The a-c filament supply and its integral control circuit are shown schematically in Fig. 6. F. Dickey of our laboratory designed this controller. The principle of its operation is that the emission current is monitored by measuring the voltage across a fixed resistance. After comparison with a voltage (variable at the operator's choice), the difference signal is used to control the d-c current to a saturable reactor and thus control the filament current. The filament current determines the filament temperature and hence the electron emission. The circuit is similar in principle to Calverly's original design.

Since control of the power input is accomplished by controlling the temperature of the cathode, optimum control is experienced when the unit is operated in the emission limited rather than the space-charge limited range. For the emitter configuration previously described, the voltage required to prevent space-charge limitation can be determined experimentally by measuring the emission current as a function of applied voltage for various cathode temperatures. Figure 7 illustrates data obtained for the emitter configuration shown in Fig. 3 and a 1/8-inch-diameter tungsten rod as the anode. Since the space-charge limited current is proportional to the 3/2 power of the voltage[4] (see Spangenberg, 1948), the data taken at low voltages can be used to predict the theoretical space-charged limited current at higher voltages. In Fig. 7 this curve is designated, $I = 3.79 \times 10^{-4} v^{3/2}$.

The curves designated 11.0$\underline{A}$ to 12.5$\underline{A}$ are data taken with the indicated filament current held fixed. If the filament current were the only power available to the filament, all of these curves should be almost horizontal at high voltages because the emission current is limited by the filament temperature. In fact, when the anode becomes hotter than the filament, the filament is back heated by radiation. This is the reason that the curves designated 12.0$\underline{A}$ and 12.5$\underline{A}$ show the upward trend at higher voltages.

Operating Characteristics and Growth Conditions

The equipment described above was used to produce all of the material used during the course of this contract. As is evident from subsequent discussion and the work of many other investigators,[1, 5, 6] refractory metals produced by electron bombardment floating zone-refining always crystallize as single crystals unless extremely high zone speeds are used.[7] High zone speeds and hence high growth rates mean a sacrifice of purity. Subsequently, all crystals were grown at 3 mm/min, a speed which represents a compromise between the best zone-refining practice and obtaining a reasonable yield since slower growth rates led to excessive volatilization of the tungsten. All crystals, unless noted otherwise, were grown in a vacuum of less than 10^{-4} mm of Hg.

Some insight into the reasons for the growth of single crystals by electron bombardment floating zone-refining can be gained by considering the temperature gradients encountered during growth. An example of the temperature variation found along the length of a 1/8-inch-diameter tungsten rod is shown in Fig. 8. The temperature was measured with an optical pyrometer and the readings were corrected for emissivity and the thickness of the glass. Higher temperature measurements were not attempted because of volatilization of the tungsten or impurities become a problem above 2400°C. Note that for the emitter configuration used the temperature gradient is in excess of 1000°C/cm. As has been demonstrated, a steep temperature gradient is conducive to the growth of single crystals whether from the liquid or by strain anneal.[8]

Structure and Purity of Tungsten Crystals Produced by Electron Bombardment Floating Zone-Refining

The single crystals of tungsten produced under the growth condition described above were 1/8 inch in diameter and about 3 1/2 inches long. As determined by etch pitting (see section on Etch Pitting for details) they have a dislocation density, exclusive of sub-boundaries of between 10^5 and 10^6 dislocation lines/cm^2. In the cross section there are about six subgrains with angular rotation between them of less than 1/2°. The subgrains are elongated along the growth axis of the crystal. In all, about 100 crystals of various orientations were grown.

Several times early in the course of this program crystals were grown under conditions of exceptionally high, $>10^{-4}$ mm Hg, pressure, and the surface of the crystal became slightly oxidized. Figure 9 shows the surface of such a crystal on which the surface layer was identified as β-W, W_3O. Although this is an isolated observation, the nature of the oxide is interesting enough to be included. There is an apparent relation between the underlying tungsten crystal and the oxide which was not investigated.

TABLE I

Typical Analysis

Element	Starting Material (wt %)	Material After Zone-Refining--2 Passes (wt %)
Ca*	0.001	<0.001
K*	.004	< .001
Na*	.002	< .001
Fe*	.001	< .001
Mo*	.004	.0001†
Si*	.002	< .001
C**	.007 ± 0.002	.001 to 0.002 ± 0.0010
O‡	.0003 ± .0005	.0001 to .0002 ± .0002
N	.00003 ± .0001***	.0001 and less
H	.00001 ± .00003	No analysis

*Spectrographic analysis--light emission spectrography.

†Special technique described by Carlson. (5) Although Carlson concluded that the Mo content varied along the crystal, further experiments indicated that the indicated variation is less than the experimental error.

**Carbon analyses were done by the conductometric technique.

‡Oxygen and nitrogen analyses were done by vacuum fusion on zone-refined material.

***Nitrogen analysis on starting material was by the micro Kjeldahl technique.

It is difficult to be very specific about the purity of the tungsten produced by zone-melting because of the limits of analytical procedures. Table I contains analyses of a typical starting material and a two-pass crystal. It is evident that all substitutional impurities are removed to a level below the detectable limits of the standard analytical procedures indicated. Interstitial impurities are also reduced but some oxygen (about 1 ± 1 ppm) and some carbon (about 10 ± 10 ppm by weight) always remain. Samples taken for analysis from a crystal at positions of the start and the end of the zone-refining pass show no difference in chemical

composition. Under the circumstances it is reasonable to ask whether or not any zone-refining is taking place. The experiments described below were performed to answer these questions.

It is well known that the low-temperature resistivity of a metal is sensitive to the concentration of defects and impurities present in solid solution[9] and hence is a useful tool for determining the relative purity of two samples which have the same thermal and mechanical history. It was hoped that a correlation between the residual resistivity ratio and mechanical properties could be made so that resistivity measurements could be used to screen samples which would be subsequently used for mechanical property studies. As will be clear from the data presented below no such general correlation could be made. However, the resistivity measurements did prove useful in that they definitely established that zone-refining is one mechanism of purification under the growth conditions used.

TABLE II

Proportional Limit as a Function of Processing

No. of Passes*	Proportional Limit† at 298°K	
	Start of Zone-Refining Pass (psi)	Finish of Zone-Refining Pass (psi)
1	38,000	40,000
2	34,000	37,000
3	30,000	32,000
4	17,000	--

*Zone-refined in vacuum of 10^{-5} at 3 mm/min.

†First deviation of load-elongation curve from linearity.

The influence of purity on mechanical properties is illustrated by the data in Table II. Four single crystals grown from the same seed and hence with the same orientation received 1, 2, 3, and 4 zone-refining passes, respectively. Tensile specimens, fabricated as described later, were made from the two halves of the crystal and their proportional limit** was determined. As is evident in the table there is a consistent variation between the samples taken at the section of the crystal which was the start and the section of the crystal which was the end of the zone-refining pass. The variation is just beyond the limits of expected error in stress but indicates there must be a higher concentration of impurity and/or point defects in the section of the crystal near the end of the zone-refining pass. The

**The first deviation of the load elongation curve from linearity.

differences between crystals which received different numbers of zone-refining passes is well beyond the limit of experiment error and definitely shows that additional melting increases the purity. The fact that zone-refining is actually occurring in the growth process is also indicated by the results given below which were taken on a two-pass crystal. The variation of residual resistivity ratio of this crystal was measured along its length; and then the crystal was cut into compression specimens 0.30 inch long and 0.10 inch in diameter. The proportional limit was measured in compression and the data are plotted in Fig. 10 along with the residual resistivity ratio. It is apparent there is a general correlation between the residual resistivity ratio and the proportional limit.

Both the strength and the residual resistivity ratio indicate a variation in composition along the length of the bar and hence that zone-refining is occurring during growth. However, as is indicated in the figure, the residual resistivity ratio goes through a maximum while the proportional limit increases as the distance from the start of the zone-refining pass increases as expected for impurities in W. The residual resistivity was measured by the eddy current technique of Bean, DeBlois, and Nesbitt[10] and the measurement was made of DeBlois. It is tempting to explain the discrepancy between strength and resisitvity on the basis of end effects encountered in the resistivity measurement and this may be the correct explanation. However, in subsequent experiments of a similar nature, described below, it was not possible to make a correlation between residual resistivity and strength, which suggests that the resistivity at low temperatures may be influenced differently by impurities than the mechanical strength is influenced. As has been pointed out[9] the resistivity is most sensitive to impurities and vacancies which are in solid solution and not sensitive to precipitate particles, while the mechanical properties are sensitive to both. The cooling rate of a zone-refined bar is more rapid at the start of a zone-refining pass than at any other time because only a limited length of the crystal has been heated and hence the bulk of the mass can act as a heat sink. Admitting that cooling rate will influence the state of solution of impurities and the vacancy concentration of the solid, it is reasonable to expect that a variation in resistivity could occur along a zone-refined bar simply due to differences in cooling rate. Hence the shape of the residual resistivity distance profile measured can be rationalized. Normally, one would expect that the mechanical properties would be similarly influenced but, as is apparent, the strength increases monotonically from the start of the zone-refining pass. In any event there is a good correlation of mechanical strength and resistivity at points in the crystal beyond the resistivity maximum, and this encouraged subsequent experiments.

Table III is a compilation of tensile strength data and the residual resistivity ratio for several crystals. Inspection of the data reveals that although there is a good correlation between strength and resistivity for a given crystal the strength of any randomly selected crystal cannot be predicted from the residual resistivity ratio. Therefore, further attempts to use resistivity as a means of predicting strength were abandoned and subsequent mechanical properties were determined on two-pass crystals unless otherwise noted.

TABLE III

Correlation of Residual Resistivity Ratio and Tensile Strength

Crystal	Residual Resistivity Ratio (ρ 298°K/ρ 4.2°K)	τP. L. on (110) $\langle\bar{1}11\rangle$ Slip Plane (psi)	Temp of Tensile Test (°K)
WB-1	3,000	12,800	298
WC-2	1,200	10,900	298
WC-3	950	12,400	298
188-1	2,700	11,500	298
189-2	1,500	12,500	298
WB-2	3,000	46,100	78
WB-3	2,100	51,200	78
WC-1	1,200	42,600	78
188-2	2,900	57,000	78
189-1	1,300	70,000	78
203-1	7,100	60,000	78
209-1	10,000-7,400	65,000	78

The resistivity data did prove useful in demonstrating that although zone-refining is a mechanism for the purification of tungsten it is not as important as the melting process itself. As Fig. 10 illustrates, there is a factor of two difference in resistivity, and presumably purity, along the length of a zone-refining bar, but comparison of the resistivity ratio of 5000 with the resistivity ratio of the starting material of 80 indicates that the primary means of purification is loss of impurities through volatilization, sacrificial volatilization, or chemical reaction and subsequent volatilization. All three of these mechanisms have been discussed by this author[8] and in a review article written by Smith.[11] There is no benefit in belaboring these points here, but only to emphasize that apparently the primary benefit of the electron beam floating zone melting process is the purification which is the result of the high temperature and relatively clean atmospheres present during growth.

Preparation of Tensile and Bend Specimens from Tungsten Crystals

The preparation of samples from the 1/8-inch-diameter single crystals of tungsten is described in this section. As will be indicated in a later discussion, the method of preparation and testing is an important variable in any single-crystal experiments with tungsten. The underlying aim in all sample preparation, whether for tensile or bend specimens, was to produce a strain free sample and, hence, the final step in all processes was electropolishing.

Tensile Specimens

Tensile specimens were produced from the 1/8-inch-diameter zone-refined crystals in the following manner. Straight sections of crystal 1 3/4 inches long, were centerless ground to 0.100 ± 0.001 inch. Since early work had indicated that such treatment introduced plastic deformation to a depth of about 0.004 inch, tensile specimens were produced from these rods by electromachining. The technique has been described by Avery et al., [12] and the equipment used is illustrated schematically in Fig. 11. The sample, held between two Jacobs chucks, was rotated in the opposite sense as the "cutting wheel" and at a tangential velocity of about 1/10 that of the stainless steel wheel. This insured an excess supply of the 10 per cent NaOH electrolyte to the specimen. Electrical contact was made to the specimen by silverplated copper braid which rested gently on the top of the specimen. This method of contact is essential if a uniform gage length is desired. A d-c potential of 20v was maintained between the specimen and the polishing wheel which was the cathode. The distance between the surface of the wheel and the specimen was adjusted to maintain a current of 2 amps. The polishing wheel was shaped so that a tensile specimen with the shape shown in Fig. 12 was produced. A 20-minute polishing time removed 0.020 inch from the radius of the specimen and insured removal of the damage produced by centerless grinding.

This procedure produces specimens of different gage diameter, but which are uniform to ± 0.001 inch over a length of about 0.400 inch. Unless noted all tensile specimens were produced by this technique.

Bend Specimens

For simple bend tests specimens with a rectangular cross section of 0.080 x 0.060 inch were made from the 1/8-inch-diameter crystals by surface grinding, electropolishing, and annealing at about 2500°C. Specimens were held for grinding by attaching them, in the desired orientation to a steel block using De Khotinsky's cement. The block had a 0.100-inch-wide groove cut to about 0.040 inch to accommodate the specimen. Considerable care was used in grinding. A self-cleaning wheel and very light cuts (less than 0.0005 inch) were used to minimize the amount of surface damage. After grinding the specimen, now in the form of a rectangular bar about 2 inches long, was electropolished in 2 per cent NaOH using 12v and a stainless steel cathode. About two mils was taken from every surface in this way so the subsequent annealing would not result in a recrystallized specimen.

The annealing treatments were carried out in an electron beam furnace whose general features are illustrated schematically in Fig. 13. In this furnace, which was attached to a standard mercury pump vacuum system, specimens were annealed for about 32 hours in four 8-hour periods. After the final anneal the crystal was cooled to room temperature in 15 minutes. This final cooling rate is similar to that which the crystals receive during growth. A vacuum of 10^{-6} mm of Hg was maintained throughout the anneal. The temperature was measured with an optical pyrometer and roughly calibrated by assuming that the emitting filament was at 2100°K. The effect of this annealing treatment on the perfection of the crystals is illustrated in Fig. 14. The etchant used to reveal dislocations has been described by Wolff.[2] The primary purpose of this treatment was to produce specimens for dislocation velocity measurements, and hence the aim was to produce samples with a low dislocation density. In part the treatment was very successful in that the dislocation density exclusive of subboundaries could be reduced consistently to about 10^5 dislocation lines/cm^2. However, about 20 per cent of the specimen had subgrains less than 0.1 mm in diameter and these could not be used successfully for velocity measurements. As the section on the "Dislocation Velocities" indicates, enough specimens were made to permit the measurements, but the cost was very high.

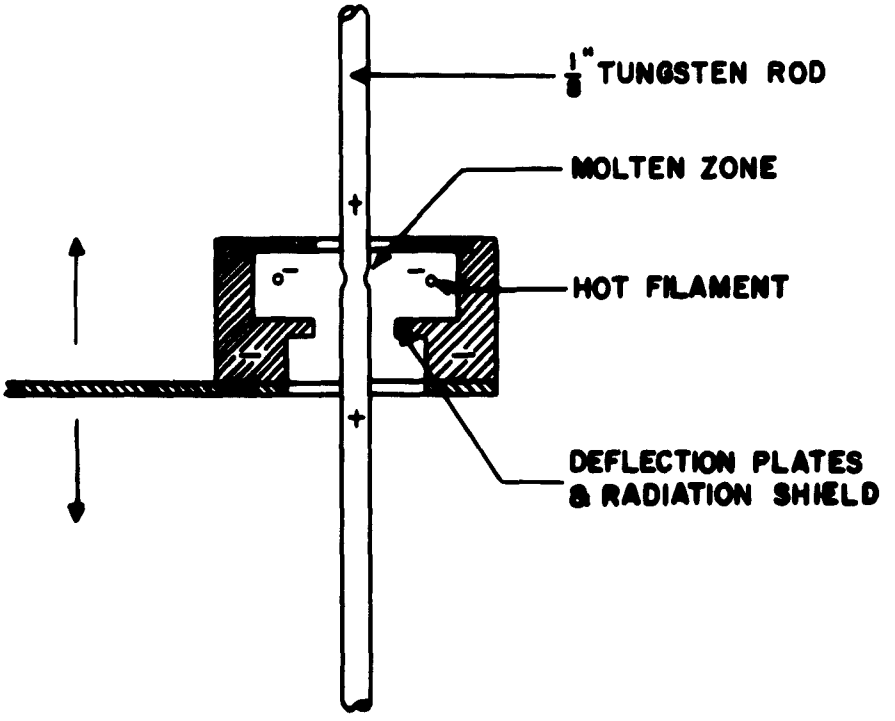

Fig. 1 Schematic diagram of electron bombardment floating zone-refining equipment.

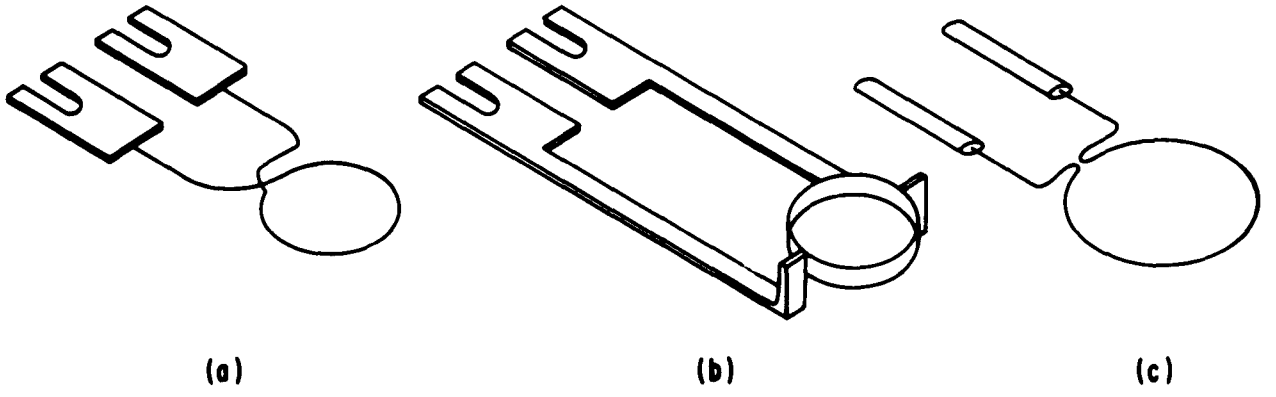

Fig. 2 Cathode designs: (a) 0.010-inch-diameter W wire spot welded to Ni lugs; (b) 2 mm x 0.001 inch W tape; (c) 0.015-inch-diameter W wire slipped into a 0.018-inch-diameter hole in a 0.100-inch-diameter Mo cylinder; (a) and (b) after Calverly.[1]

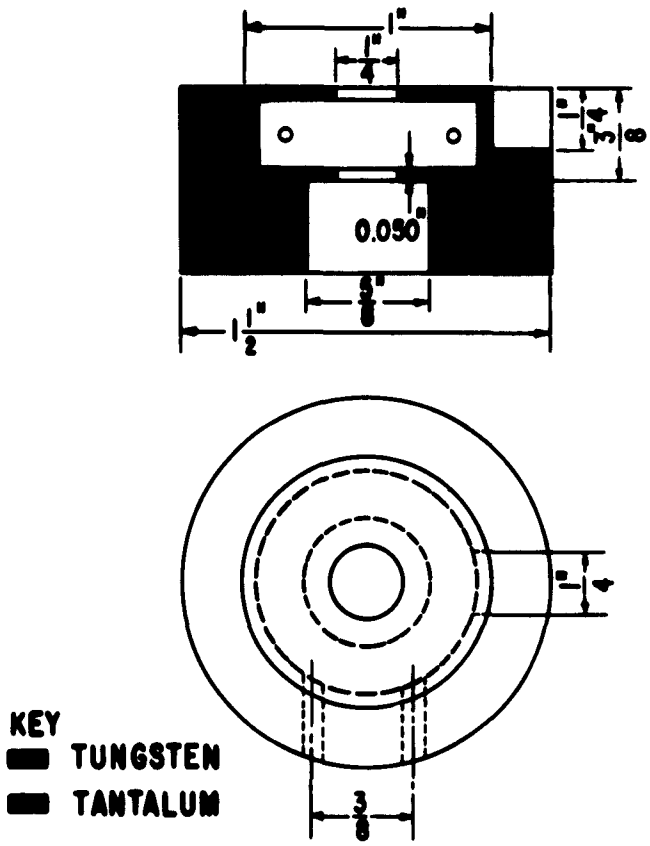

Fig. 3 Details of focusing shields and cathode arrangement used for 1/8-inch-diameter rods.

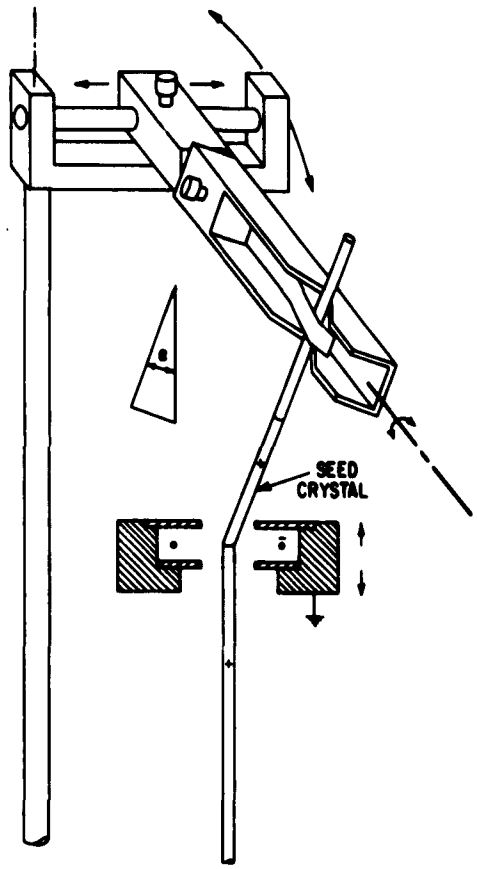

Fig. 4 Simple goniometer arrangement used to hold seed crystals when growing a crystal of a specific orientation.

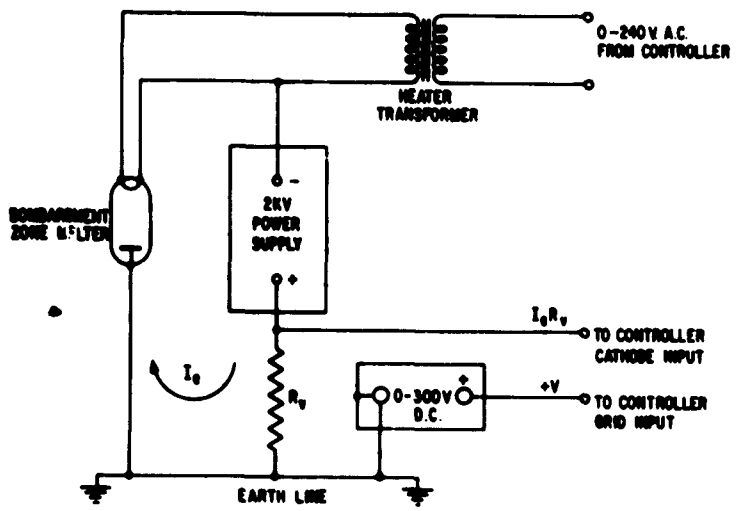

Fig. 5 Block diagram of electrical circuit used for electron bombardment taken from Calverly.[1]

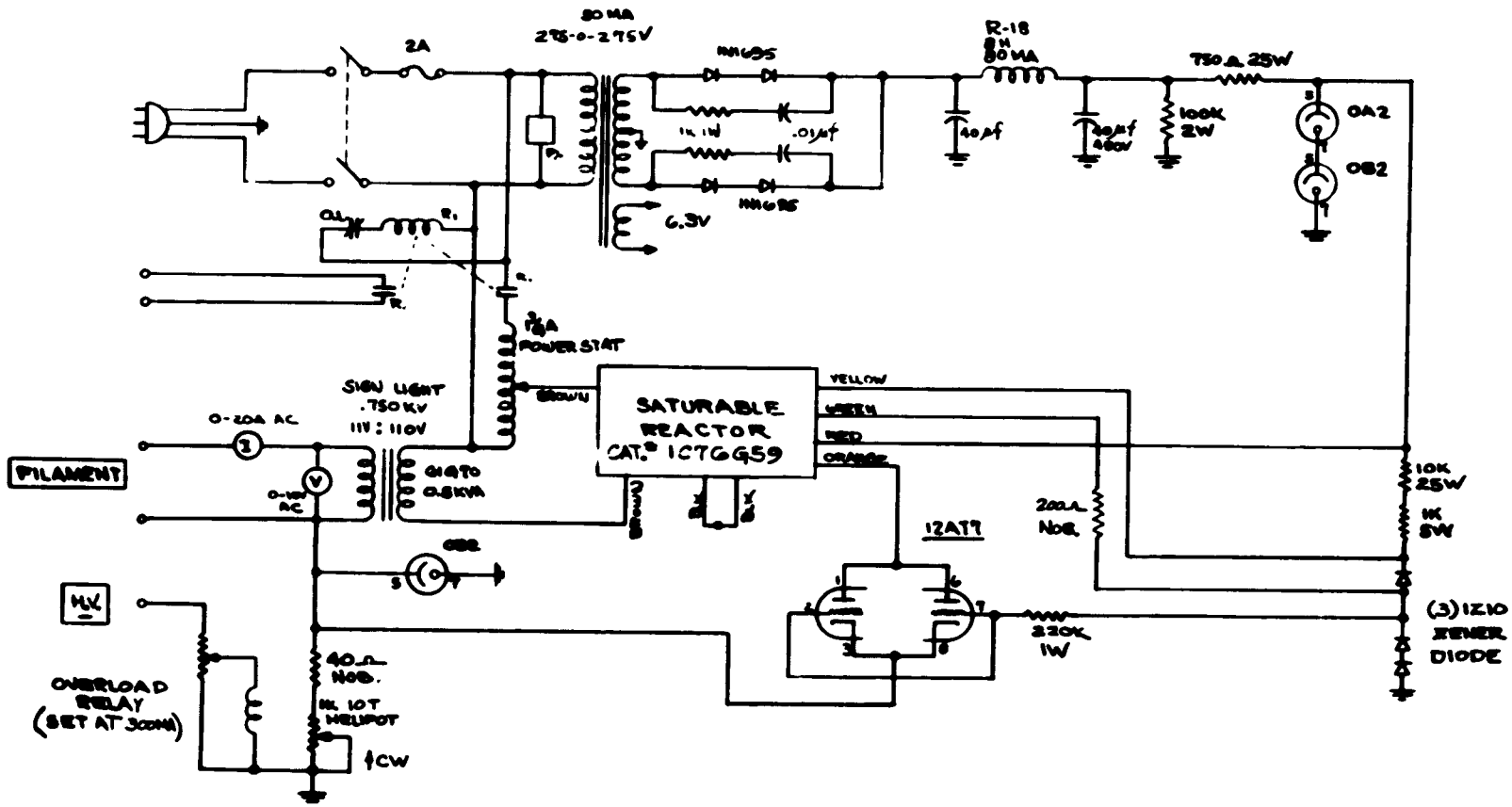

Fig. 6 Details of control circuits used for emission limited control of bombardment current. Designed and built by F. Dickey, General Electric Research Laboratory.

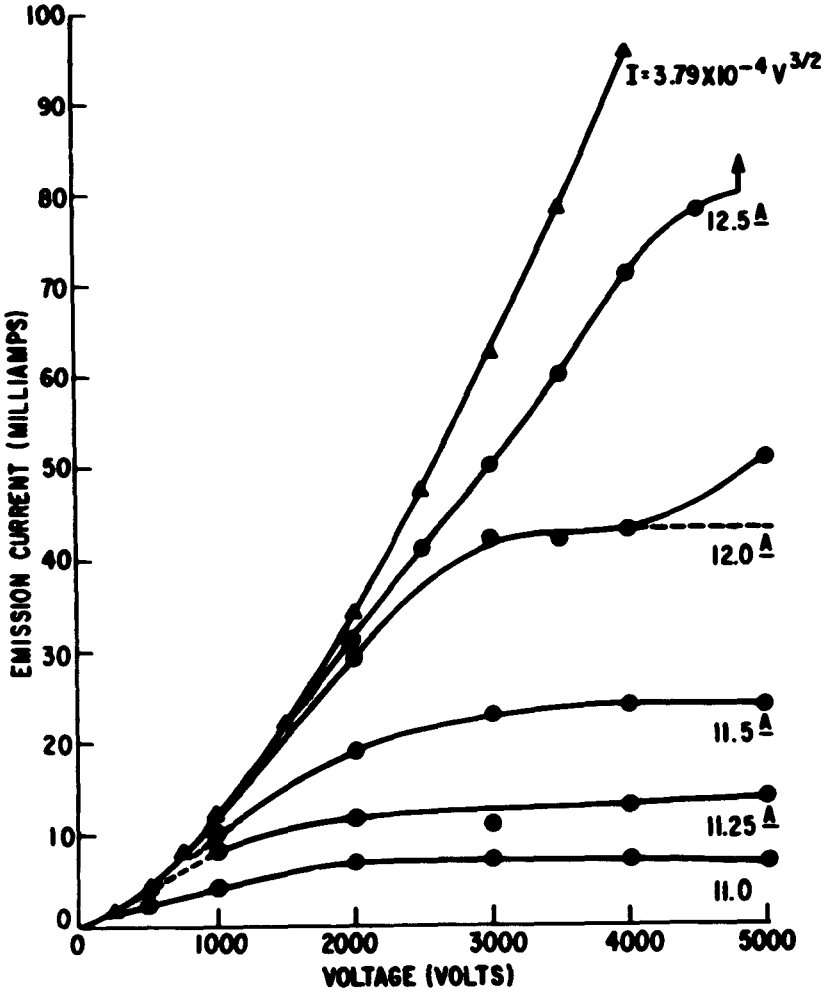

Fig. 7 Voltage current characteristics of the emitter configuration shown in Fig. 3. Specimen bombarded was a 1/8-inch-diameter tungsten rod.

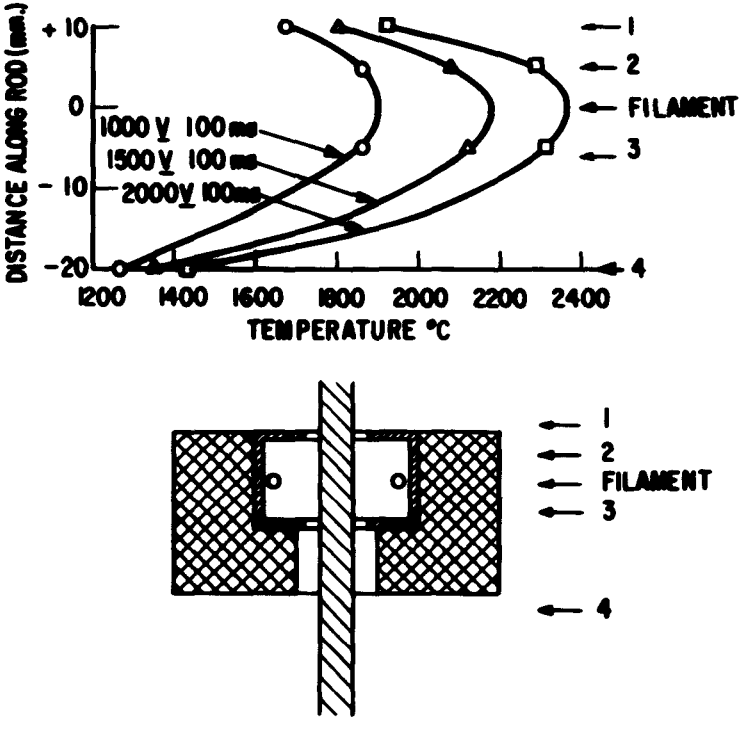

Fig. 8 Temperature gradient along a 1/8-inch-diameter W rod heated by electron bombardment. Temperature was measured with an optical pyrometer and the readings were corrected for emissivity and the glass bell jar.

Fig. 9 Surface of tungsten single crystal grown in a vacuum of $>10^{-4}$ mm of Hg. Pattern results from formation of β-W, W_3O, on the surface of the crystal. 500X

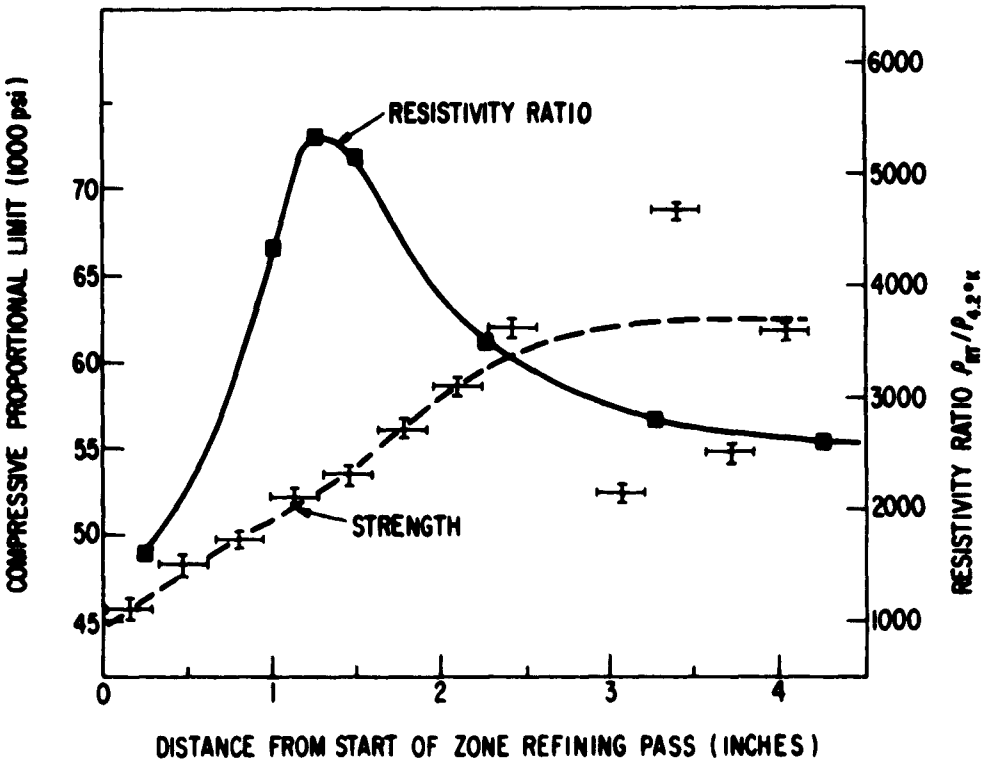

Fig. 10 Strength and residual resistivity ratio along the length of a two-pass electron beam floating zone-refined tungsten crystal.

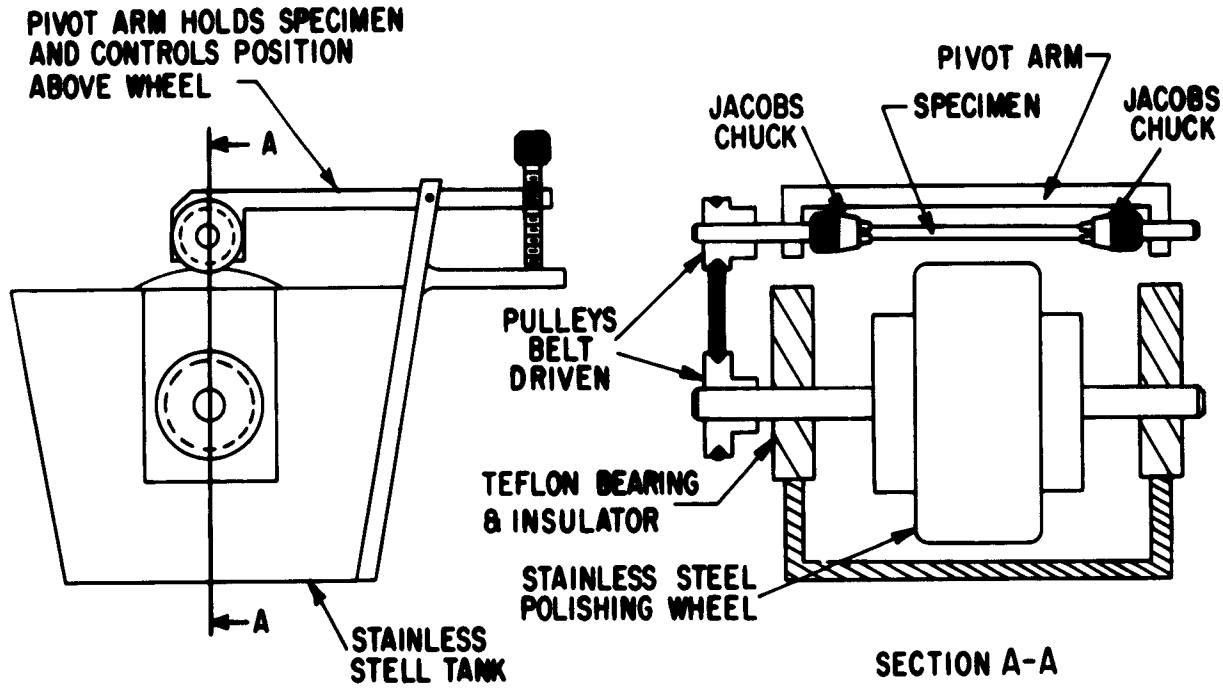

Fig. 11 Electromachining device used to produce tensile specimens from 1/8-inch-diameter tungsten crystals.

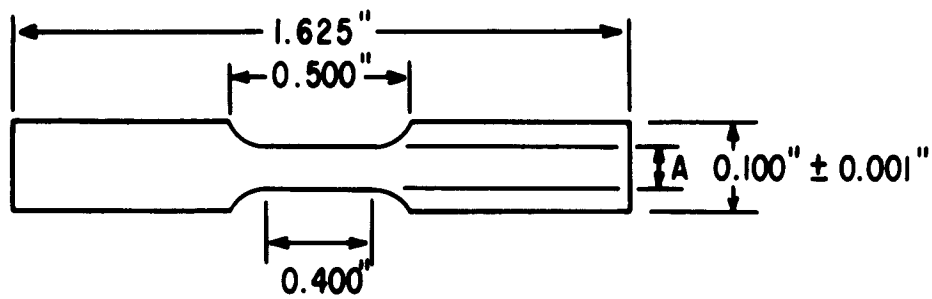

A = 0.050" TO 0.060" DEPENDING ON SPECIMEN,
BUT UNIFORM TO ±0.001" OVER 0.400"

Fig. 12 Nominal dimension of tensile specimens produced by electromachining.

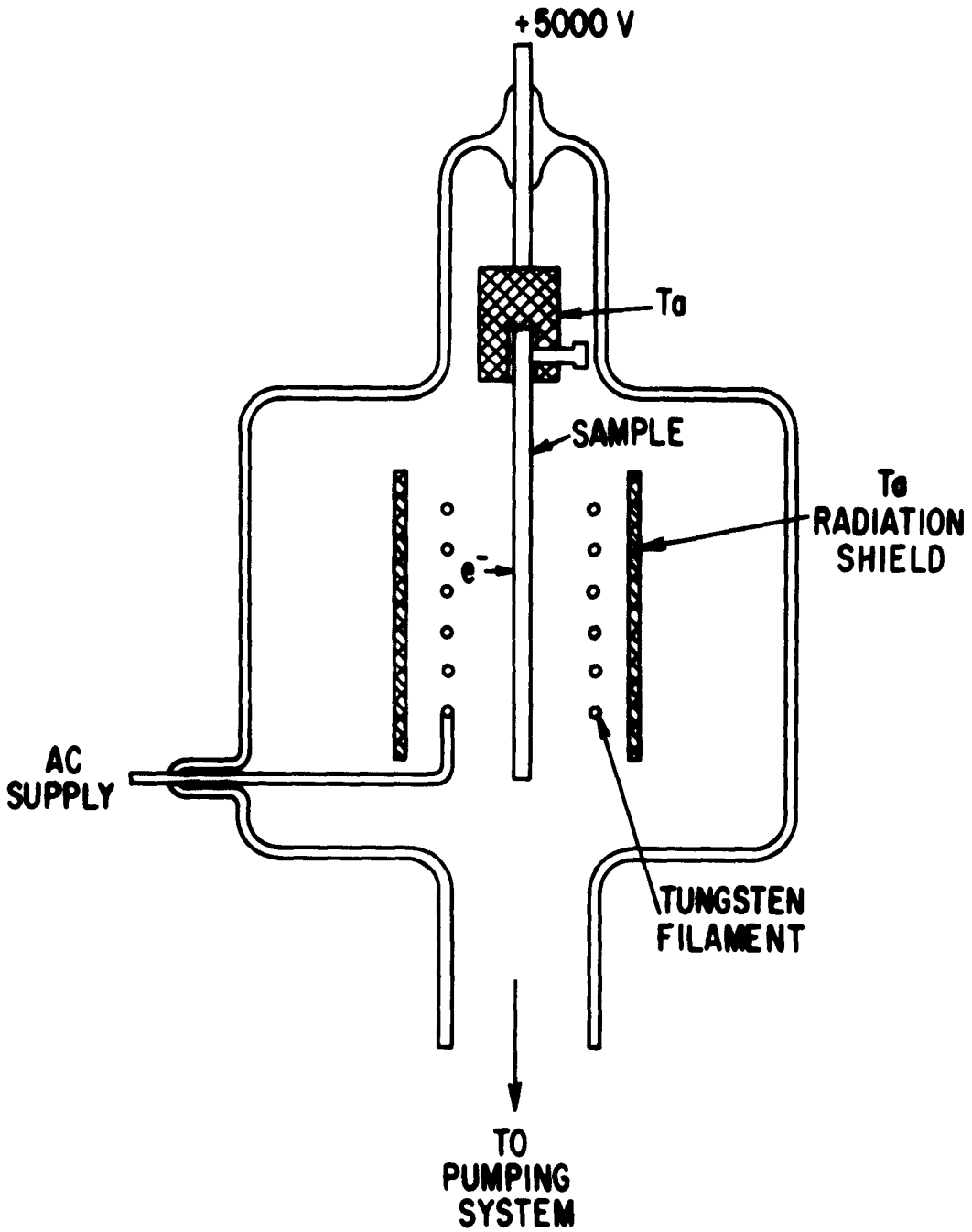

Fig. 13 Cross section of electron beam annealing furnace used for long-time anneals at temperatures in excess of 2500°K.

(a)

(b)

(c)

Fig. 14 Influence of annealing on the substructure of a tungsten single crystal: (a) 50X photograph of (112) type surface on a crystal annealed 8 hours at 2000°C; (b) 150X photograph of same crystal after 8 hours additional heating at 2500°C; (c) 150X photograph of (112) type surface after a total of 32 hours at 2500°C. In (c) note the elongation of subgrains. This elongation is in the same direction as the direction of growth.

III. THE CORRELATION OF ETCH PITS AND DISLOCATION IN TUNGSTEN

Introduction

Etch-pitting reagents which reveal the sites of emergence of dislocations from the surface of a crystal have recently been used to study the effect of an applied stress of the behavior of individual dislocations,[3, 13, 14] and have thereby contributed greatly to the understanding of the role which dislocations play in determining the mechanical properties of LiF, silicon-iron, and Ge. Before the etch-pitting reagent reported by Wolff[2] to reveal dislocation in tungsten could be used for similar studies described subsequently in this report, conclusive evidence that the pits formed by this reagent are associated with dislocations had to be obtained.

The question of how to prove experimentally that etch pits correspond to dislocations has been discussed recently in great detail by Johnston.[15] The characteristics of a dislocation etchant which have been used in this study to establish a correlation between pits and dislocations are listed below:

1. A dislocation etchant should reveal the qualitative features of the substructure of the crystal, and the pit density should not be a sensitive function of etching time.

2. A dislocation etchant should reveal evidence of plastic deformation, and it should reveal quantitatively the number of dislocations in a bent and annealed crystal which Nye's[16] formula predicts.

As Johnston points out, it is difficult to prove that all dislocations or only dislocations form etch pits with a given reagent, but experiments performed in both of the above categories to establish that the Millner and Sass[17] etching reagent develops pits at dislocations on the surface of a tungsten crystal.

Etch-Pitting Reagent and Material

The etchant for tungsten developed by Millner and Sass[17] and described more fully by Wolff[2] is a solution composed of two parts by volume of a 25 wt per cent solution of $CuSO_4$ and one part by volume of reagent grade NH_4OH. Wolff recommends use of the etchant immediately after mixing, but it can be used after several hours if it is reheated to 45°C. (This temperature is the same as that attained due to the heat of mixing if 20 cc of the $CuSO_4$ solution is mixed with 10 cc of NH_4OH in a 50 cc test tube.) Etching is accomplished by immersing the specimen for 15 seconds and moving it gently but continuously. After etching, the specimen should be rinsed in flowing water, then in alcohol, and blown dry.

The tungsten single crystals used for this study were prepared as described previously.

Experimental Results. I

The Millner and Sass reagent reveals the qualitative features of the substructure of a tungsten single crystal as is shown by the two photographs in Fig. 15. Figure 15(a) is a light micrograph of the {112} surface of a tungsten single crystal etched for 15 seconds. The subgrain boundaries are evident and there are individual pits present within the subgrains. Figure 15(b) is an x-ray diffraction micrograph of the same area taken prior to etching using the modified Berg-Barrett technique of Newkirk.[18] Characteristic radiation from a Cu target was used. The arrows indicate the same triangular subgrain in both pictures. Although there is some foreshortening of the x-ray image, the sub-boundaries evident in Fig. 16(a) are reproduced faithfully in Fig. 16(b). Unfortunately the x-ray technique, as used, does not have sufficient resolution to reveal the sites of individual dislocations, and hence a direct correlation of etch pits with dislocation is not possible. Nevertheless these two photographs show that the $CuSO_4$-NH_4OH etchant reveals accurately the subgrains present in the crystal.

That the pit density is not a sensitive function of etching time is illustrated in Fig. 16. Figures 16(a) and (b), the same area on a {112} surface after electrolytic polishing and repeated etchings so that the total etching times are 30 and 45 seconds, respectively. The general features of the substructure are reproduced independently of the etching time. The total number of pits, exclusive of sub-boundaries, increases 6 per cent between Figs. 16(a) and (b). If the surface of a specimen collects dust between etches in a double etch experiment, the pit density may increase very markedly. Apparently, dust particles can nucleate pits. For this reason the specimen should be etched immediately after electropolishing or carefully cleaned by rinsing in flowing water or alcohol prior to etching.

Figure 16 also illustrates the fact that the pits increase in size as the etching time is increased. The rate of growth and the shape of the pits will be discussed in a later section.

One very satisfying proof of the correlation between etch pits and dislocations is obtained by etching the matching halves of a cleaved crystal. Since cleavage divides the crystal into two parts, any dislocation threading through the cleavage plane should be revealed as pits, after etching, on both faces of the cleaved crystal. Figures 17(a) and (b) show the matching halves of a cleaved crystal. The photograph in Fig. 17(b) has been reversed in printing. The surface is a {100} plane, the cleavage plane for tungsten. Where individual pits are distinguishable on these photographs there is a one-to-one correspondence for 85 per cent of the pits. Where individual pits are not distinguishable, there is very good correspondence between the dark areas. This indicates that the reagent is attacking deformed areas, but the spacing of dislocations in these areas is too close to allow resolution of individual pits. As Gilman has shown in LiF[19] when cleavage cracks travel at less than some critical velocity, plastic deformation can occur ahead of the crack. Figure 17(c) shows that the crack must have gone through this critical velocity several times before finally slowing down enough to permit a large amount of plastic strain

ahead of the crack front. The direction of crack propagation is indicated by the arrow. The fact that there is matching of the pit arrangement on the two fracture surfaces is good evidence that this reagent reveals dislocations.

Experimental Results. II

The etchant reveals evidence of plastic deformation. Figure 18 shows a {112} surface on the tension side of a specimen deformed in bending at 78°K. The specimen was prepared by first electropolishing and then etching to reveal the dislocations present in the crystal (larger pits). After scratching with a diamond stylus (the scratch is the horizontal line) the sample was bent to a maximum plastic strain at the surface of a few tenths of a per cent and then re-etched. The smaller pits, representing dislocations introduced by bending, are arranged in glide bands. Note that apparently dislocations present prior to scratching also moved under the applied stress. At higher strains the glide bands are no longer distinguishable, as will be evident in subsequent photographs.

A quantitative argument for the correlation between etch pits and dislocations in tungsten is illustrated in Figs. 19(a) and (b) which show the side, 19(a), and top, 19(b), surfaces of a specimen bent at room temperature. Because of some torsional strain imposed during bending, the slip plane operating is the one indicated in Fig. 6 by the plane AEFH. The Burgers vector is neither parallel nor perpendicular to the side and top surfaces of the crystal and, therefore, slip lines appear on both surfaces. The etched specimen reveals that these slip lines terminate in a row of pits and in several cases the slip line is broken by a group of pits. Knowledge of the step height and the orientation of the Burgers vector permits a calculation of the number of dislocations required to form the slip step, and this can be correlated with the number of pits. An interference micrograph taken from the area outlined in Fig. 19(a) shows that the difference in step height between the slip line at the points marked A and B in Fig. 19(a) is given as: $(215\,A \pm 50\,A) - (150\,A \pm 40\,A)$ or 65 A. This corresponds to 56 dislocations and an electron micrograph of the group of pits marked C in Fig. 19(a) shows about 45 pits. Considering the inaccuracy of the determination, the agreement is good. However, independent of the quantitative aspects of this observation, the fact that the slip lines in Figs. 19(a) and (b) terminate in pits is qualitative evidence that the pits represent dislocations.

One additional quantitative test was employed to correlate etch pits with dislocations. Nye[16] has calculated that for the special case of uniform plane bending, the equilibrium number of dislocations of one sign which must be present in a bent crystal is:

$$N = \frac{1}{\rho b \cos \chi_0}$$

where N is the dislocation density measured on a surface which is perpendicular to the axis of bending, ρ is the radius of curvature, and χ_0 is the angle between the Burgers vector, b, and the neutral plane. The crystal must deform by slip on one

slip system only for this equation to apply. If a single crystal of the orientation shown in Fig. 20 is bent about the [112] axis, the shear stress is a maximum on the $(1\bar{1}0)$ $[\bar{1}\bar{1}1]$ slip system and χ_0 for this system is 45°. Dislocations emerging perpendicular to the (112) surface are edge dislocations. A single crystal of this orientation, having an initial dislocation density of 5×10^5 dislocation lines per cm^2 on the (112) surface, was bent at 78°K to a radius of 13 ± 1 centimeters. Etching showed that a single slip system, the $(1\bar{1}0)$ $[\bar{1}\bar{1}1]$, was operative and that the average dislocation density was 7.5×10^6 dislocation lines per square centimeter. The density in the region of maximum strain was 1.5×10^7 dislocations per square centimeter and at the neutral axis was zero. Figure 21 shows a region of intermediate density, and Fig. 22 shows the region near the neutral axis. Nye's formula predicts a density of 4×10^6 dislocations/cm^2 in the fully annealed sample. After annealing for 4 hours at 1600°C in hydrogen the dislocation density was uniform across the crystal and had dropped to 3.7×10^6 dislocations/cm^2. Subsequent annealing at 2400°C in vacuum produced no further change. Figure 23 shows the sample after annealing at 2400°C. Note the absence of any arrangement of dislocations into long-range polygon walls.

The theoretical density of 4.0×10^6 dislocations/cm^2 and the experimental density of 3.7×10^6 dislocations/cm^2 for this bend specimen are in agreement within experimental error, and this agreement is good evidence that the etch pits correspond to the sites of emergence of dislocations.

Experimental Results: Pit Characteristics

The crystallography of the pits formed with the Millner and Sass reagent and the kinetics of their formation require some comment because they are distinctively different from the pits formed in LiF[20] and Cu.[21, 22] Figure 24 shows the type of pit formed on {100} surfaces and Fig. 25 shows the pits formed on {112} surfaces. These pits are formed by the preferential formation of crystallographically identical surfaces. The pits formed on {100} surfaces are in the form of an inverted truncated right pyramid. The bottom of the pit is microscopically very rough, but macroscopically parallel to the {100} plane which is parallel to the surface. The sloping sides of the pit are roughly parallel to {110} planes. The pits formed on {112} surfaces are crystallographically equivalent except that the truncated pyramid is inclined at 55° to the {112} surface. The form of these pits can be rationalized assuming that there is strong preference for solution of surfaces other than those bounded by {110} and {100} planes.

It is obvious from Fig. 16 that the pits increase in size with increased etching time. The change of any linear dimensions of the pit is roughly proportional to the square root of time. For LiF[20] and Cu[22] the pit size is a linear function of etching time.

Discussion

The experimental results described above indicate that the $CuSO_4$-NH_4OH reagent of Millner and Sass reveals dislocations which emerge from {112} and {100}

surfaces of tungsten crystals. They also reveal several interesting facts about dislocation motion in tungsten and show that intentional decoration of the dislocations by an impurity is not necessary. Consider the specimen shown in Fig. 22. The specimen was etched prior to bending and again within 15 seconds after deformation. The larger pits represent dislocations present prior to deformation, and the smaller pits represent dislocations resulting from plastic deformation. This result indicates that no intentional aging of the crystal is necessary as Wolff suggested might be the case. This is particularly surprising in the case of tungsten since the range of crystal orientations which respond to etching[2] is much broader than is to be expected of undecorated dislocations if the experience gained from etch-pitting reagents for LiF[20] and Cu[21, 22] can be generalized.

Figure 22 illustrates another point which is really secondary to etch pitting but is important in the understanding of dislocation interactions. Note the alignment of pits near the neutral axis into rows perpendicular to the glide plane. The trace of the glide plane is parallel to the line marked S. Glide polygonization is the name given by Livingston[22] to describe this alignment of dislocations into polygon walls as the result of plastic deformation and is distinguished from ordinary polygonization in that no thermal treatment is involved.

Another interesting feature of the deformation behavior of tungsten as revealed by the etch pitting technique is illustrated by Fig. 19(a). Consider the slip line marked A-B. The slip step is laterally displaced at the point where the row of pits marked C is evident and the offset slip steps are connected by the row of pits. The offset is characteristic of cross slip, and there are several additional examples of cross slip in Fig. 19. Just why the dislocations are held up in the region at C is not understood.

Also apparent from Fig. 19 is the fact that slip steps do not act as preferred sites for the nucleation of pits as is the case for some reagents used on Al.[23] In addition, it is clear that under some conditions dislocations can move long distances in tungsten without multiplying.

One final comment concerning the response of dislocations with various Burgers vectors to etching is necessary. These experiments have shown that dislocations with strong edge character and mixed dislocations having both edge and screw components can be etched with the Millner and Sass reagent. As Fig. 20 illustrates for specimens of the orientation indicated, dislocations on the $(1\bar{1}0)$ $[\bar{1}\bar{1}1]$ slip system have a Burgers vector which is parallel to the (112) plane, and such dislocations emerging from the (112) surface have strong edge character. Figures 21 and 22 show that these dislocations respond to etching. Because all crystallographic surfaces don't respond to the Millner and Sass reagent (see Ref. 2) it is not possible to etch pit dislocations of strong screw character. However, the dislocations emerging from the top and side surfaces of the crystal shown in Fig. 19 are revealed by this reagent; and as Fig. 20 shows, these dislocations are of mixed character. Thus the $CuSC_4$-NH_4CH reagent attacks both dislocations with strong edge character and mixed dislocations with both edge and screw components.

Conclusions

In summary, the $CuSO_4$-NH_4OH reagent described by Millner and Sass does reveal the sites of emergence of dislocations from single crystals of tungsten of suitable orientation. Dislocations with edge character and mixed dislocations with edge and screw character are attacked. Further, dislocation etch pits are produced without any deliberate aging of the crystal.

Acknowledgments

The author gratefully acknowledges the help of J.M. Lommel who very kindly took the x-ray extinction photograph shown in Fig. 15(b) and E. Koch and Miss A.M. Turkalo for the electron microscope pictures in Figs. 24 and 25, respectively.

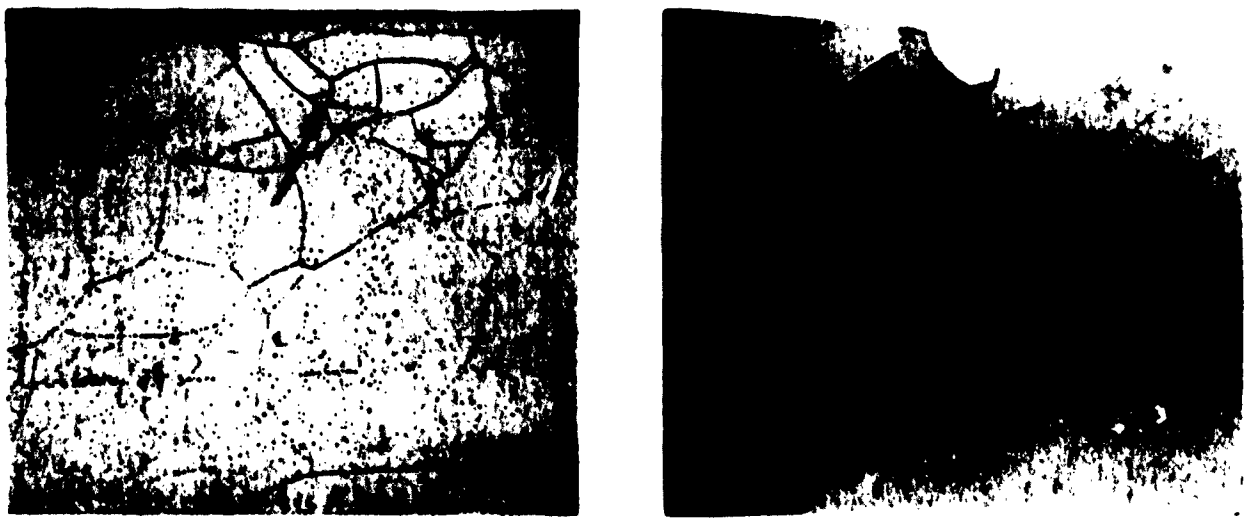

(a) (b)

Fig. 15 |112| Surface of a tungsten single crystal: (a) after etching in the Millner and Sass[7] reagent for 15 seconds, 50X; (b) x-ray extinction photograph of same area prior to etching, 50X.

(a) (b)

Fig. 16 |112| Surface of a tungsten single crystal: (a) etched for 30 seconds; (b) same area etched for an additional 15 seconds. 250X

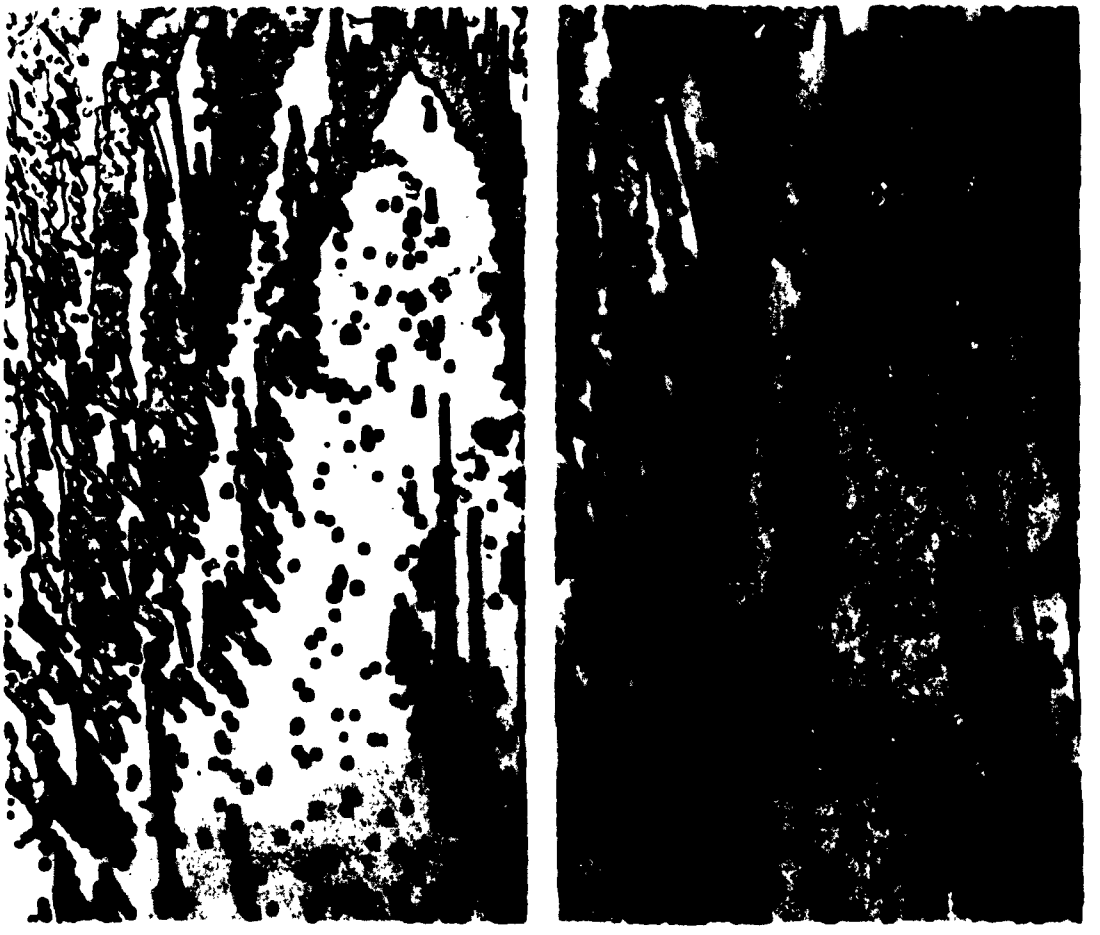

(a) (b)

Fig. 17 Etched cleavage surface of a tungsten crystal: (a) and (b) are matched faces at 1000X. The photograph in (b) has been reversed in printing; (c) same area at 250X. Note that the lateral spreading of the crack occurred at a velocity low enough that considerable plastic deformation took place.

Fig. 17 (continued)

(c)

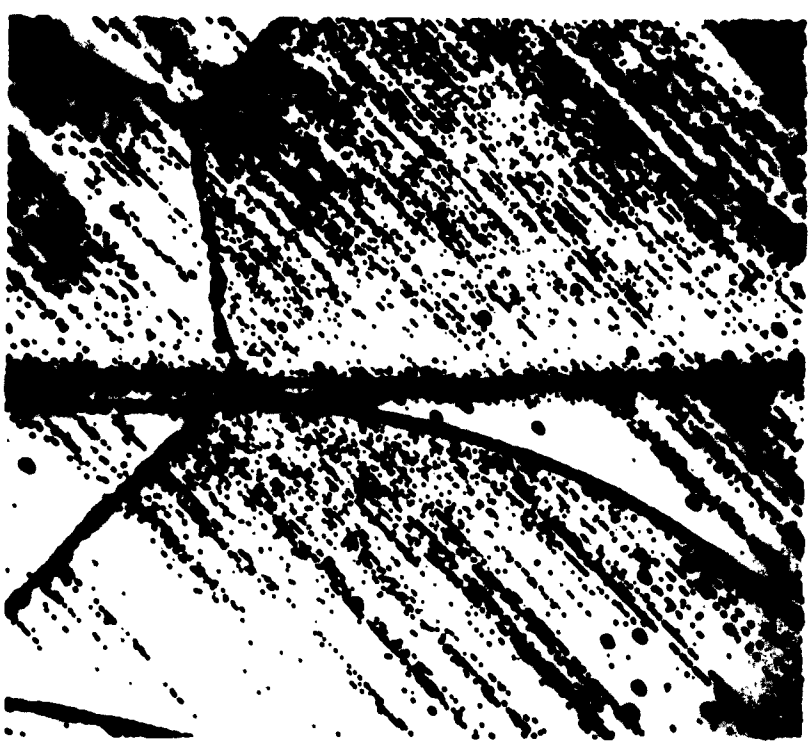

Fig. 18 {112} Surface of specimen deformed at 78°K. 250X

(a) (b)

Fig. 19 (a) Side and (b) top surfaces of a crystal deformed at room temperature in bending: (a) 500X; (b) 250X.

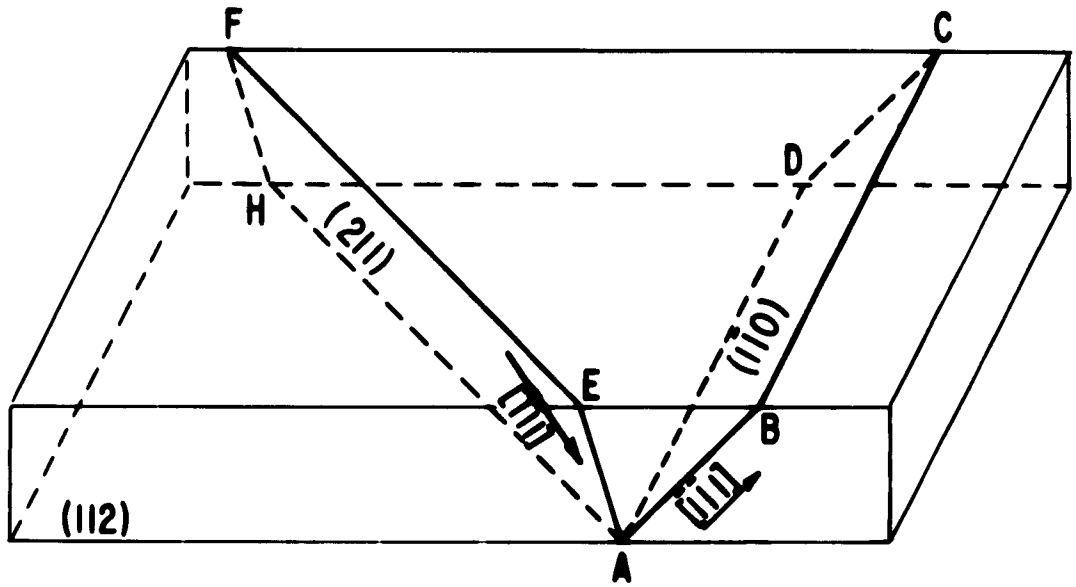

Fig. 20 Schematic representation of crystal orientations used for specimens shown in Figs. 19 and 21.

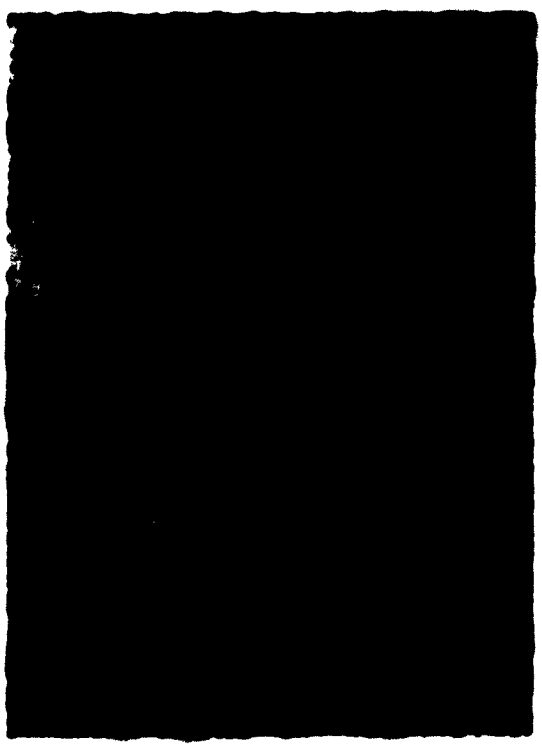

Fig. 21 Etch pits near region of maximum strain on the (112) surface of crystal bent about [112] axis. 500X

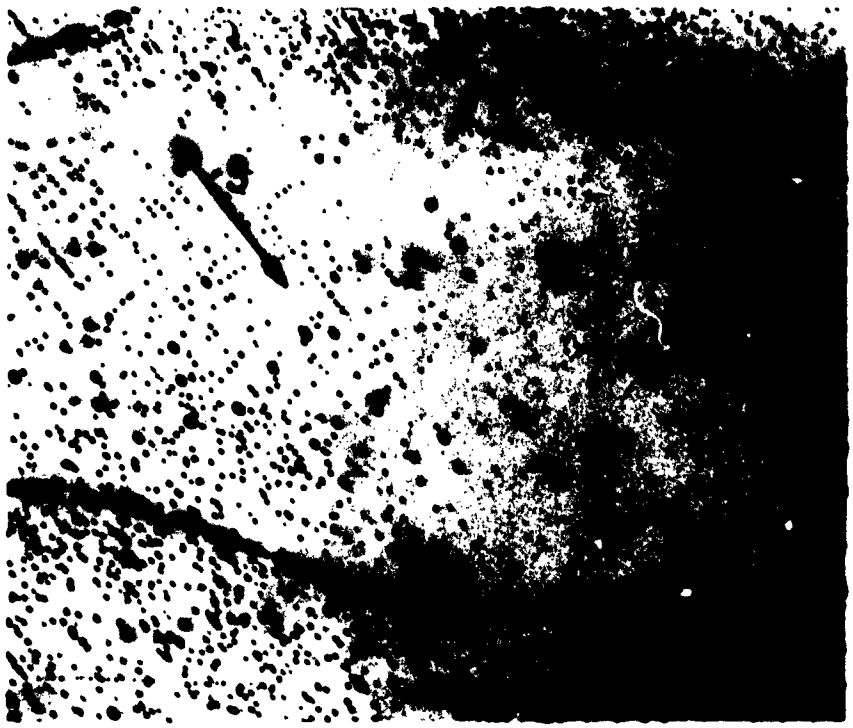

Fig. 22 Etch pits near neutral axis on the (112) surface of crystal bent about [112] axis--500X. Note the glide polygonization evident perpenducular to the glide bands marked S.

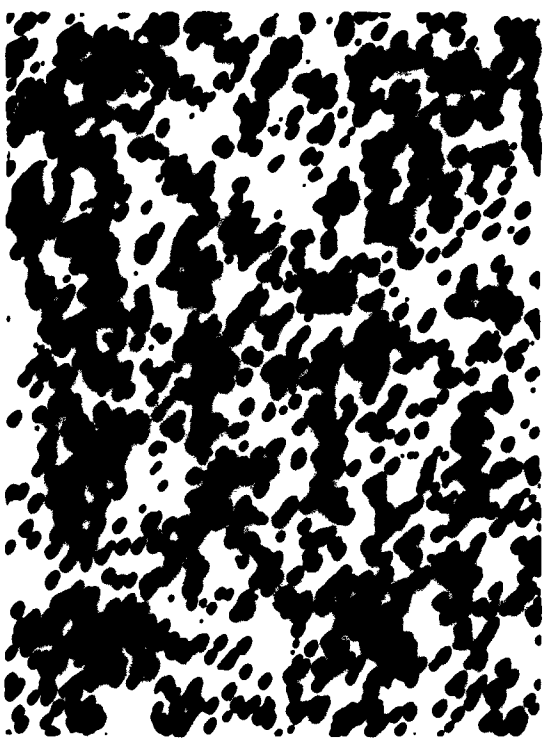

Fig. 23 Photograph of (112) surface of crystal bent about [112] axis after annealing at 2400°C in vacuum for 4 hours.
250X

Fig. 24 Electron microscope picture of pits formed {100} surface of tungsten crystal. 10,000X

Fig. 25 Electron microscope picture of pits formed on {112} surface of tungsten crystal. 12,400X

IV. DEFORMATION BEHAVIOR OF ZONE-MELTED TUNGSTEN SINGLE CRYSTALS

Introduction

Current models for the initiation of brittle fracture in crystalline materials are based on a knowledge of the details of their plastic deformation.[24] Body-centered cubic tungsten exhibits brittle failure at temperatures below about 500°K, yet the modes and crystallography of its plastic deformation have not been studied below 1000°K. In 1924, Goucher[25] reported that tungsten single crystals with a total impurity content of less than 0.01 wt per cent deformed by slip on the (112) $[11\bar{1}]$ system in the temperature range 1000° to 3000°K. He also observed (001) [010] slip in one crystal which was constrained by the presence of a large fissure. According to Barrett,[26] tungsten also deforms by twinning on the (112) plane in the $[11\bar{1}]$ direction, but he gives no details on the tendency for twin formation or the temperature range in which twinning occurs. Therefore, as a necessary part of a study of the factors influencing the brittle fracture of tungsten, the modes and crystallography of the plastic deformation were determined at 298°, 77°, and 20°K.

Test Specimens and Testing Procedure

The range of crystal orientation used in this study is indicated in Fig. 26. The point on the unit stereographic triangle identified by the crystal number represents the crystal axis and the direction of the applied tensile stress. A typical tensile specimen, described previously, is shown in Fig. 27(a). The tensile tests were performed on a standard Instron machine at a strain rate of 2 per cent per minute using standard wire grips, and the bend specimens were deformed either in four-point or cantilever loading to a maximum strain of 2 per cent.

Determination of the Slip and Twinning Elements

The crystallography of the slip and twinning planes which were evident after plastic deformation was determined from the orientation of traces of the planes on the crystal surface by a technique described by Barrett,[26] and illustrated schematically in Fig. 28. The orientation of the crystal was determined with respect to the crystal axis and a scratch placed just outside of the gage section by the Laue back reflection x-ray technique. The angles α and β for a single trace were measured as the crystal was rotated through the angle over which the trace was visible. The experimental points were plotted on a stereographic projection of the crystal orientation, and the great circle passing through these points represents the trace of the observed plane.

The slip direction was determined by measuring the angular rotation of the crystal lattice, caused by tensile deformation, with respect to the specimen axis. In tensile deformation of a single crystal the specimen axis will move toward the slip direction as deformation proceeds.[27]

Results

A typical example of the surface offset produced by slip and twinning is shown in Fig. 29. Figure 29(a) shows slip lines on crystal 159 which was deformed at 298°K. Figure 29(b) is a photograph of crystal 171 after 2 per cent deformation at 77°K and shows both slip lines, marked S, and twins, marked T. Electron microscope pictures of the slip lines formed at 77°K are included in Figs. 29(c) and (d). The apparent curvature of the twins is due to the curvature of the crystal surface. Although the optically visible twins extend over a large portion of the crystal cross section, they are very thin and therefore account for very small strains. The existence of twins was established by the standard polishing and etching procedure using 2 per cent NaOH solution for electropolishing and a 1:1 solution of HNO_3 and HF for etching. Figures 30(a) and (b) illustrate this procedure. Both slip lines and twins are evident before polishing and etching [30(a)], but only twins are apparent after polishing and etching [30(b)]. The electron micrographs in Fig. 29(c) and (d) illustrate the straight nature of the slip lines formed but also show that the individual slip steps are relatively short (5μ to 10μ).

The formation of twins was not apparent from the Instron load-deflection curve. The crystals deformed at 298° and 77° or 20°K showed the same general features, namely, a high rate of work hardening with no evidence of a yield point or the discontinuities which are usually associated with twinning. Apparently the tensile machine was too soft to detect very fine twins.

The results of observations of 46 slip and twinning plane traces on 20 crystals deformed at 298°, 77°, and 28°K are present in Figs. 31 and 32 and Table IV. The poles of the slip and twinning planes observed on crystals deformed at 200°, 77°, and 20°K are plotted in Fig. 31. Crystals 180-1 and 184-1 were tested at 20°K and the others at 77°K. These poles cluster within ± 5° of the (011) pole and (112) pole, respectively, indicating that at 200°, 77°, and 20°K the active slip plane is of the (011) type and the twinning plane is of the (112) type. The poles of the traces which were shown to result from twinning are marked with a T.

Figure 32 gives the poles of the observed traces for crystals deformed at 298°K and one crystal, 152, deformed at 725°K. There is a larger spread in the room temperature data than in the low-temperature data, but the poles of the observed deformation planes cluster within 6° of either the (011) pole or the (112) pole. Electrolytic polishing and etching of these samples failed to reveal the presence of deformation twins; and, therefore, the deformation on both the (011) and the (112) planes is presumed to be slip.

In Table IV the positions of the poles of the observed slip and twin plane traces plotted in Figs. 31 and 32 for both the low-temperature and room temperature data are noted as latitude and longitude deviations from the (001) pole and the (001)-(011) join, respectively. Also included in Table IV are the length of arc over which the trace was observable, the number of measurements, and the standard deviation of the experimental points from the nearest (011) or (112) pole of the crystal. The standard deviation was determined by assuming that the pole of the trace was either

TABLE IV-a

Positions of Poles of Observed Slip and Twinning Plane Traces

Crystal No.	Observed Slip Plane Type	Angle from (011) Pole Along (011)-(111) Zone (°)	Angle from (011)-(111) Zone (°)	Length of Arc of Trace Observed (°)	No. of Measurements	Standard Deviation (°)	T_1, °K
157	(112)	26.5	18	125	7	6.4	298
	(112)	29	22	100	4	4.1	
	(011)	41	2	95	3	4.2	
158	(112)	30	21	100	4	3.0	298
	(011)	43	1	100	4	7.0	
	(011)	44	1	95	3	1.0	
159	(011)	36	5	100	4	9.3	298
	(112)	29	16	95	11	9.7	
160	(011)	43	2	120	3	6.3	298
	(011)	43.5	6	100	5	1.4	
161	(011)	43	1.5	105	4	2.8	298
	(011)	44	2.5	10	3	1.0	
	(011)	44	2	100	4	4.7	
168	(011)	41	4	225	7	7.1	298
	(011)	42	3	45	3	5.7	
154	(112)	27	24.5	90	2	5.7	298
	(011)	44	0	100	3	1.0	
180-2	(011)	43	0	100	13	2.2	298
	(011)	44	1	170	6	6.1	
	(112)	27	19	140	6	2.7	
184-2	(112)	26	28	40	7	3.7	298
	(011)	43	1	65	7	5.6	
152	(112)	29	24	90	2	3.6	725
166	(011)	44	2	120	5	2.5	77
	(011)	44	2	140	3	4.4	
	(011)	36	4	70	4	4.7	
167	(011)	46	0	90	6	3.1	77
	(011)	43	1.5	155	4	2.5	
169	(011)	43	1	45	5	3.3	77
170	(011)	44	1.5	70	11	4.4	77
	(011)	43	1	80	8	7.1	
171	(011)	41	3	125	5	6.0	77
	(112)T	28	22	140	2	1.6	
	(112)T	28	24	35	6	4.4	
172	(011)	34	4	110	5	5.5	77
	(011)	42	2	135	4	2.2	
	(112)T	26.5	25.5	90	4	12.5	
128	(011)	43.5	1	90	3	2.8	77
	(112)	26.5	25.5	45	2	2.2	
180-1	(112)T	29	24.5	120	16	3.5	20
184-1	(011)	44	3	130	7	3.2	20
	(011)	46	1	30	3	7.6	
	(011)	43	3	35	3	2.5	
154	(011)	44	2	90	2	0.7	77
	(011)	43	2	90	2	1.4	
	(011)	44	3	90	2	1	

TABLE IV-b

Summary of Early Resolved Shear Stress Data

Crystal No.	Proportional Limit (psi)	Orientation Factor cos X cos φ	Resolved Shear Stress (011) [11$\bar{1}$] (psi)
At 298°K			
180-1	30,000	0.481	14,000
180-1	34,000	.491	17,000
180-1	36,000	.492	18,000
161-1	32,000	.489	16,000
180-2	31,000	.491	15,000
180-2	37,000	.491	18,000
180-2	41,000	.492	20,000
161-2	41,000	.489	20,000
168	29,000	.484	14,000
185	37,000	.487	18,000
180-2	46,000	.478	22,000 Avg = 17,700 ± 2500
At 77°K			
184	80,000	0.488	36,000
185	79,000	.491	38,000
167	96,000	.468	45,000
169	117,000	.299	35,000
170	88,000	.400	35,000
171	102,000	.440	45,000
172	94,000	.411	38,000 Avg = 39,000 ± 3900
At 20°K			
184-1	326,000	0.418	136,000
180-1	268,000	.478	127,000 Avg = 131,500 ± 4500

a (011) or (112) pole of the crystal, and 90° was taken as the average deviation of the pole from the trace of the plane it represents (X = 90°). The standard deviation includes, therefore, the error in the determination of the crystal orientation as well as the error in the measurements of α and β (see Fig. 28).

To emphasize the fact that slip does not occur on (112) type planes at 77°K or below, two specimens were made from each of three crystals: 180, 184, and 154. One specimen from each crystal was strained at 298°K and the other at 77° or 20°K. Specimens from crystal 154 were strained in bending, and specimens from crystals 180 and 184 were strained in tension. All three of the specimens strained at 298°K deformed by slip on planes of the type (011) and (112). The specimens, 180-1 and 184-1, strained at 20°K deformed by slip on (011) type planes

or twinning on (112) type planes or a combination of both. The part of crystal 154 strained at 77°K deformed by slip on (011) type planes only.

Observations of dislocation etch pits on bend specimens also support the conclusions that at 77° and 20°K tungsten deforms by slip on the (011) type planes and twinning on the (112) type planes; and that at room temperature, deformation is by slip on both the (011) and (112) type planes with no evidence of twinning. Figure 33 shows dislocation motion off a scratch which was purposely put into a crystal to nucleate fresh dislocations. The crystal was electrolytically polished and etched in Wolff's reagent to reveal grown-in dislocations, then scratched at 77°K and bent at room temperature at a stress below the yield stress so that gross yielding was avoided. The crystal was oriented with the (112) plane in the surface of the photograph and the maximum resolved shear stress on the (011) [$11\bar{1}$] system. Dislocation motion on the (011) plane is indicated. Although there is evidence for seemingly random dislocation motion in the vicinity of the scratch there is a line array of dislocations indicated (112). This trace corresponds to dislocation motion on a system of the (112) [$11\bar{1}$] type which has the highest resolved shear stress. Figure 34 shows dislocation etch pits in a crystal which was bent at room temperature and the two traces evident are traces of (011) and (112) type planes as indicated. In contrast to the arrays of pits which are indicative of slip deformation, Fig. 35 shows etch pits which are associated with twins. These markings on a crystal which was deformed at 77°K and failed brittlely, are presumed to be twins because they are evident after polishing and etching in HNO_3-HF and are evident as pits after polishing and etching in Wolff's reagent. They lie along traces of (112) type planes. The difference in the spacing of these pits from the arrays of pits revealed along slip traces is evident.

Figure 36 shows the shift of the specimen axis which occurred as the result of tensile deformation for crystals 132, 135, and 152. As slip progresses the specimen axis rotates toward a [111] direction, and the particular direction depends on the tensile axis of the crystal. The unit triangle in Fig. 36 has been divided into three regions in which the resolved shear stress is largest on three separate slip systems. In determining this division it was assumed that: (1) only systems of the type (011) [$11\bar{1}$] and (112) [$11\bar{1}$] were operative, and (2) that the critical shear stress on both (011) and (112) type planes are equal. The data of Calnan and Clews[28] was used to determine the boundaries of the three regions. The crystal axes of crystals 132, 135, and 152 rotate toward the [111] direction predicted. These results do not imply that the critical shear stress on planes of the type (011) and (112) is equal, but they do indicate that the slip direction is [111] as Goucher found for higher temperature deformation.

Observations on the Fracture of Tungsten Single Crystals

Figure 27 illustrates the relative ductility of tungsten single crystals at 298° and 77°K. Figure 27(a) shows a tensile specimen prior to testing. Figures 27(b) and (c) show specimens deformed at 298°K. These specimens showed 15 per cent elongation prior to necking and 90 to 100 per cent reduction in area. At room temperature, failure occurred either by the knife-edge fracture typical of soft single

crystals [27(b)] or by cleavage on (001) type planes just outside of the necked region [27(c)]. The cleavage plane has been reported previously by Goucher.[25] At 77° and 20,°K failure occurs by cleavage along (001) type planes with little or no plastic strain [28(d)] or after 2 to 4 per cent elongation by slip and twinning failure occurs by fracture along the twin interface and cleavage on (001) type planes.

Typical cleavage failures are illustrated in Fig. 37. Figure 37(a) shows the [100] fracture surface of a crystal which failed at 77°K. Note the river patterns evident along the three crystallographic directions indicated. Figure 37(b) shows the same area after etching to reveal dislocations. Note that pits are present along the traces which would be expected to result from slip and twinning, but that no evidence for plastic flow along [001] traces is evident as would be expected from the previous results.

The role of twinning in the fracture process is illustrated in Figs. 38 and 39. Figure 38 is a photograph of an as-cleaved crystal. This specimen failed in bending after about 5 per cent surface strain. It was deformed very rapidly at room temperature by bending over the edge of a table to demonstrate its ductility to a visitor. The specular reflections indicated by the arrows in Fig. 38 were identified as (112) type planes using a light goniometer and are twins. As is evident from this result and attempts to draw the tungsten single crystals at room temperature, twinning can occur in tungsten at room temperature if the strain rate is great enough. Recently there have been reports of twinning in tungsten at room temperature and above by several authors.[29, 30, 31] In an effort to prove that the surface irregularities illustrated in Fig. 38 were really twins the specimen was sectioned on a plane perpendicular to the trace of the twins and the [001] surface. Upon polishing and etching the result shown in Fig. 39 was obtained. The twins marked T_1 are the twins revealed as specular reflection in Fig. 39, and the twin marked T_2 is probably an accommodation twin formed to relieve the stress ahead of the crack indicated C. Of course, it is also possible that twin T_2 nucleated the crack, C, but neither conclusion can be proven definitely. Similar observations have been made by Sheely[30] in polycrystalline tungsten deformed at 77°K.

Another example of twins in tungsten is shown in Fig. 40 which was taken on the same specimen as that illustrated previously in Fig. 38. Figure 40(a) shows a very broad twin which apparently nucleated along the straight line on the bottom of the picture and grew upward. Note that in some regions the twin does not appear to have grown and along the original twin interface holes appear in these regions. As additional proof of the fact that these are really holes, examine Fig. 40(b) which is an electron microscope picture of the region indicated with the arrow in Fig. 40(a). Note the long shadows produced by replicating material which had penetrated the fissures and which stand up on the replica. The exact position of these cracks with respect to the original twin is difficult to determine, but they apparently occurred subsequent to the initial twin formation, but prior to its growth. This series of photographs illustrates that twins and cracks are sometimes associated and it raises but leaves unanswered the question of the role of twinning in brittle fracture in tungsten.

Critical Shear Stress

The tensile tests performed to determine the deformation modes in tungsten were conducted so that the stress-strain curve was obtained and the critical shear stress was measured. For this discussion the first deviation of the load-elongation curve from linearity was defined as the proportional limit, and the values obtained are presented in Table IV. Although we have shown that at room temperature both (110) $\langle \bar{1}11 \rangle$ type and (211) $\langle \bar{1}11 \rangle$ type slip systems are operative, the data are given as resolved shear stress on the (110) $\langle \bar{1}11 \rangle$ type slip system. Assuming (211) $\langle \bar{1}11 \rangle$ type slip does not alter the average values of critical shear stress. It was pointed out in an earlier report that these data fit the temperature dependence predicted by the Fisher[34] modification of the Cottrell-Bilby[35] theory of yielding. Further work has raised some question about this result which will be discussed in a later section of this report.

Recently, Wolff[29] and Probst[31] have observed twinning in tungsten at much higher temperatures than previously reported. The evidence reported here that high strain rates promote twinning at higher temperatures can account for this difference. As Rose,[32] Sheely,[30] and Bechtold[33] have all observed, the yield strength of tungsten is a sensitive function of strain rate at high strain rates (i.e., greater than about 2.5×10^{-2}/min). Hence, if there is a critical resolved shear stress for twinning or better a stress where twins can be nucleated if the dislocation density is low (see Sheely), then higher strain rates will promote twinning at higher temperatures. Of course, purity will influence the yield strength and hence also affect the temperature range in which twinning is observed. Wolff also pointed out that the frequency of twinning along a fractured tensile bar is brightest in the vicinity of the fracture. Their presence near the fracture is evidence that the two processes are related but is not a priori evidence that the twins nucleated the fracture. They could be found subsequent to the fracture also. Evidence that both situations are possible is illustrated by the picture of a fracture polycrystalline sample shown in Fig. 41. Note that in region A the fracture path lies along twin interfaces, while in region B one surface, to the left of the crack, shows the presence of twins while the region to the right shows no twin indicating that the twins formed subsequent to failure.

Discussion

The poles of the observed slip and twin plane traces presented in Figs. 31 and 32 show a deviation from the poles of the low index (011) and (112) planes. The average standard deviation, calculated as described previously, is $\pm 4.2°$ and the estimated experimental error is $\pm 5°$ consisting of $\pm 2°$ in the determination of the crystal orientation and $\pm 3°$ in the determination of the angles α and β. Since the average standard deviation is less than the estimated experimental error, the deviation of the experimentally determined poles of the deformation traces from the low index (011) and ($\bar{1}12$) planes can be attributed to experimental error.

The crystallography of plastic deformation of the metal single crystals was reviewed by Maddin and Chen[36] in 1954. Body-centered cubic metals have been

reported to slip on three different types of planes in the [111] zone: (110), (112), and (123). Andrade and Chow[37] found a correlation between the active slip plane and the temperature of deformation which is given in Table V. T is the absolute temperature of deformation and T_m is the absolute melting point. This correlation does not apply in the case of 4 per cent silicon-iron, molybdenum, niobium, or tungsten. Barrett, Ansel, and Mehl[38] showed that 4 per cent silicon-iron deformed by slip on (110) type planes only at temperatures from 77° to 973°K. For niobium[39] and molybdenum,[40] Chen and Maddin found that (011) [11$\bar{1}$] type slip explained all of their results.

TABLE V

Andrade's Correlation of Slip Planes
in Body-centered Cubic Metals and Temperature

Metal or Alloy	T/T_m	Slip Plane
W, Mo, Na	0.08-0.24	112
Mo, Na, B-Brass	.26- .50	110
Na, K	.80	123

In the case of tungsten this investigation shows that the number and type of operative slip planes are temperature dependent, but the behavior is not what Andrade and Chow would predict. Their correlation would predict slip on (112) type planes at low temperatures and (110) slip at intermediate temperatures. The present data show that at temperatures below 77°K (T/T_m = 0.02) slip occurs on (011) [11$\bar{1}$] type systems only while at 298°K (T/T_m = 0.08) the (011) [11$\bar{1}$] and (112) [11$\bar{1}$] type systems are both active. Although Frank and Nicholas[41] have predicted that dislocations with a [001] Burgers vector are stable in the body-centered cubic lattice and Goucher[25] has reported a single observation of (001) [010] type slip, no evidence of (001) [010] type slip was found in this study. As Goucher indicates, the conditions under which he observed slip on cube planes were very restrictive.

Although several reference works give the twinning plane and direction for tungsten as (112) [11$\bar{1}$], no original reference has been found. The present work shows that twins are formed in tungsten at 77° and 20°K on (112) type planes, but the twinning direction was not established. The twins which form as a result of tensile strain at these temperatures are few in number and are very thin so that the volume of twinned material is too small to be detected with back reflection microbeam x-ray techniques. At strain rates of 2 per cent per minute no twins were found to result from tensile deformation of tungsten single crystals at 298°K. However, twins have been seen in crystals which were deformed at 298°K at a strain rate in excess of 10 per cent per minute.

Conclusions

1. At 298°K and a strain rate of 2 per cent per minute, tungsten single crystals deform by a slip mechanism, and the operative slip systems are of the type (011) [11$\bar{1}$] and (112) [11$\bar{1}$]. At 200°K a single observation indicates (011) [11$\bar{1}$] type slip only.

2. At 77° and 20°K tungsten, single crystals deform by slip on (011) [11$\bar{1}$] type systems and by twinning on (112) type planes.

3. At 77°K tungsten, single crystals fail by cleavage along (001) planes or by a combination of cleavage and fracture along twin interfaces after 2 to 4 per cent plastic deformation.

4. The slip plane of tungsten does not change with temperature as the correlation of Andrade and Chow would predict.

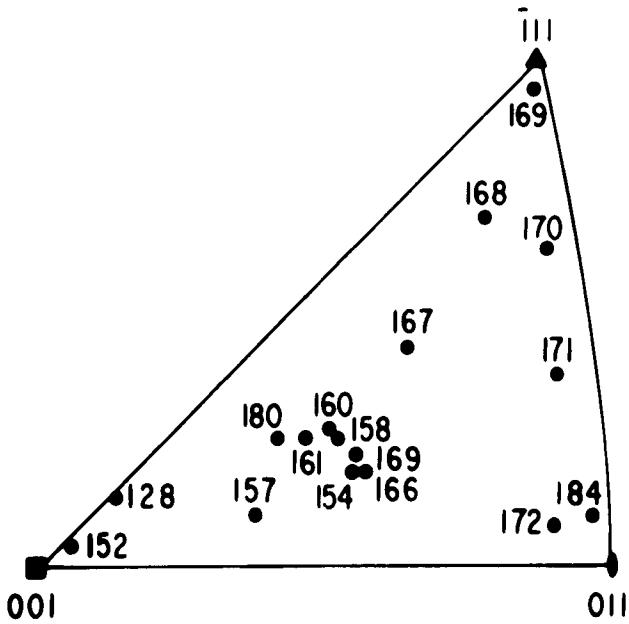

Fig. 26 Orientations of tungsten single crystals used for deformation study. The point represents the crystal axis.

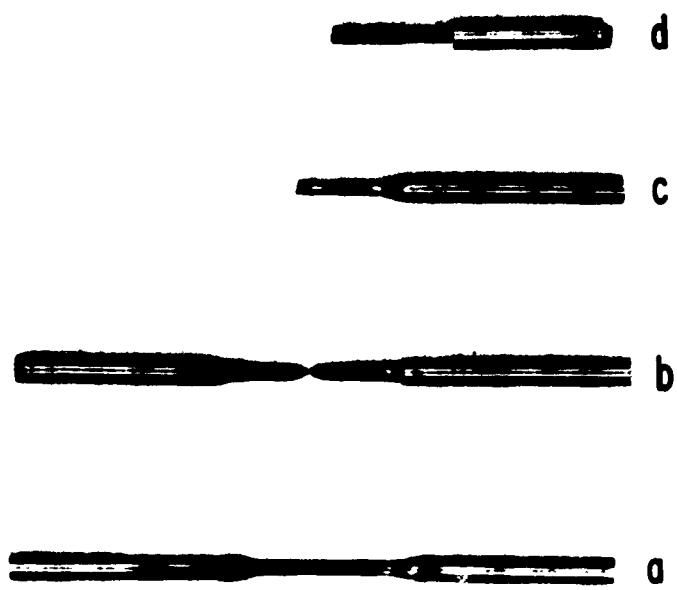

Fig. 27 Tensile specimens: (a) undeformed; (b) and (c) deformed at 298°K; (d) deformed at 77°K. 2X

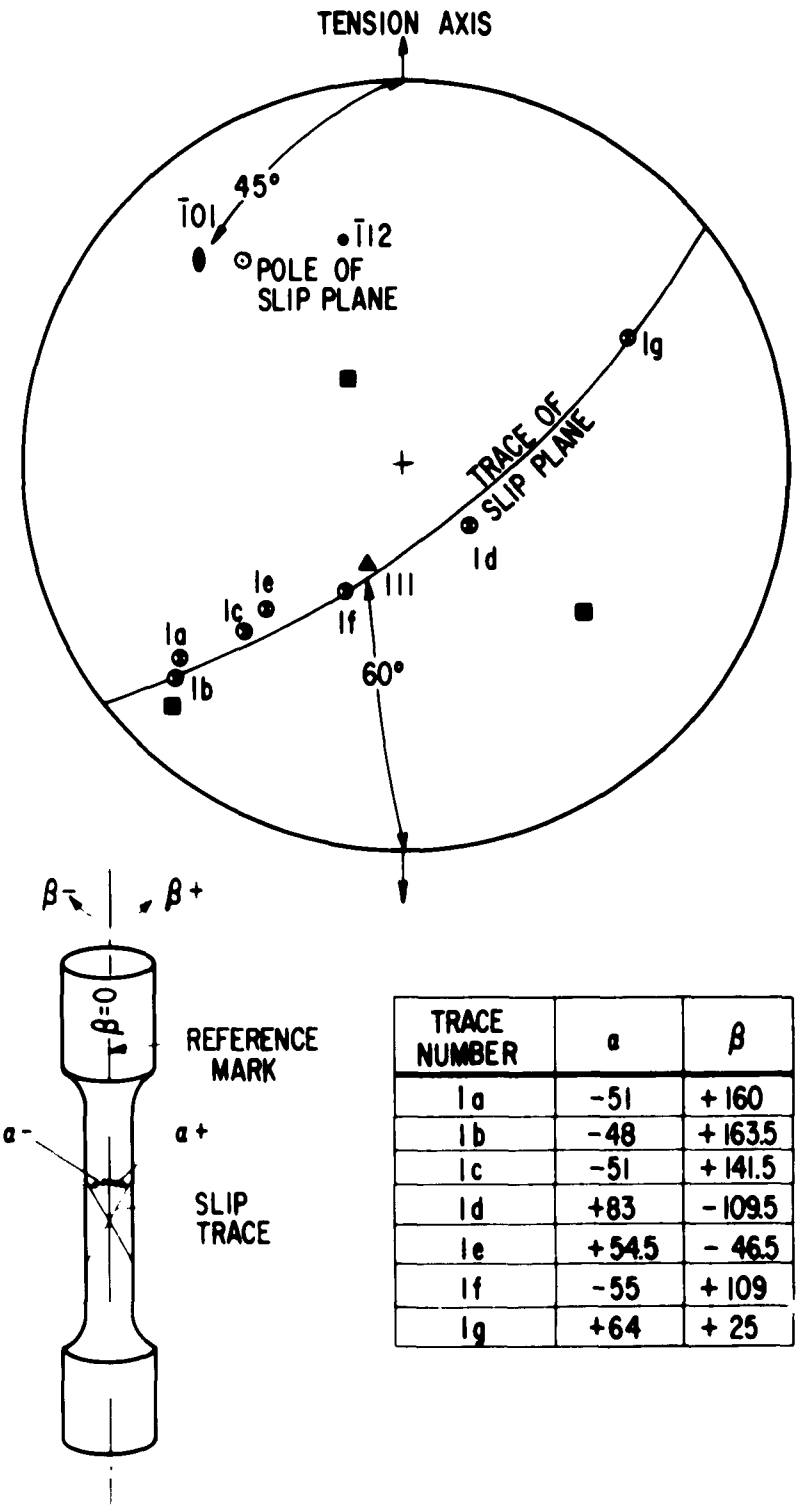

TRACE NUMBER	α	β
1a	-51	+160
1b	-48	+163.5
1c	-51	+141.5
1d	+83	-109.5
1e	+54.5	- 46.5
1f	-55	+109
1g	+64	+ 25

Fig. 1. Schematic illustration of technique for determining the pole of a plane from its trace.

(a)

(c)

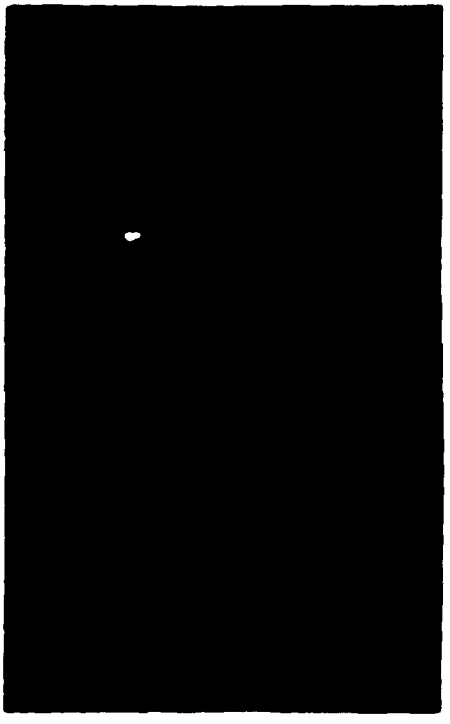

(b)

(d)

Fig. 29 Slip lines and twins: (a) crystal 159 deformed at 89°K. Slip lines only (1500X); (b) crystal 171 deformed at 77°K, S indicates slip lines and T twins (1500X; (c) 7500X, same as (a); (d) 30,000X, same as (b).

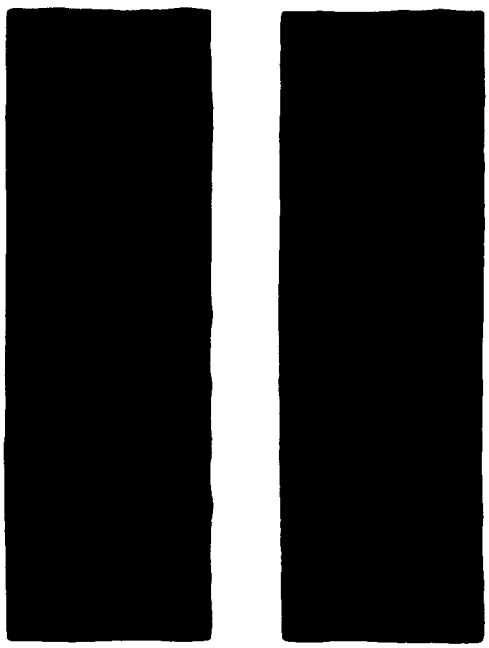

(a) (b)

Fig. 30 Slip lines and twins on crystal 171; (a) after 2 per cent tensile strain; (b) after repolishing and etching. 250X

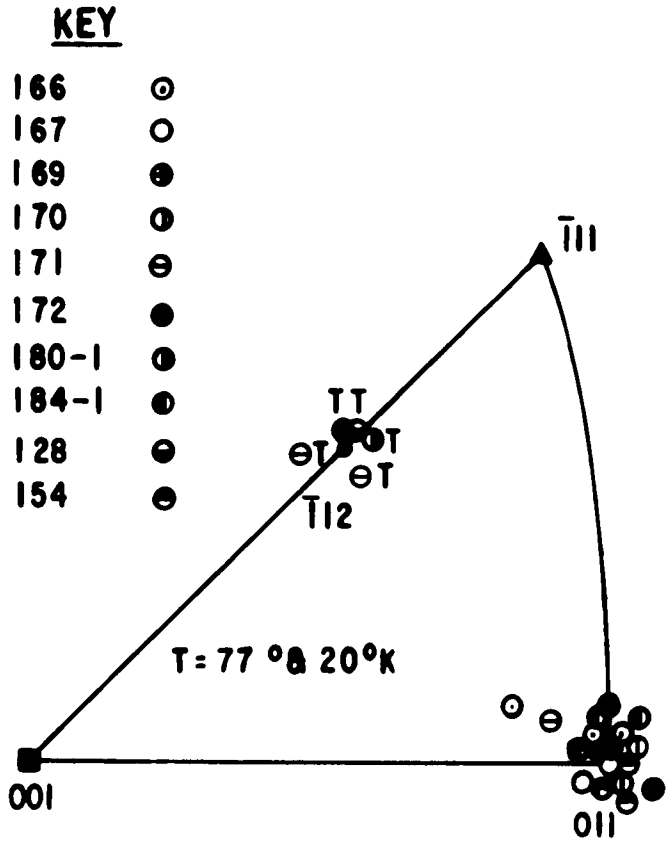

Fig. 31 Poles of slip and twinning planes for crystals deformed at 77° and 20°K.

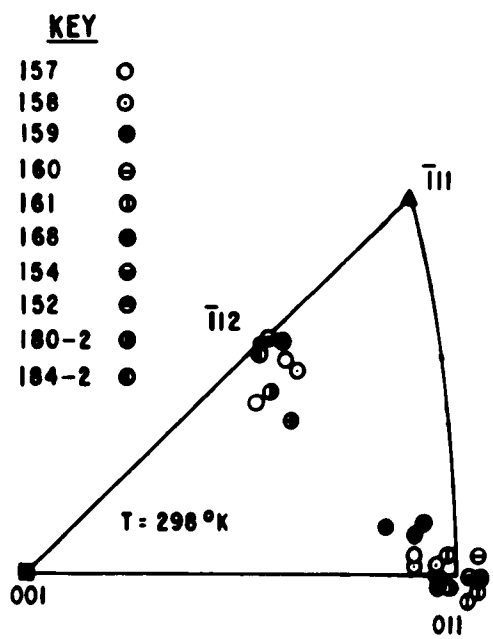

Fig. 32 Poles of slip planes for crystals deformed at 298°K.

Fig. 33 Dislocation etch pits aligned near scratch. (011) Indicates dislocation motion on (011) type planes and (112) motion on (112) type planes. 1000X

Fig. 34 Dislocation etch pits aligned along (011) and (112) type planes in crystal 109. 150X

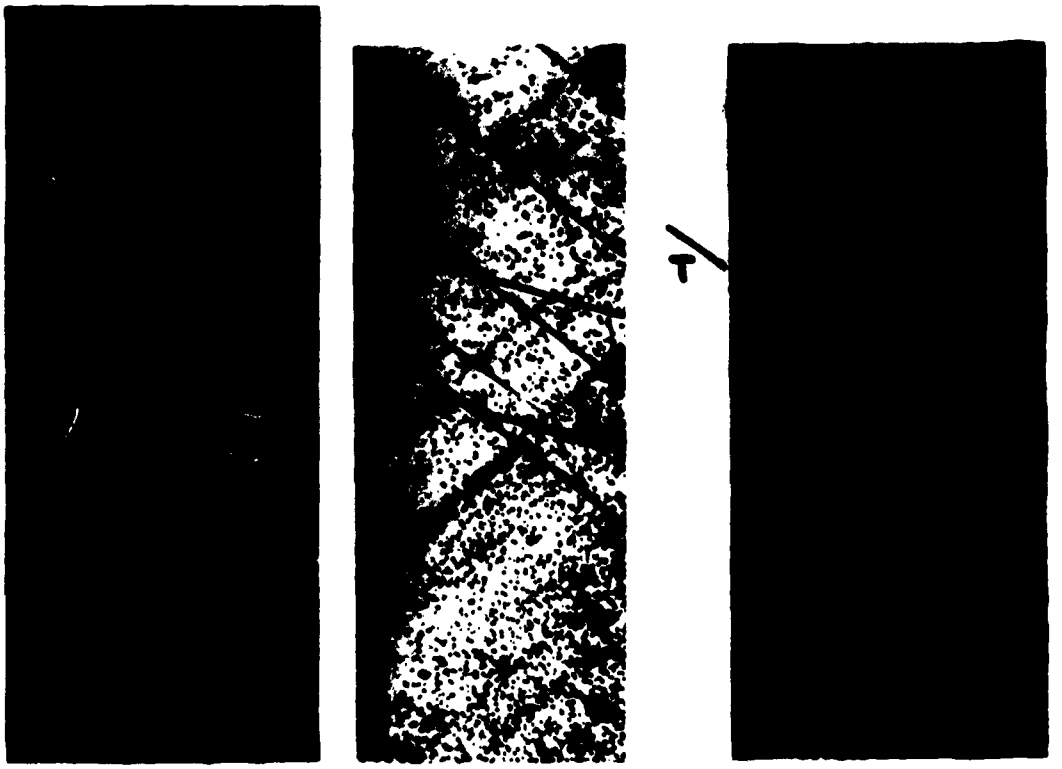

Fig. 35 Dislocation etch pits aligned along (112) type planes on crystal deformed at 77°K which are characteristic of deformation twins. (a) 500X; (b) 250X; (c) 500X. Note the glide bands evident as rows of etch pits at about 90° to the twins.

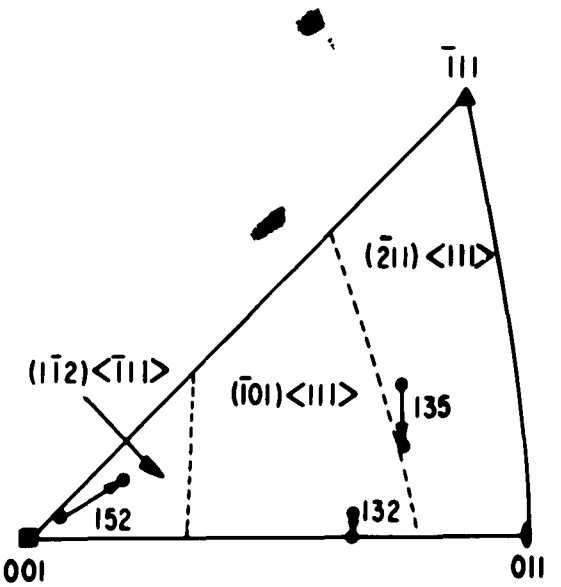

Fig. 36 Determination of slip direction. The tail and head of an arrow indicate the specimen axis before and after tensile deformation.

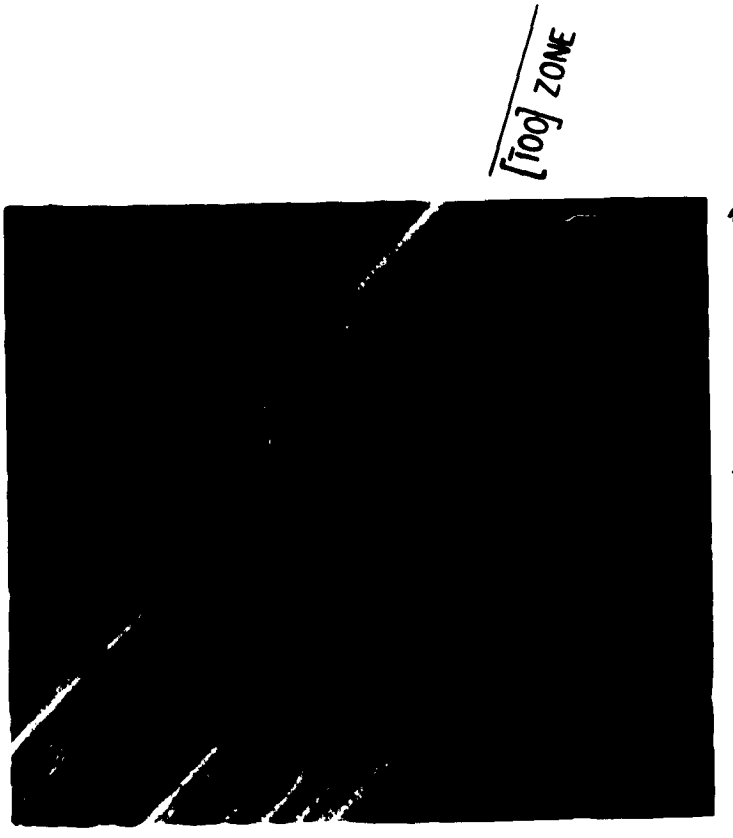

(a)

(b)

Fig. 37 Cleavage failure of a tungsten crystal at 77°K: (a) as-cleaved, 50X; (b) etched, 50X. The traces indicated on the [001] type surface are identified as slip (011) and twinning (112) planes. The (110) trace is also indicated although this trace could represent any plane in the [01] zone.

Fig. 38 [001] Cleavage failure of tungsten deformed rapidly at 298°K. Specular reflections indicated by arrow are from surface twins. 30X

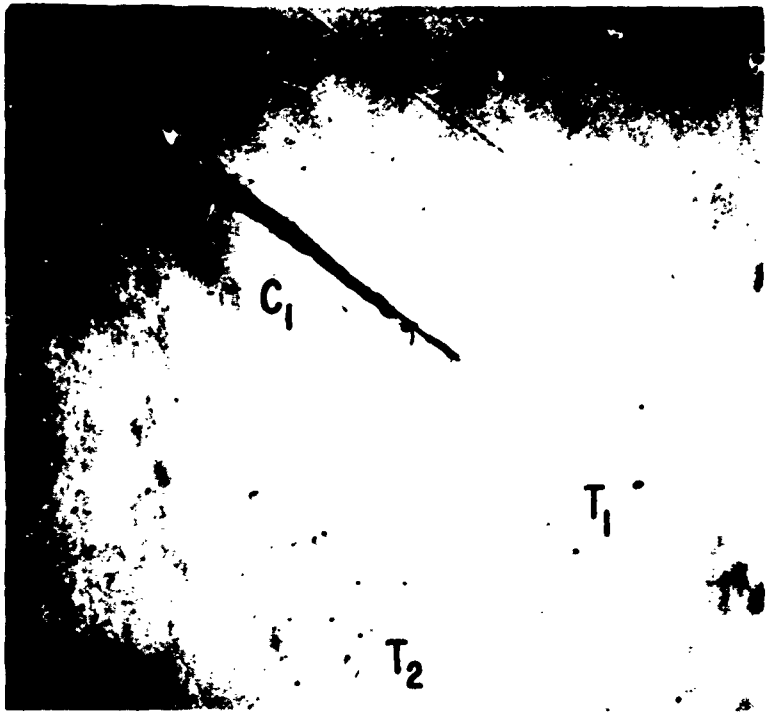

Fig. 39 Polished and etched surface of specimen shown in Fig. 38. Plane of polish is at 90° to [211] cleavage surface and at 90° to trace of twins indicated in Fig. 38. 500X

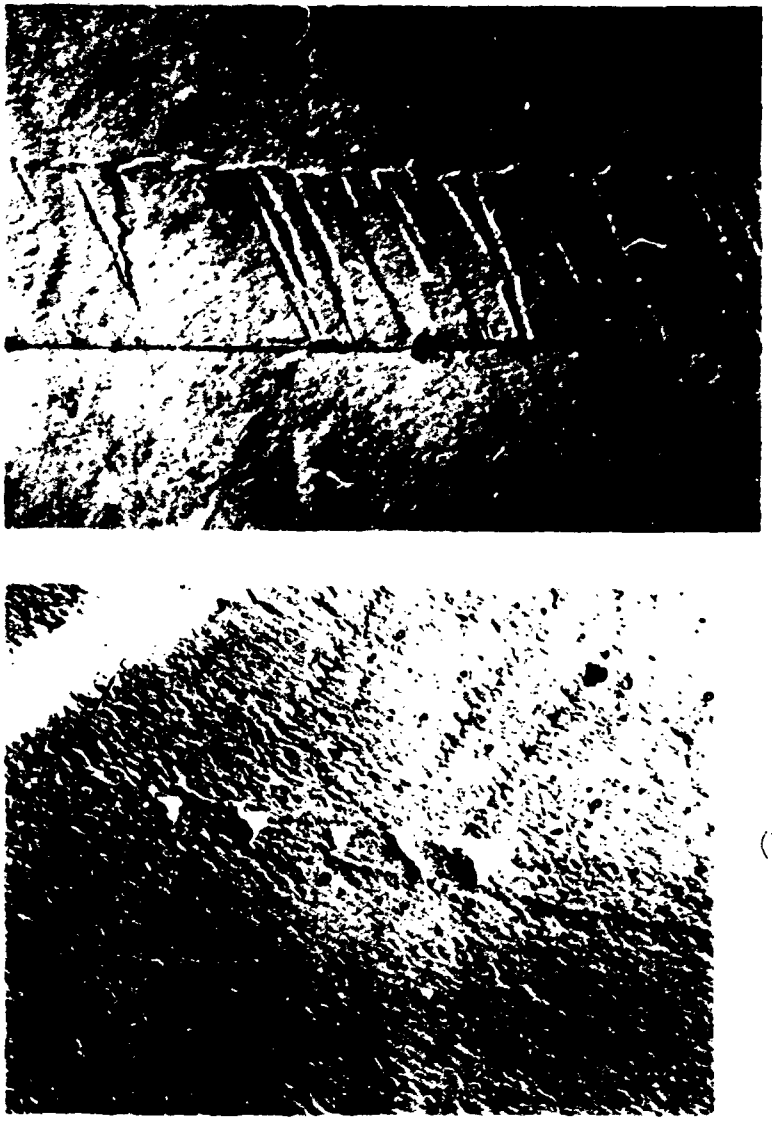

Fig. 40 Additional examples of twins in tungsten: (a) 2000X; (b) 9000X. See text for explanation.

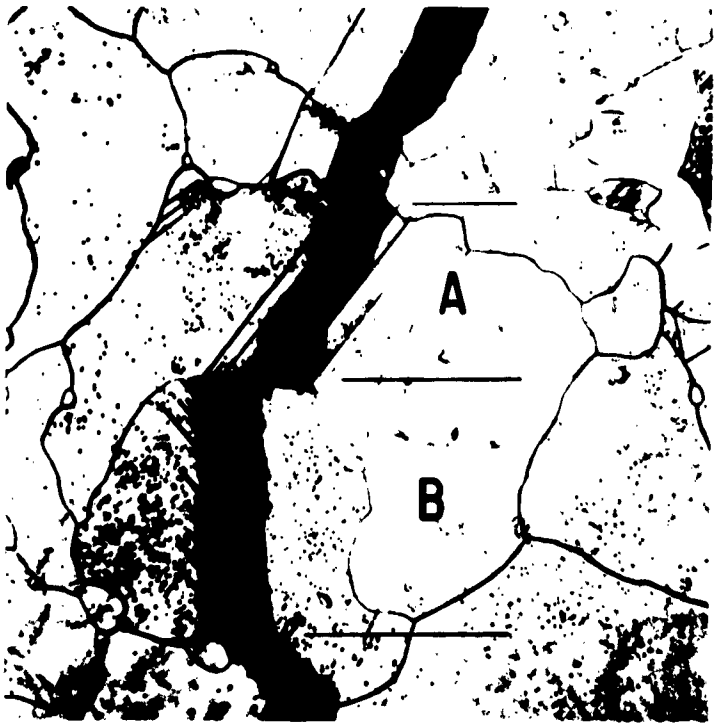

Fig. 41 Brittle failure in a polycrystalline sample of tungsten. Note that the photograph shows that twinning can occur in tungsten both prior to and subsequent to fracture. 250X

V. THE STRESS-STRAIN BEHAVIOR OF TUNGSTEN SINGLE CRYSTALS

Introduction

The preliminary work on the strength of electron beam zone-refined crystals of tungsten carried out in conjunction with the study of the modes of deformation of these crystals had indicated that the temperature dependence of the proportional limit could be described by the Fisher[34] modification of Cottrell's[35] model of yielding. However, there was considerable scatter in the data and also sometimes the crystals exhibited a very small yield drop which couldn't be consistently reproduced. In addition, since polycrystalline tungsten was reported by Bechtold[42] to exhibit a similar temperature dependence it was felt that further examination of single crystals to low temperatures would be beneficial.

Further, in retesting some of the crystals used for the earlier work there were indications that strain aging might be occurring in tungsten at room temperature. It was felt that this should be followed up since Bechtold and Shewmon[42] had previously reported strain aging in tungsten and it had already been found that an aging treatment was required to pin "grown-in" dislocations in the crystals used for the dislocation velocity measurements.

Single crystals with a [001] tensile axis were selected for this study since it was felt they would yield the required information and at the same time give the most information on the brittle behavior of tungsten single crystals. The latter supposition proved to be incorrect for the temperature range studied, but nevertheless useful information on the stress strain curve, aging effects in tungsten, and the work-hardening rate was obtained.

Experimental Procedure

Early load-elongation curves on tungsten single crystals had shown that the standard Instron testing machine was too soft to use for accurate measures of yield strength and yield point phenomenon in tungsten single crystals. On the advice of W. G. Johnston of our Laboratory and with the able assistance of D. C. Lord, modification of the loading arrangement on the Instron machine was undertaken. The primary source of nonelastic behavior in the standard loading string on the Instron machine is the bayonet coupling between the load cell and the pull rods. This joint and all others in the loading string were eliminated by making the upper specimen grip an integral part of the load cell. The pull rod-grip assembly was bolted directly to the load cell using a flange and six holding screws which permitted accurate alignment of the pull rod-grip assembly and the flat surface of the load cell. The pull rod-grip assembly was perpendicular to the mating surface of the load cell to within $\pm$ 0.001 inch in a runout of 30 inches. The lower grip was mounted on a bridge beneath the crosshead of the machine to permit testing at various temperatures and aligned with the upper grip using shims between the bridge and the crosshead. The alignment between upper and lower

grips was accomplished with the aid of a drill sleeve bearing which slid over the outside of both grips simultaneously. Axiality between upper and lower grips was better than 0.0005 inch over the 6-inch length of the drill sleeve bearing. This was checked with suitably positioned dial gages. As the sleeve bearing was lowered from the upper grip down onto the lower grip, the dial gages indicated the shift of the grip. The sense of touch of the operator was actually as sensitive as the indicating gages.

The grips themselves were of the standart split, wire type designed to accept a 0.100-inch sample. For temperatures above and below room temperature the heads and holding screws were appropriately stainless steel and machine steel. Thus differential thermal expansion aided the gripping. At room temperature, extra force was applied to the holding screws and if slipping was detected the data obtained fromthat test were discarded.

Experimental Results and Discussion

The experimental results are summarized and discussed in this section in three parts: the temperature dependence of the strength, aging of tungsten crystals, and strain rate sensitivity.

Temperature Dependence of the Strength

Figure 42 shows a typical load-elongation curve for an as-grown tungsten single crystal strained at 298°K. The strain rate used in all tests described in this section was 0.002 in/min in an 0.400-inch gage length or 5×10^{-3}/min (8×10^{-5}/sec). Several features of this curve should be noted: first is the absence of any yielding phenomenon and second is the relatively high work-hardening rate. For as-grown crystals this curve is typical for all crystals tested from 20° to 473°K. In contrast is the curve at the right for a sample cut from the same crystal and prepared in the same manner except for an aging treatment. The crystal was aged for 1.5 hours at 600°C and subsequently furnace cooled to room temperature over an 8-hour period. The aging treatment was carried out in an evacuated quartz capsule. Evacuation pressure is less than 10^{-6} mm of Hg. For this specimen note the presence of an abrupt load drop and the short lower yield point extension. For most specimens aged in a similar fashion and also at 1000°C the region of lower yield point extension is not present. The abrupt yield drop is a consistent feature of the aged crystals. Note also that the work-hardening rate of the aged crystal is slightly greater than the as-grown crystal. Figure 43 shows that the same sharp load drop occurs for an aged crystal tested at 77°K and similar results were obtained up to the highest test temperature used, 473°K.

Table VI summarizes the yield strength and work-hardening characteristics of as-grown and aged [001] axis single crystals as a function of test temperature. Also included are some crystals of random orientation to illustrate that this yield point phenomenon is not peculiar to [001] axis crystals. Figure 44 shows the temperature dependence of the upper and lower yield points for aged [001] axis crystals

TABLE VI

Summary of Yield Strength and Work-Hardening Coefficient for [001] Tungsten Single Crystals

A. As-grown Crystals

Crystal No.	Test Temp (°K)	$\tau_{P.L.}$* (10^3 psi)	$n = \frac{d \ln \sigma}{d \ln \epsilon}$	$\left(\frac{\partial \sigma}{\partial \epsilon}\right)_{\epsilon = 0.03}$ (x 10^{-6} psi)
244T1	473	7.3	0.316	0.63
228T1	298	10.6	.378	1.64
229T2	298	7.7	.463	1.57
226T2	208	13.0	.402	1.40
228T2	197	19.3	.396	2.24
233T1	78	49.7	.323	1.34
242T1	78	35.0	--	--
242T2	78	39.3	--	--
244T2	20	80.5	--	--
234T1	20	87.9	--	--
222T2†	298	20.7	--	--
160T2†	298	20.0	--	--

*$\tau_{P.L.}$ is the tensile stress measured as the first deviation of the load-elongation curve from linearity resolved onto the (011) [11$\bar{1}$] slip plane which has the maximum resolved shear stress factor.

†Not [001] axis crystals.

Table VI (continued)

B. Crystals Aged at 600°C for 1.5 hours and Furnace Cooled

Crystal No.	Test Temp (°K)	$\tau_{U.Y.P.}$* (10^3 psi)	$\tau_{L.Y.P.}$* (10^3 psi)	n	$\left(\frac{\partial\sigma}{\partial\epsilon}\right)_{\epsilon=0.03}$ (x 10^{-6} psi)	%Load Prop.
236T2	473	12.5	10.5	0.373	0.785	16
229T1	298	25.2	15.4	--	--	39
246JT1	298	16.1	14.1	--		12.4
224T1†	298	26.4	13.1	.568	1.51	50.3
235T1	197	32.9	25.9	.469	1.79	21
230T1	78	80.4	55.7	.261	--	30.7
236T1	78	80.5	53.7	--	--	33
222T1**	78	119.3	113.3	--	--	5
225T1**	78	125.0	121.0	--	--	3

*Stress has been resolved onto (011) [11$\bar{1}$] slip system with the maximum resolved shear stress.

†Aged 1 3/4 hours at 1000°C.

**Not [001] axis crystals.

and the proportional limit for as-grown crystals. As was expected, the upper yield point, lower yield point, and proportional limit all show a rapid increase with decreasing temperature. Both the upper and lower yield stress can be approximated by a straight line when τ is plotted vs 1/T, but the upper yield strength also fits equally well a straight line relation when log τ is plotted vs T. This is not true for the lower yield strength. The temperature dependence of the proportional limit of unaged crystals can be fitted to a straight line when τ is plotted vs 1/T but not as log τ vs T. The scatter in this case is very hard and in the absence of more information it is unreasonable to consider that this empirical fit is meaningful. Similarly, since the upper yield strength data fit equally well to both type of plots these data are no proof that either relation is correct. One thing is apparent from these data, however, and that is that the strength of the [001] crystals is below that of the average of the larger number of crystals measured earlier. Figure 45 compares the proportional limit shear stress values for the two sets of data. There are three differences between this set of data and the earlier work reported in the section on "Deformation Behavior." First, the

difference in the testing machine referred to earlier; second, the possible difference in purity of these [001] crystals; and third, the difference in strain rate. The softness of the tensile machine will influence the determination of the proportion limit. However, the second difference between the two sets of tests is probably more important. The [001] crystals and all crystals numbered 120 through 150 were grown from material which had been vacuum degassed prior to receipt. Standard procedure followed in the growth of early crystals included annealing the crystals in the vacuum system at about 3000°K for 10 minutes prior to melting. In an effort to eliminate this step and hopefully to obtain purer starting material, the 1/8-inch rod used to grow the crystals was heated at 2500°K for several hours prior to shipment from our Cleveland plant. Analysis of the material shows little improvement in purity, and analyses after growth of the single crystals show that the only difference in purity is in the average level of carbon that has been reduced from about 20 ppm by weight to about 10 ppm by weight. Since Lawley[43] has shown that small differences in purity as inferred from differences in zone-refining procedure influence the temperature dependence of the yield strength in Mo single crystals, it is probably that the same phenomenon is illustrated here. Apparently the difference in carbon content of the crystals used for these experiments and those used in the early work is responsible for this difference although the evidence is not at all conclusive.

Although the importance of strain rate on the proportional limit was not evaluated in this work, Rose has examined this variable. The data taken from his paper for [001] axis crystals and presented in Table VII show that for the range of strain rates used in our experiments there is no effect of strain rate on the proportional limit. Further, it should be noted on Fig. 45 that his data for a strain rate of 2.5×10^{-2}/min fall for the most part below our data for a strain rate of 2×10^{-2}/min.

TABLE VII

Shear Strength of [001] Axis Tungsten Crystals as a Function of Temperature and Strain Rate [after Rose[32]]

Crystal No.	Test Temp (°K)	$\dot{\epsilon}$ (per min)	σ (10^3 psi)	$\tau_{(011)[11\bar{1}]}$ (10^3 psi)
17b	77	2.5×10^{-2}	107.0	43.6
27b	195	2.5×10^{-2}	51.0	20.8
17a	300	2.5×10^{-2}	31.0	12.6
27a	373	2.5×10^{-2}	24.0	9.8
48	300	2.5×10^{-1}	65.0	26.5
37a	300	2.5×10^{-3}	24.0	9.8
7	300	2.5×10^{-0}	132.0	53.9

Another reason for the difference in strength of the [001] axis crystals and crystals of random orientation could be that there is an influence of orientation on the critical resolved shear stress. Although we never considered our data accurate enough to draw this conclusion without reservation, Rose's data indicate a marked increase in strength and a marked decrease in apparent work-hardening rate of [011] axis crystals. Since an abrupt discontinuity of the influence of orientation on critical resolved shear stress is not to be expected it is reasonable too that strength of a particular orientation might be less than the average strength of many crystals of different orientations.

The work-hardening rate for the [001] crystals is also included in Table VI and the work-hardening exponent, $d \ln \tau / d \ln \epsilon$, is plotted as a function of temperature in Fig. 46. These data are of particular interest because they show a difference between the as-grown and the aged crystals, and they also show that the work-hardening rate is a maximum near room temperature. The difference in work-hardening exponent between aged and as-grown crystals is to be expected, but without more information on the nature of the aging phenomenon it would be difficult to predict which treatment would result in the highest work hardening. The maximum in the work-hardening exponent at room temperature is more readily understood since as we have shown earlier slip deformation at 20°, 77°, and 200°K takes place on (110) $\langle 11\bar{1} \rangle$ type slip systems. At room temperature, however, both (110) $\langle 11\bar{1} \rangle$ type and (211) $\langle 11\bar{1} \rangle$ type slip systems are active. Hence one would expect an increase in work-hardening rate from 77° to 298°K. The reason for the decrease in work-hardening rate above 298°K is not as precisely explained because deformation modes have not been as exhaustively determined above 298°K. However, what evidence there is was presented in an earlier section of this report; and since (211) $\langle 11\bar{1} \rangle$ type slip is preferred at 725°K and also at very high temperatures as Goucher[25] and more recently Pugh and Lever[44] have shown, it is reasonable to expect a decrease in work-hardening rate above 298°K. The slope of the shear stress-shear strain curve at 3 per cent strain is also presented in Table VI. Note that the same general trend is apparent here also although there is greater scatter in the data. The data of Bechtold[33] on the work-hardening coefficient indicate that $d \ln \sigma / d \ln \epsilon$ is temperature dependent but in his case they reached a maximum at 350°C. Because of the brittleness of polycrystalline specimens at lower temperatures he could not make measurements at low temperature and hence the polycrystalline data cannot be compared with the single crystal data.

The most interesting feature of the load-elongation curve of the aged single crystals is not apparent on the stress strain curve. The yield point load drop was often accompanied by an audible "click" reminiscent of twinning. However, close inspection of these samples failed to reveal the presence of twins for any test temperature from 77° to 473°K. Realizing that any noise associated with a load drop phenomenon in body-centered cubic metals is always assumed to be twinning, this phenomenon was investigated further by performing some delay time experiments of an unusual kind. A tensile specimen was loaded to a stress below the upper yield strength and then the motion of the crosshead stopped. After a certain

time which depends on the maximum stress reached, the specimen began to unload itself by exchanging plastic for elastic strain. The total strain, elastic strain plus plastic strain, was held fixed. The results of such a test are illustrated in Fig. 47. This experiment performed at 298°K is convincing evidence that rapid unloading can occur in tungsten without twinning since again no twins were found upon examination and also on reloading the specimen behaved as would be expected of an as-grown crystal. The aging treatment results in a locking of dislocations by an impurity, presumably an interstitial impurity because the aging occurs at relatively low temperatures. The yield points resulting from such a locking process should not be presumed to be of the Cottrell type, and this point will be considered in the section on "Dislocation Velocities."

Several comments about the character and distribution of slip lines in these specimens are appropriate. Consider the photograph shown in Fig. 48(a) which was taken after etching the crystal used in the delayed yielding experiment indicated as W247-T1 in Fig. 47. Note that the glide bands delineated by the rows of etch pits (revealing dislocations) are widely spaced along the length of the specimen. Figure 48(b) shows the crystal whose mechanical history is indicated by the curve marked W247-T2 in Fig. 47. In this case the glide bands are no longer narrow, but have widened. Their number has not changed. Also interesting is the fact that in the aged crystal, shown in Fig. 48(b) and at higher magnification in Fig. 48(c), considerable work hardening has occurred but the widening glide bands have not yet impinged on one another. The bands widen only with <u>increasing</u> stress. This has been observed previously in LiF.(45)

The character of the slip lines present after deformation of the aged crystals is illustrated in Fig. 49. It is apparent that they are extremely sharp and straight. These pictures were taken on a specimen deformed just beyond the lower yield point. The broad band present in Fig. 49(a) produced enough offset to account for about 20 per cent of the load drop. Reference to this observation will be made in the discussion which appears at the end of the next section.

<u>Aging Effects</u>

Some preliminary experiments on the effects of aging on strained tungsten single crystals are discussed in this section and summarized in Table VIII. The observation that a 600°C anneal produced an abrupt yielding phenomenon in as-grown, unstrained single crystals raised the question as to what impurity or impurities in tungsten are responsible for the aging effects. Since at the present time it is not possible to eliminate all impurities and further since current analytical techniques don't permit reliable measurement of the level of impurities present in tungsten, it was decided to investigate briefly the influence of time and temperature on the production of the yield point.

Hardness measurements seemed a reasonable approach if sensitive to aging, since small samples could be used and hence experiments could be completed on one single crystal. Two samples were prepared to investigate this possibility by cutting a single crystal transversely and polishing the opposite faces using

TABLE VIII

Aging Experiments

Sample No.	Orientation	Heat Treatment	Test Temp (°K)	Yield Strength $\sigma_{P.L.}$ (10^3 psi)	Yield Strength $\sigma_{U.Y.}$ (10^3 psi)	Yield Strength $\sigma_{L.Y.}$ (10^3 psi)	ϵ (%)	σ_{max} 1st Test (10^3 psi)	Heat Treatment	Test Temp (°K)	Yield Strength $\sigma_{P.L.}$ (10^3 psi)	Yield Strength $\sigma_{U.Y.}$ (10^3 psi)	Yield Strength $\sigma_{L.Y.}$ (10^3 psi)
Tensile Tests													
347T2	[100]	1.5 hr at 600°C	298	--	--	29.8	1	61.2	6 hr at 400°C	298	--	86.6	86.0
347T1	[100]	1.5 hr at 600°C	298	--	--	27.0	0.32	27.0	1.5 hr at 600°C	298	37.0	40.2	38.6
225T1		1.5 hr at 600°C	78	--	254.0	187.5	1.2	187.5	1.5 hr at 600°C	298	75.8	80.2	70.2
226T1	[100]	1.5 hr at 600°C	206	46.65	--	--	2.56	134.7	1.5 hr at 600°C	298	85.4	--	--
236T2	[100]	1.5 hr at 600°C	473	--	28.5	23.9	15	83.0	1.5 hr at 400°C	298	59.3	--	--
246R	[100]	1.5 hr at 600°C	298	--	--	35.0	3.5	123.2	1.5 hr at 400°C	298	55.8	--	--
216T2		As-grown	No previous test						1.5 hr at 600°C	298	--	200.7	157.6
219T1	[100]	As-grown	298	18.9	--	--	5.8	135.7	6 hr at 400°C	298	82.0	--	--
217T1		As-grown	No previous test						1.5 hr at 600°C	298	--	84.6	55.9
215T1		1.75 hr at 1000°C	78	--	241.0	188.6	9.8	245.0	6 hr at 400°C	298	51.9	--	--
238T1	[100]	As-grown	197	46.5	--	--	7.9	250.0	1.5 hr at 400°C	298	84.4	--	--
206T1	[100]	As-grown	208	31.8	--	--	2.62	128.7	1.5 hr at 600°C	298	54.5	--	--
Compression Tests													
338T1	[100]	4.5 hr at 600°C F.C.	298	32.5	32.5	--							
338T2	[100]	1.5 hr at 600°C F.C.	298	31.2	36.7	--							
338T3	[100]	1.75 hr at 600°C F.C.	298	35.0	38.6	--							
338T4	[100]	1.5 hr at 600°C W.C.	298	32.5	36.1	36.1							
445T1	[100]	1 hr at 600°C F.C.	298	37.6	40.3	--							
445T3	[100]	19 hr at 600°C F.C.	298	33.1	38.7								
445T4	[100]	1.5 hr at 600°C F.C.	298	32.5	32.5	--							
445T4	[100]	3.5 hr at 600°C F.C.	298	33.1	--	--							

standard metallographic procedures. The final step was electropolishing. Using opposite faces eliminated orientation effects and minimized purity differences. One section of the crystal was aged for 1.5 hours at 600°C and the second was used as a control. No significant difference in hardness of the two specimens was measurable. The aged crystal had a Vickers hardness of 344 ± 13 and the as-grown crystal a Vickers hardness of 340 ± 16 for a 500-gram load and a loading rate of 0.04 mm/min. Loads of from 50 to 1000 grams and loading rates from 0.1 mm/min to 0.01 mm/min were investigated with similar results. It was noted that loading rate influences the hardness value obtained, but no combination of load and loading rate distinguished between the two samples.

Since hardness will not distinguish between as-grown and aged crystals several [001] crystals were cut into 0.250 inch long by 0.100 inch diameter cylinders for compression tests. The aging treatments are summarized in Table VIII and the strength levels are indicated. As is evident from the table, these samples did not exhibit the large yield drops which had been seen in the tensile tests. As Johnston[46] has emphasized, yield points are very difficult to obtain in compression unless the specimens are aged under a light load while in place in the testing machine. Since sufficient time did not remain to design equipment to accomplish this the compression tests were abandoned.

However, tensile tests summarized in Table VIII give enough information to prove that further investigation of this aging phenomenon should be made. The table illustrates several points. First is the fact that strain-aging produces a yield point in tungsten crystals only if the prior strain is less than about 1 per cent. Second is the fact that 1.5 hours at 600°C is sufficient to produce return of the yield point. At 400°C, 1.5 hours is not sufficient while 6 hours is sufficient to bring a return of the yield point. Further, the yield point produced by the strain aging is quite different from the yield point observed in crystals which received no strain prior to aging. In the case of the strain aged crystals, the sample exhibits pre-yield microstrain and a proportional limit is measurable. In the case of crystals aged prior to straining, no pre-yield microstrain is detectable. Also note that in the case of the strain aged crystals the load drop from upper to lower yield point is only a few per cent while for crystals aged prior to straining Table VI indicates load drops of tens of per cents. Apparently in crystals with a dislocation density greater than about 2×10^7 dislocations/cm^2 (the density observed in crystals strained 1 per cent--see the section on "Etch Pitting") the dislocations cannot be pinned as effectively by the impurity. Assuming that one impurity atom per plane along a dislocation line is required to completely immobilize a dislocation, a dislocation density of 2×10^7 would require only about 0.01 atom ppm. Since C, O, and N are all present in amounts greater than this, it is difficult to say what impurity is responsible. Some progress on the identification of the impurity responsible for this aging phenomenon is being made by Sell[47] and co-workers. They have identified an internal friction peak at 300°C which disappears after a solution treated specimen is aged at 600°C or above for a short time. The impurity responsible for this internal friction peak is probably the same one responsible for the observed aging phenomenon.

The limitation of time prevented further investigation of the aging and/or the strain aging effects, but the data are included here to point out the existence of the phenomenon.

Strain Rate Sensitivity
of Tungsten Single Crystals

Early in this work it was noted that tungsten crystals exhibited considerable ductility if deformed slowly, but fractured with little or no plastic deformation if deformed rapidly indicating that the flow properties were strain rate sensitive. Previous measurements of strain rate sensitivity in tungsten by Pugh[48] and Bechtold[33] were made at temperatures above 250°C. Since no data were available for temperatures below 250°C, the strain rate sensitivity of several crystals was investigated at 77° and 298°K.

$$n = \left(\frac{\log \sigma_1/\sigma_2}{\log \dot{\epsilon}_1/\dot{\epsilon}_2}\right)_{\epsilon}$$

where n is the strain rate sensitivity;

σ_1 is the flow stress at a strain rate $\dot{\epsilon}_1$ and a strain, ϵ ;

σ_2 is the flow stress at a strain rate $\dot{\epsilon}_2$ and the same strain, ϵ.

n is usually measured in one of two ways. The first involves determining the stress-strain curve for two similar samples deformed at two different strain rates and the calculated n at different strains. A simpler technique which involves only one specimen is to change strain rates in the middle of the test and determine the change in the flow stress. This process can be repeated several times in order to determine n as a function of strain. The change of rate type tests were used, and the strain rate was varied by a factor of 10 from 0.4 per cent/min to 4.0 per cent/min. The strain range investigated was from 0.5 to 10 per cent. Crystals of different orientations were used to see if there was any effect of orientation.

The data are presented in Table IX and n is given as a function of increasing strain. Except for crystal WB-2, there appears to be no influence of strain or orientation on n. However, n is a function of temperature having a value at 77°K which is 60 per cent of the room temperature value. These values are similar to the values reported by Pugh[48] at 400°C but are considerably below the values of Bechtold[33] reported at 250°C. However, it is evident from the data of Carreker and Guard[49] and Bechtold[50] on Mo the strain rate sensitivity is not a monotonic function of temperature.

TABLE IX

Strain Rate Sensitivity of Tungsten Single Crystals

Sample No.	Strain (%)	$n = \left(\frac{\log \sigma_1/\sigma_2}{\log \dot{\epsilon}_1/\dot{\epsilon}_2}\right)_\epsilon$	$\bar{n}$	Temp (°K)
WB2	2	0.0160		77
	2.9	.0140		
	4.9	.0140	0.0138	
	7.0	.0125		
	8.9	.0115		
	9.2	.0150		
WC1		.0125	.0122	77
		.0120		
WB3		.0140		77
		.0195		77
		.0190		
		.0140	.0161	
		.0140		
W188-2		.0145	.0145	77
W189-1		.0135		77
		.0135	.0135	
		.0135		
		Grand Average 0.0140 ± 0.0013		
W180		.0240		298
		.0255		
		.0255	.0252	
		.0255		
		.0255		
W160-1		.0215		298
		.0280		
		.0260	.0258	
		.0275		
		.0260		
WC-2		.0260		298
		.0235		
		.0215		
		.0225	.0240	
		.0250		
		.0250		
		.0260		

Table IX (continued)

Sample No.	Strain (%)	$n = \left(\frac{\log \sigma_1/\sigma_2}{\log \dot{\epsilon}_1/\dot{\epsilon}_2}\right)_\epsilon$	$\bar{n}$	Temp (°K)
WC3		0.0205		298
		.0220		
		.0220	0.0224	
		.0225		
		.0225		
		.0240		
		.0260		

Grand Average 0.0243 ± 0.0013

Summary

The temperature dependence of the proportional limit of as-grown tungsten crystals and the temperature dependence of the upper and lower yield points of aged crystals was measured. As expected, the data showed a rapid increase as the temperature was lowered. The data plot reasonably well as a straight line if τ is plotted vs the reciprocal of the absolute temperature, but equally as well as log τ vs temperature at temperatures below room temperature. Therefore, it is not reasonable to assume that any particular model of yielding is correct.

The dramatic effect of aging on the shape of the stress-strain properties is reported, but the impurity or impurities responsible was not identified.

The work-hardening coefficient of [001] axis single crystals is temperature dependent and is a maximum (over the temperature range 77° to 473°K) near room temperature. Aged crystals have a larger work-hardening coefficient than as-grown crystals for all temperatures investigated.

The strain rate sensitivity was measured by the rate-change technique at 77° and 298°K. As Guard(51) and Hahn(52) have recently indicated, the strain rate sensitivity should be related to the stress dependence of the velocity of individual dislocations, and this point will be considered further in the next section.

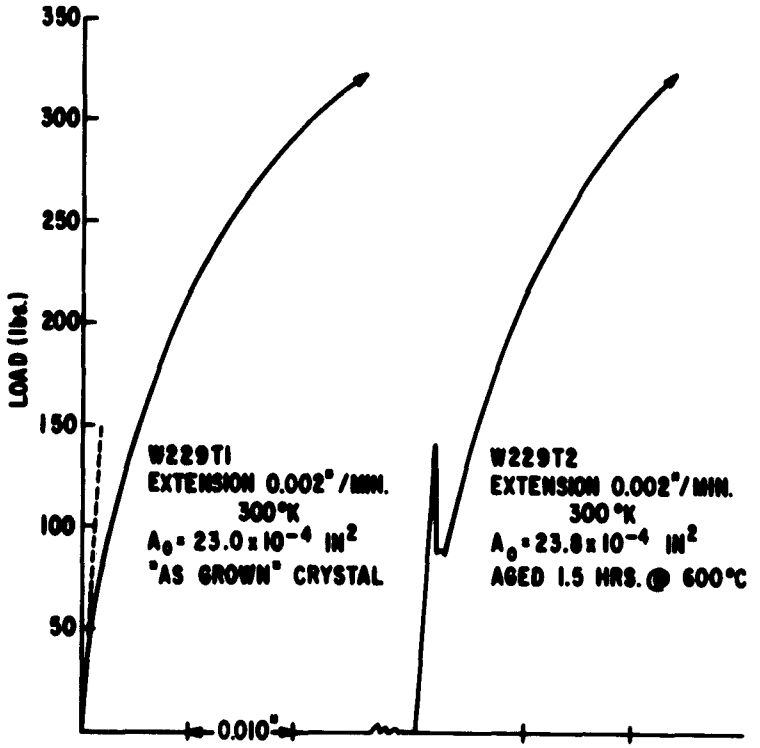

Fig. 42 Typical load-elongation at 300°K for as-grown and aged tungsten single crystals. Although the samples illustrated had a [001] tensile axis, the behavior is typical of random orientations. The load drops are less spectacular for the random orientations.

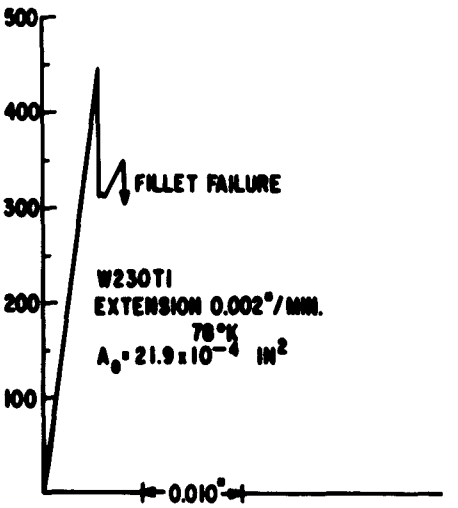

Fig. 43 Load-elongation curve for [001] axis crystal tested at 77°K. Note failure was premature and actually occurred in the fillet.

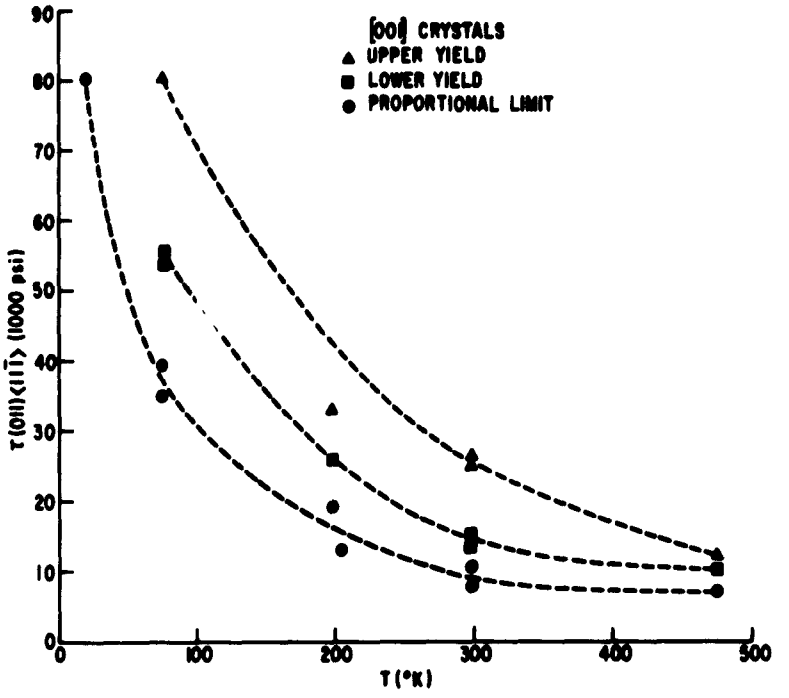

Fig. 44 The temperature dependence of the proportional limit and upper and lower yield point of [001] axis single crystals. No tests of aged crystals were made at 20°K.

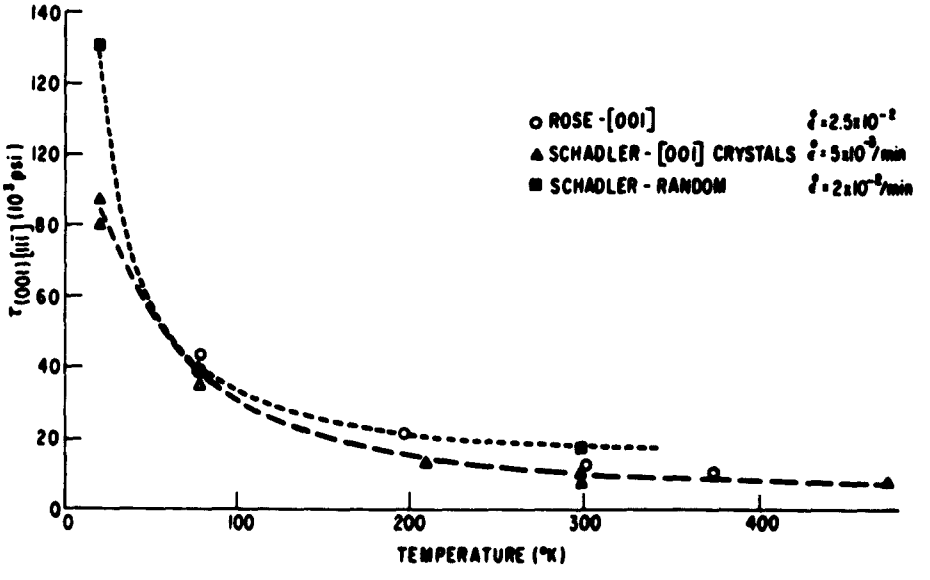

Fig. 45 Temperature dependence of the proportional limit of [001] axis and random axis tungsten single crystals. Also included are strengths of [001] axis crystals obtained by Rose. (32)

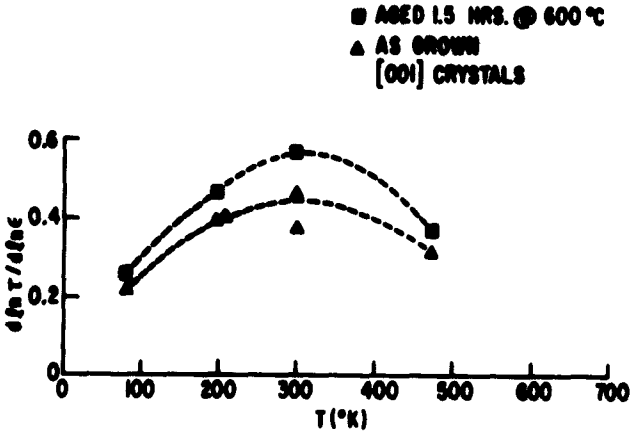

Fig. 46 Temperature dependence of the work hardening exponent, $d\ln\tau/d\ln\epsilon$, of [001] axis tungsten single crystals.

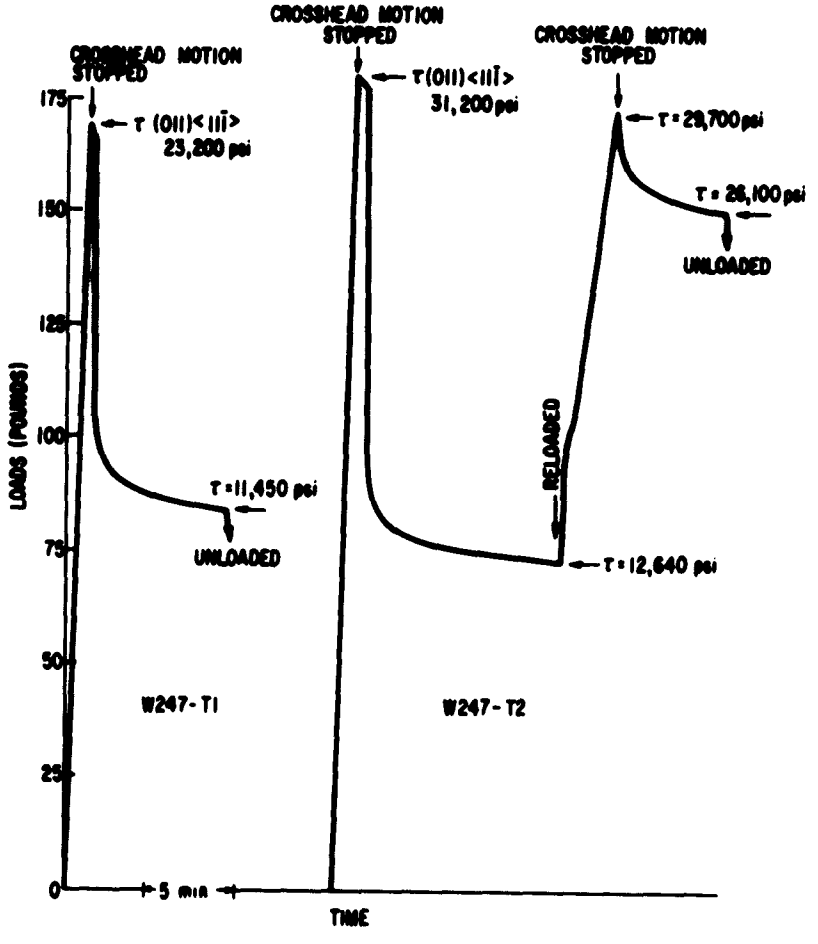

Fig. 47 Illustration of delayed yielding in tungsten. Experiment conducted at 298°K.

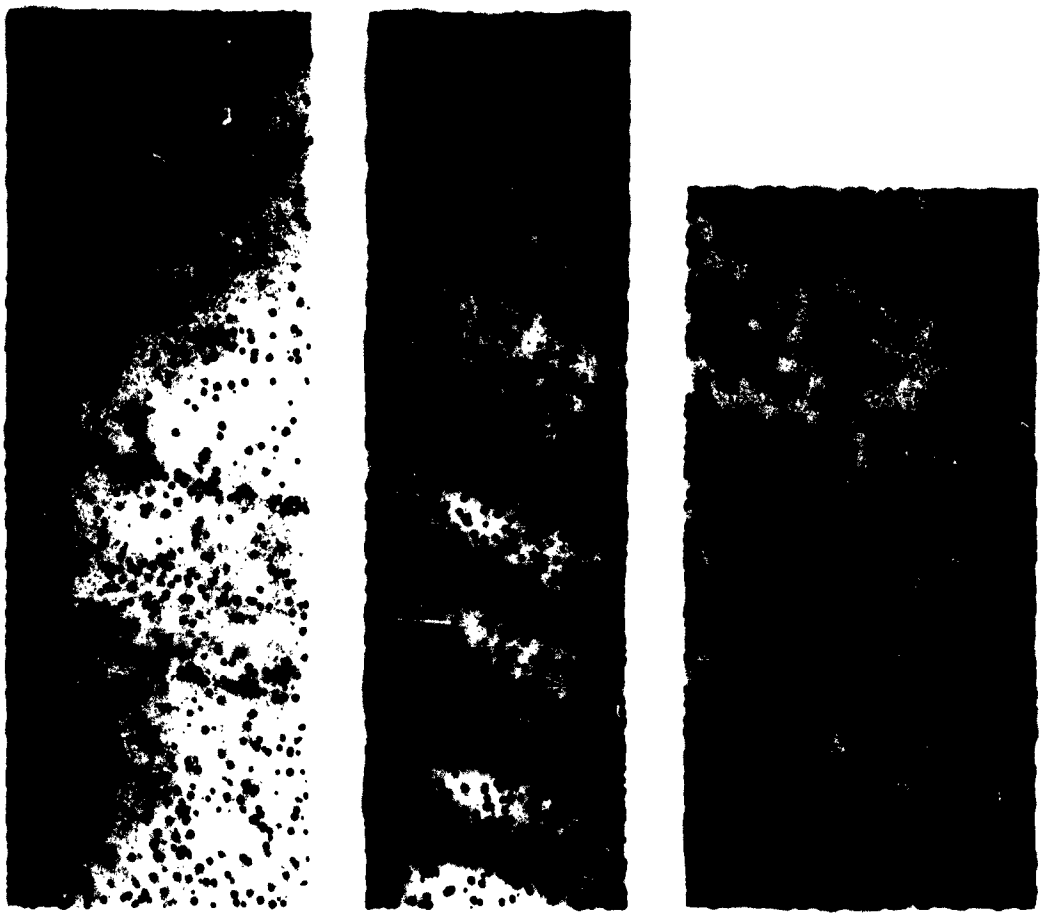

Fig. 48 Etched surface of crystals used for delay time experiments illustrated in Fig. 47. (a) Crystal W247-T1, 250X; (b) crystal W247-T2, 250X; (c) same as (b), 500X.

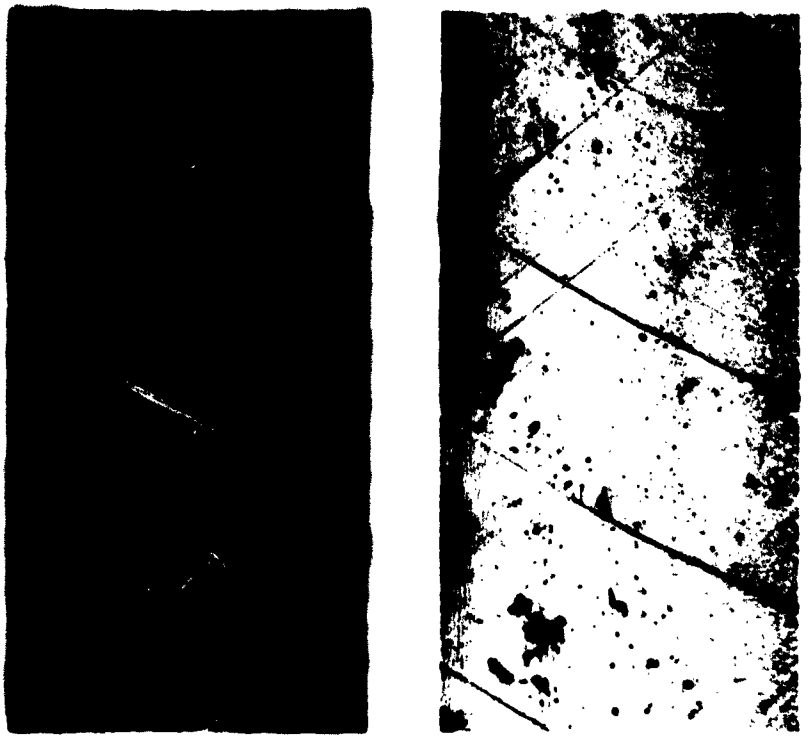

(a) (b)

Fig. 49 Slip lines on surface of aged crystal deformed at 77°K--250X. Large deformation band in (a) produced enough strain to account for 20 per cent of the load drop.

VI. MOBILITY OF DISLOCATIONS IN TUNGSTEN

Introduction

The recent work of Johnston,[46] Johnston and Gilman,[53] Stein and Low,[3] and Chaudhuri and Patel[14] on the behavior of individual dislocations in single crystals of LiF, 3.25 per cent Si-Fe, and Ge and Si has demonstrated that a knowledge of the dislocation behavior in a crystal can be used to explain the mechanical properties of single crystals. These authors have used dislocation etch-pitting techniques to observe the behavior of individual dislocations under the application of stress at various temperatures. In addition to the fact that these authors have illustrated that the average velocity of a dislocation is a very sensitive function of stress and temperature, they have raised the question of the importance of the Cottrell explanation of the rapid drop in load which occurs subsequent to the upper yield point in iron. Cottrell's[35] theory says that load drop following the upper yield point is the result of dislocations breaking away from their impurity "atmospheres" whence they are free to move and multiply at a stress lower than that required to free them from their atmospheres. Using their data on the stress dependence of the dislocation velocity and the dislocation velocity as a function of strain, Johnston and Gilman[53] and more recently Johnston[46] have shown that the yield point can be explained using the two parameters mentioned above with the assumption that the original crystal had relatively few, but some (10^2 to 10^4 dislocations/cm^2), mobile dislocations. Johnston also points out that in addition to these parameters, in a real crystal the rate of work hardening will influence the magnitude of the yield point.

A second and independent indication that Cottrell's explanation may not be the complete explanation of the yield point is the results of Stein and Low.[3] They measured the stress dependence of the average velocity of dislocations in single crystals of 3.25 per cent Si-Fe and found that the temperature dependence of the stress required to maintain a dislocation velocity of 10^{-3} cm/sec was the same as the temperature dependence of the flow stress. Further, they found that gross yielding of a single crystal initiates at inclusions in the crystal and thus that stress concentrations may be important to yielding.

In an effort to broaden the quantitative knowledge of the role which dislocations play in yielding of single crystals in general and in tungsten crystals specifically, the technique of Stein and Low was used to determine the stress dependence of the average velocity of dislocations in tungsten single crystals at 77° and 298°K.

Experimental Procedure

The growth of the single crystals and their preparation for the velocity measurements has been described previously. In addition to the treatments described for bend specimens it was found to be necessary to age the crystals at

600°C for about 1.5 hours and slow cool them to room temperature to prevent the motion of the dislocations grown into the crystal. Since the success of the experiment depends on knowing the location of a group of dislocations before and after the application of a stress, random motion from grown in dislocations cannot be tolerated. This aging process effectively pinned the grown-in dislocations for tests run at 77°K, but unpinning became a problem at 298°K. The effect of this treatment on the stress-strain behavior has been previously discussed in this report.

The specimen was cut to have the orientation indicated in Fig. 50 so that when loaded in bending along the axis indicated the maximum resolved shear stress was on the (011) [11$\bar{1}$] type slip system. Dislocations moving on this plane have a Burgers vector parallel to the surface of the specimen and hence are pure edge dislocations. Fresh dislocations were introduced on the (112) surface of the crystal along a line perpendicular to the bend axis in the same manner and with the same diamond indentor described by Stein and Low.[3] The character of the scratch produced is shown in Fig. 51. Scratching was always carried out at 77°K and the lapsed time between scratching and loading was never more than 5 minutes. Note that the scratch shown in Fig. 51 is not symmetrical and dislocations moving from the scratch along the (110) trace always moved from the side of the scratch showing fewer dislocations. At high stress dislocation motion from both sides of the scratch was observed. Figure 33 indicates this as well as illustrating the character of the glide bands formed.

The velocity measurements were made by taking a previously polished and etched specimen, scratching it at 77°K and then loading it in three-point bending for a predetermined time at a predetermined temperature, and then re-etching. The loading time was usually long enough so that only a small error was introduced by reading the time from the recording chart. For short-time pulses the load signal was fed into the vertical scale of an oscilloscope and the time was read from a photograph of the horizontal sweep. A Tinius Olsen testing machine was used for all but the short time experiments, where an Instron was used. The force applied to the specimen was used to calculate the applied stress in the specimen assuming elastic behavior. Since all stress used were below the stress for general yielding for the aged crystal, this approximation introduces no error. However, there are several sources of error which must be considered.

Sources of Error

The following sources of error will be considered: subgrain boundaries, nonuniformity of specimen shape, and residual stress in the scratch. The presence of subgrain boundaries was a constant source of difficulty. If dislocations moving from the scratch encountered a subgrain boundary they were held up by the boundary for two reasons: first, by the interaction of the stress field of the boundary with the stress field of the dislocation and, second, because the initial etching had removed material and hence the moving dislocation encountered a hole in the material. The obvious solution of moving the dislocations short enough distances to

avoid this interaction effect was adopted. This meant that total distances of motion of 400μ or less were used. The problem of the nonuniformity of the specimen is troublesome in that it introduces an error in the stress calculation which requires knowledge of the moment of inertia of the specimen, and also because it means a nonuniform stress field across the surface of the specimen. The latter part of the problem was minimized by using only the center section of the surface of the crystal. At most, the error in the moment of inertia was less than about 5 per cent which is about the same as the maximum error in the knowledge of the absolute load.

The residual stress in the scratch could be very troublesome except that it can be estimated from the experiment and hence subtracted from the data. Consider Fig. 52 which schematically illustrates the problem. Since Stein has shown that the residual stress introduced by the diamond scriber falls off linearly with the distance from the scratch, we assume the stress distance profile indicated by τ_c. For an applied stress, τ, the stress profile across any given cross section is represented by the dotted line and is the sum of the applied stress and the residual stress. Since for a given time of an experiment the dislocations will move a distance which is

$$\int_0^t \bar{v}dt,$$

there is some arbitrary stress below which no dislocation motion will be observed, and hence dislocations will move away from the scratch the distance indicated. As the applied stress is varied, this distance moved from the scratch will change and the profile of the distance moved vs stress, τ, is indicated schematically in Fig. 53. X_0 is the distance over which the scratching process itself has caused motion. This curve was constructed assuming that the average dislocation velocity, $\bar{v}$, is power function of τ. This figure emphasizes that X_c, the distance over which the residual stress of the scratch is felt, is not easily measurable, but also that failing to take it into consideration introduces an error of less than 10 per cent as long as the data are taken for stresses close to τ_{max}. In practice this was done. Actually the expression for the shape of the curve indicated from τ_{max} to $\tau = \tau_c$ is:

$$X = X_0 + \left(\frac{\tau}{\tau_0}\right)^m t - \frac{X_c}{\tau\tau_c(n+1)}$$

where X_0 and X_c are as defined in the figure and $\bar{v} = (\tau/\tau_0)^n$ an empirical relation found by Gilman and Johnston, Stein and Low, and Schadler to fit the data.

Hence, $$\bar{v} = \frac{X - X_c - X_0}{t}\sqrt{2}$$

From the experiments X_0 is 14μ, X_c is 14μ, and τ_c about 15,000 psi, and 28μ was subtracted from the measured distance to calculate the average velocity defined as above. The $\sqrt{2}$ factor is to correct for the actual distance moved since X was measured perpendicular to the scratch and the dislocations are moving on a plane

which is 45° to the scratch. Figure 54 shows motion of dislocations from the scratch. The specimen shown in Fig. 54(a) was stressed at 77°K and that shown in Fig. 54(b) was stressed at 298°K.

Results

The stress dependence of the average edge dislocation velocity on (011) [11$\bar{1}$] type slip planes at 77°K is indicated in Fig. 55 and in Table X. The solid line with the dashed extensions is the least squares line for all the data obtained, and Table X contains the constants in the equation

$$\bar{v} = \left(\frac{\tau}{\tau_0}\right)^m$$

which were obtained from a least squares fit to the data from individual crystals. Also included in the figure are the least squares line and the individual data points for crystals W205-2 and W249-1 which have the largest and smallest values of m, respectively, for all crystals tested. There is a variation of the functional relation between different crystals as might be expected both from experimental error and from variation in properties of the crystals due to variations in purity. Although these crystals have not been analyzed due to recent completion of the test, we know from previously presented data there is no significantly measurable variation in purity. This fact alone is sufficient to permit anticipation of the fact that the influence of purity on the stress dependence of the velocity was not made and should probably not be attempted with interstitial impurities until better methods of analysis and/or doping become available.

TABLE X

Summary of Dislocation Velocity Data

Crystal No.	Temp (°K)	m	log τ_0
W205-2	77	9.3	4.84
W238-2	77	14.6	4.73
W209B	77	12.5	4.88
W249-1	77	11.9	4.70
All crystals	77	10.5	4.79
W238-2	298	4.0	4.90
W213-2	298	6.2	4.41
W239-1	298	3.1	5.01
All crystals	298	4.8	4.65

Also presented in Fig. 55 is the least squares line for all of the results obtained at 298°K. The data in this case are not presented since the data do not cover a broad enough velocity range and are probably not as reliable as the data obtained at 77°K. Data were not taken at higher velocities because, at the high stresses required, dislocations began to move from the subgrain boundaries of the crystal hence obscuring the measurements and invalidating the results. Apparently the aging treatment was not sufficient to permit complete pinning at room temperature a point to which we'll return in the subsequent discussion.

Discussion of Results

Because of the difficulties encountered in specimen preparation, measurements of dislocation velocity were attempted only at the two temperatures indicated, and hence any attempt to correlate the stress required to maintain a fixed velocity and the flow stress at various temperatures will be incomplete. However, it is interesting to note that at 77°K the proportional limit (the first deviation of the load elongation curve) occurs at a dislocation velocity of about 4×10^{-3} cm/sec, and at 298°K the velocity at the proportional limit is 10^{-3} cm/sec. This factor of 4 is in good agreement considering the difficulties encountered in the 298°K velocity measurements, the inaccuracy in the determination of the proportional limit, and the variation in the measured values. The stress values used are those obtained for the [001] axis crystals described in the previous section because these crystals were grown using the same starting material and under the same conditions (two passes) as those used for the velocity measurements.

As Guard[51] and more recently Hahn[52] have pointed out, there should be a simple relation between the strain rate sensitivity and the power dependence of the dislocation velocity on stress. This relation is derived from the equation $\dot{\gamma} = nb\bar{v}$, where $\dot{\gamma}$ is the strain rate, n is the number of mobile dislocations, $\bar{v}$ is the velocity of the dislocations, and b is the Burgers vector. Guard gives the equation as

$$\frac{d \ln \dot{\epsilon}}{d \ln \sigma} = \frac{d \ln \bar{v}}{d \ln \sigma} + \frac{d \ln n}{d \ln \sigma}$$

The first term is the reciprocal of the strain rate sensitivity and second is the power dependence of the dislocation velocity on stress. They are related by the third term which is the change in the density of dislocations moving in a crystal as a function of stress. As Johnston has recently shown for LiF,[46] $d \ln \bar{v} / d \ln \sigma$ can be measured by measuring the strain rate sensitivity as a function of strain. He finds that the strain rate sensitivity is a function of strain in LiF and if a linear plot of strain rate sensitivity vs strain is made the extrapolation to zero strain gives the reciprocal of the power dependence of the dislocation velocity on stress. It is unfortunate for science that this procedure is not applicable to all materials as can be seen by comparing the previously measured strain rate sensitivities of tungsten with the dislocation velocity results. As was pointed out previously, the strain rate sensitivity of tungsten single crystals is not strain dependent in the

range of strain investigated (0.5 to 10 per cent). Measurements at lower strain proved unsuccessful primarily because of the high apparent work-hardening rate of the crystals. In one case, crystal WB-2, the strain rate sensitivity was apparently strain dependent, but the reciprocal of the strain rate sensitivity extrapolated to zero strain indicates that the dislocation velocity should be proportional to the 60th power of stress, a value six times the measured value. It is apparent that the third term in the equation above has a large influence on the strain rate sensitivity. This is also consistent with the observations of a high apparent work-hardening rate in tungsten.

A striking feature of these results is the very high dislocation velocity at the upper yield strength which the extrapolated data at 77°K would indicate. $\bar{v}$ at τ = 80,000 psi is in excess of 10^{1} cm/sec. This is far from the limiting velocity of sound in tungsten, but is higher than any velocity encountered under normal testing conditions in the other materials for which velocity measurements have been made. This one fact raises an important question as to the relation between dislocation mobility and the brittle behavior of tungsten.

Consider the slip line data and yield point observations presented in the previous section. There it was shown that the plastic deformation associated with the yield point load drop was confined to a series of narrow glide bands, and in one case a single shear band accounted for 20 per cent of the total elongation. Further, this deformation occurred fast enough to produce a shock wave which could be heard. Such rapid plastic flow must be the result of (1) a high dislocation velocity and (2) the motion of a large number of dislocations.

Whether Johnston's[46] model of the yield point or Cottrell's[35] model is assumed to be correct, the presence of the large yield drop in aged tungsten crystals is indicative of the presence of a small number of mobile dislocations. Hence the requirement that there be a large number of mobile dislocations to account for the rapid unloading of a crystal is tantamount to saying that the rate of dislocation multiplication must be high. It is entirely possible that these two phenomena when occurring in a polycrystalline sample could produce a large tensile stress at a grain boundary. If the adjacent grain has pinned dislocations and the stress cannot be relieved immediately by plastic flow, cleavage or grain boundary failure will result. There is nothing new in this general idea, but here is direct evidence that very high dislocation velocities are possible at nominal stress and, second, that when high velocities are possible, plastic strain can be limited to very narrow regions in a crystal. The results of the current work by Hahn and co-workers on Cr will be very interesting in light of these observations.

The observation that at room temperature high stresses can move dislocations which were apparently pinned at lower temperatures has important speculative bearing on the current argument over the yield point phenomenon. Cottrell has argued that the yield point phenomenon encountered in body-centered cubic metals is the direct result of the thermal assisted escape of dislocations from their impurity atmospheres. He assumes that unpinning will result in an immediate

load drop. Johnston and Hahn argue, on the other hand, that it is the number of mobile dislocations present in a crystal, their multiplication rate, the stress dependence of the velocity, and the work hardening which determine the yielding phenomenon.

Both points of view cannot be right, but a slight modification of the Cottrell model brings both points of view into agreement; namely, permit thermal unpinning at a stress below the upper yield point, and now Johnston's model describes the further behavior of the specimen. I believe the observations made on the tungsten crystals support this point of view. Since unpinning and motion of dislocations were observed to occur above the lower yield point and below the upper yield point, then some dislocations must be moving below the upper yield point. Even though pre-yield microstrain was seldom observed in previously described tensile experiments, it was observed. The exact shape of the expected stress strain curve for tungsten cannot be constructed using Johnson's model since the multiplication rate is not known. However, the densities of mobile dislocations present at the upper yield point, calculated from the equation:

$\dot{\gamma} = nb\bar{v}$ $\quad$ $\dot{\gamma}$ = shear strain rate = 4×10^{-5}/sec

n = density of mobile dislocations

b = Burgers vector

$\bar{v}$ = dislocation velocity

= 1.5×10^{1} cm/sec at $\tau_{U.Y.P.}$

are consistent with Johnston's[46] and Hahn's[52] conclusions. The calculated density of mobile dislocations are 10^2 dislocations/cm^2 at 77°K and 10^4 dislocations/cm^2 at 298°K. Hence at the upper yield point only between 10^2 and 10^4 dislocations/cm^2 are required to be moving. Considering the rate of multiplication evidenced by the rate of load drop and assuming an equivalent multiplication rate prior to the upper yield point, it is understandable that pre-yield microstrain might not be observed.

While in a speculative mode it is reasonable to carry the arguments one step further. It is common practice to assume that if the yield strength of a material vs the reciprocal of the absolute temperature is a straight line, then yielding is a thermally activated process. By the arguments stated above it is obvious that such a conclusion is justified only if the material under investigation exhibits no pre-yield microstrain, i.e., that thermal unpinning of previously immobilized dislocations results in an immediate load drop. If pre-yield microstrain is present, the upper yield point will be controlled in Johnston's model by the multiplication rate for dislocations, the velocity of the dislocations apropos of the existing stress, and the work-hardening characteristics of the crystal. It is not clear that such a complex process would be expected to have a temperature dependence characteristic of a thermally activated process except by coincidence. It is also clear from the evidence of the load drop experienced in tungsten that the absence of pre-yield microstrain, in standard testing practice, means that no dislocation motion is possible below the upper yield point.

Summary

The stress dependence of the velocity of dislocations in tungsten can be represented by the now familiar equation:

$$\tau = \left(\frac{\tau}{\tau_0}\right)^m .$$

The power, m, is a function of temperature and, as is true for LiF and 3.25 per cent Si-Fe, m decreases with increasing temperature. Arguments are presented which support the Johnston model of yielding in single crystals, and a modification of the Cottrell model is suggested which would make both theories compatible.

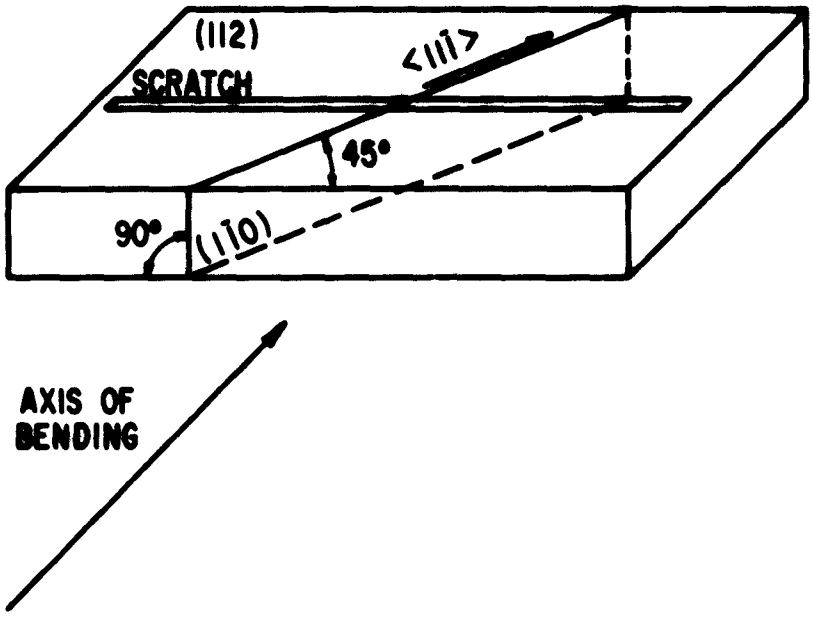

Fig. 50 Orientation of crystals used for dislocation velocity measurements.

Fig. 51 Character of scratch formed on (112) type surface of tungsten crystal scratched at 77°K. 250X

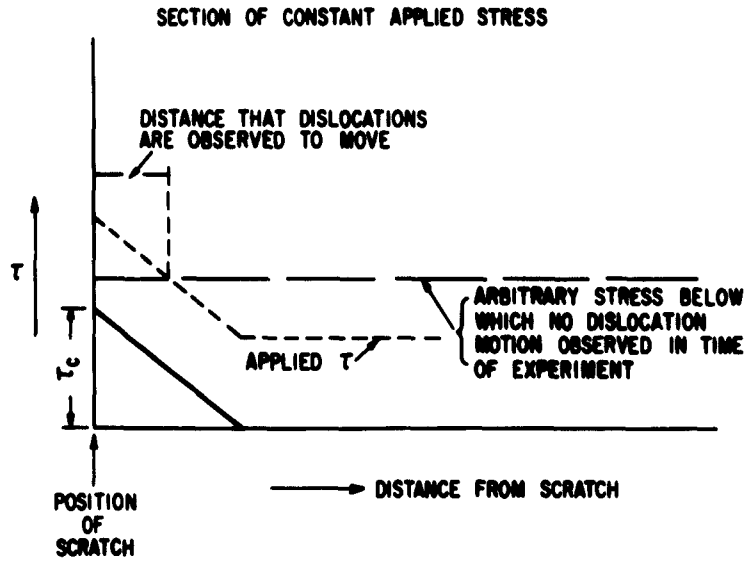

Fig. 52 Schematic illustration of influence of residual stresses created by the scratching process on the movement of dislocations in the vicinity of the scratch. See text.

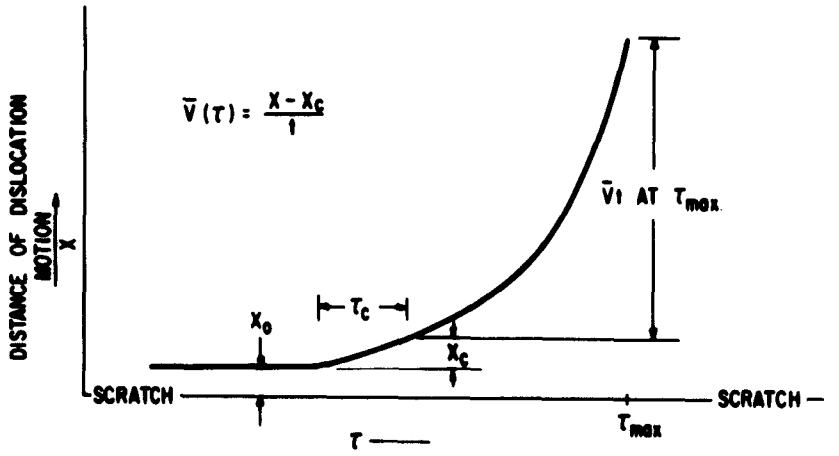

Fig. 53 Schematic illustration of dislocation motion from a scratch as a function of the applied stress and the stress concentration at the scratch. See text.

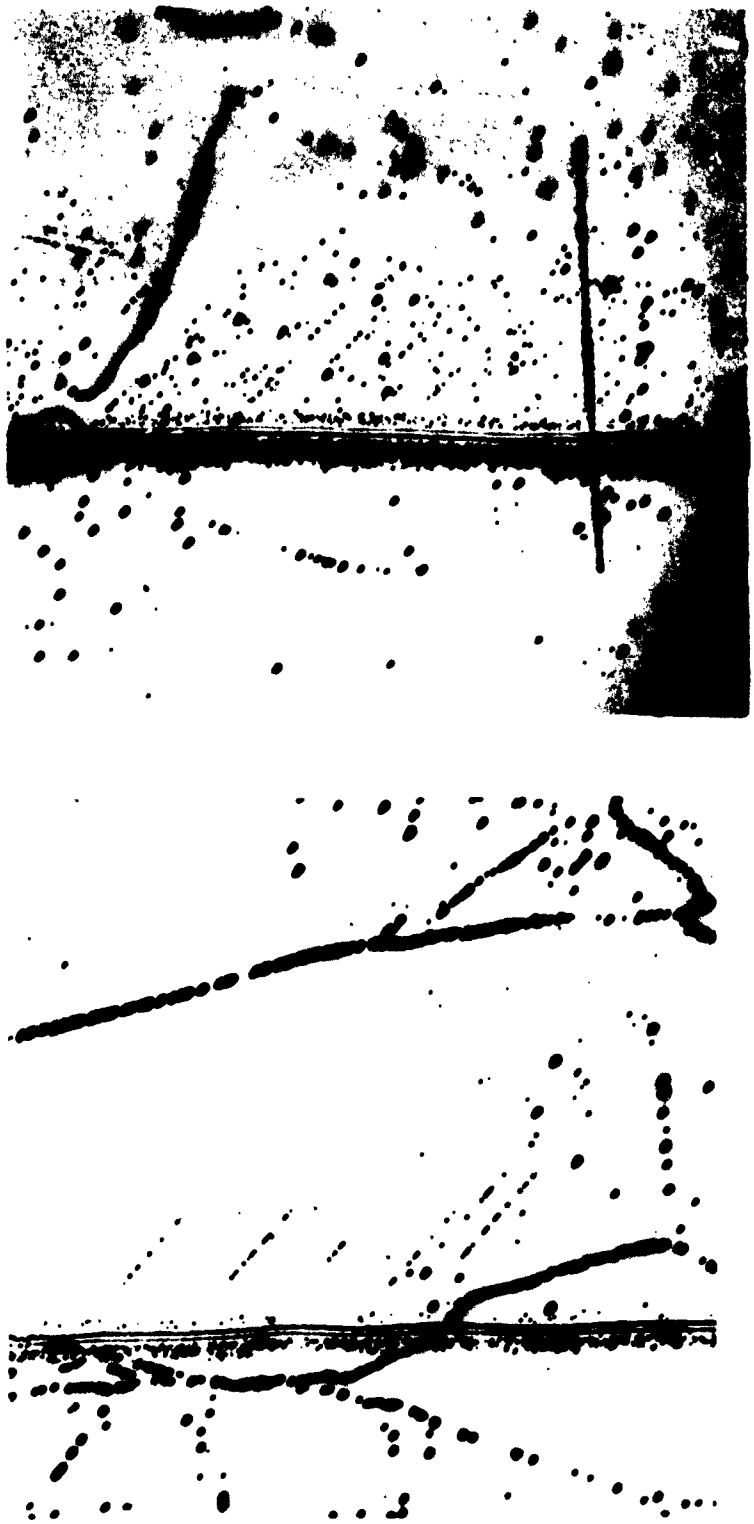

Fig. 54 Dislocation motion from a scratch in tungsten, 250X. (a) Crystal stressed at 77°K; (b) crystal stressed at 298°K. Difference in number of dislocations moving from the scratch is the result of both temperature and applied stress.

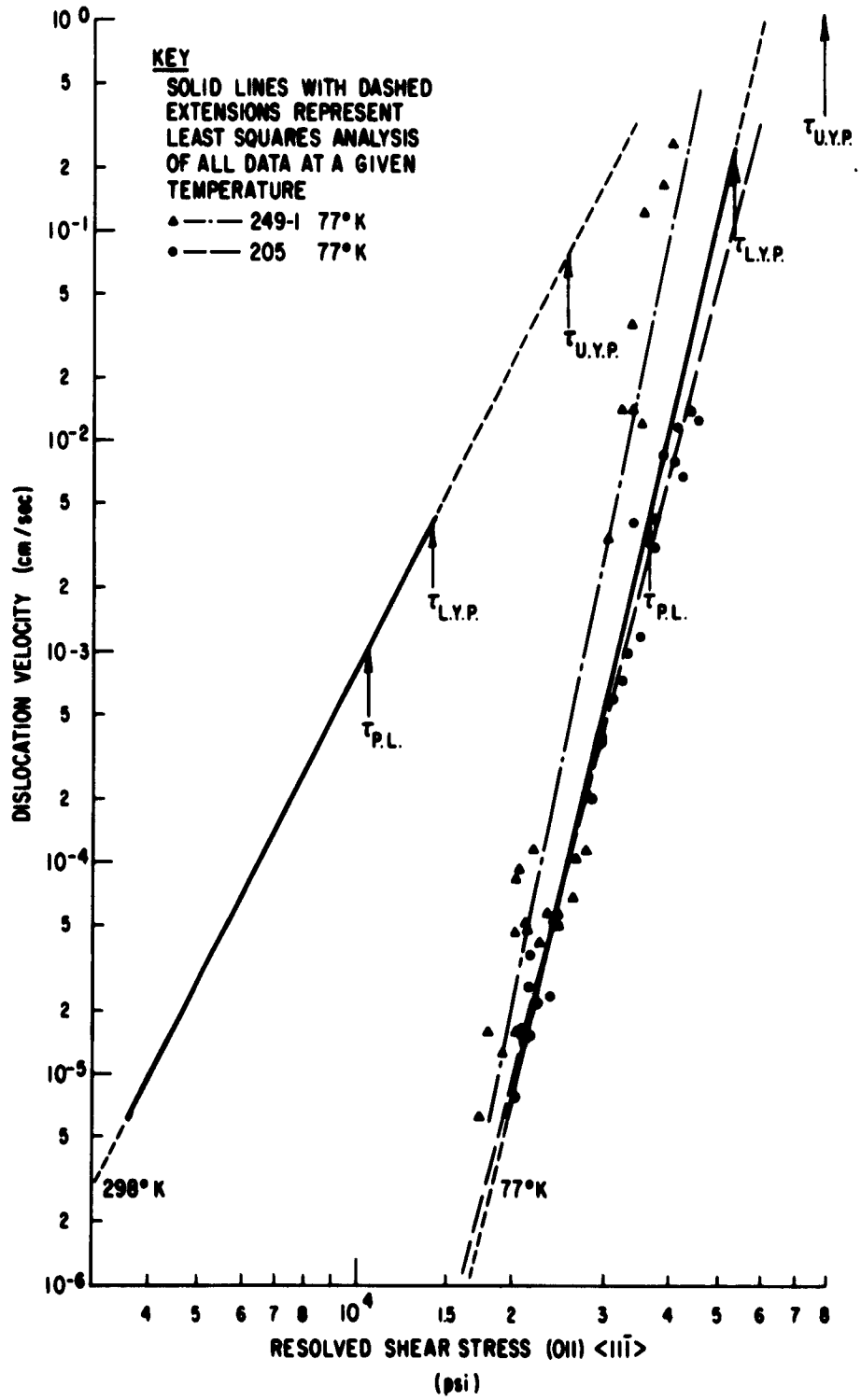

Fig. 55 Stress dependence of the average velocity of edge dislocations moving on (011) type planes in tungsten at 77° and 298°K.

REFERENCES

1. A. Calverly, M. Davis, and R. Lever, J. Sci. Instr., 34, 142 (1957).
2. U.E. Wolff, Acta Met., 6, 559 (1958).
3. D.F. Stein and J.R. Low, Jr., J. Appl. Phys., 31, 362 (1960).
4. K.R. Spangenberg, Vacuum Tubes, McGraw-Hill Book Co., Inc., New York (1948), p. 176.
5. R.G. Carlson, J. Electrochem. Soc., 106, 49 (1959).
6. B.C. Allen, D.J. Maykuth, and R.I. Jaffee, J. Inst. Metals, 90, 120 (1961).
7. H.G. Sell, "Physical Metallurgy of Tungsten and Tungsten Base Alloys," Westinghouse Electric Corp., WADD Rept. No. 60-37, p. 28ff.
8. The Art and Science of Crystal Growth, J.J. Gilman, ed., to be published by John Wiley and Sons, Inc., New York.
9. See, for example, J.H. Wernick, D. Dorsi, and J.J. Byrnes, J. Electrochem. Soc., 106, 245 (1959) or J.E. Kunzler and J.H. Wernick, Trans. AIME, 212, 856 (1958).
10. C.P. Bean, R.W. DeBlois, and L.B. Nesbitt, J. Appl. Phys., 30, 1976 (1959).
11. H.R. Smith, Vacuum Metallurgy, R. Bunshah, ed., Reinhold Publ. Co., New York, p. 221ff.
12. D.H. Avery, M.L. Ekner, and W.A. Backofen, Trans. AIME, 212, 256 (1958).
13. W.G. Johnston and J.J. Gilman, J. Appl. Phys., 30, 129 (1959).
14. A.R. Chaudhuri and J.R. Patel, presented at 1960 Fall Meeting of Metallurgical Soc. of AIME and recently summarized in report entitled "Velocities and Densities of Dislocations in Ge and Other Semiconducting Crystals" dated February 15, 1962.
15. W.G. Johnston, to be published in Progr. Ceram. Sci.
16. J.F. Nye, Acta Met., 1, 153 (1953).
17. T. Millner and L. Sass, Aluminum (Budapest), 5 (1953) 214; also Henry Brutcher Translation No. 3281.
18. J. Newkirk, Trans. AIME, 215, 483 (1959).
19. J.J. Gilman, C. Knudson, and W.P. Walsh, J. Appl. Phys., 29, 601 (1958).
20. J.J. Gilman, W.G. Johnston, and G.W. Sears, J. Appl. Phys., 29, 747 (1958).
21. F.W. Young, Jr., J. Appl. Phys., 31, 604 (1960).

22. J.D. Livingston, J. Appl. Phys., 31, 1071 (1960).

23. P.J.E. Forsyth, Phil. Mag., 45, 344 (1954).

24. A.H. Cottrell, "Theoretical Aspects of Fracture," Conf. on Fracture, Swampscott, Mass. (April 1959).

25. F.S. Goucher, Phil. Mag., 48, 228, 800 (1924).

26. C.S. Barrett, Structure of Metals, McGraw-Hill Book Co., Inc., New York (1952), pp. 40, 379.

27. H. Mark, M. Polanyi, and E. Schmid, Z. Physik, 12, 58, 78 (1929).

28. E.A. Calnan and C.J.B. Clews, Phil. Mag., 41, 1085 (1950); 42, 616 (1951).

29. U.E. Wolff, "Tungsten Crystals-Twinning," Trans. AIME, 224 (1962).

30. W. Sheely, "Investigation of Ternary Base Alloys," Final Report to Materials Central, Air Force Contract No. 33(616)-7255, April 1961, p. 18ff.

31. H.B. Probst, Trans. AIME, 221, 741 (1961).

32. R.M. Rose, "Yield and Plastic Flow in Single Crystals of Tungsten," to be published Trans. AIME.

33. J.H. Bechtold, Trans. AIME, 206, 142 (1956).

34. J.C. Fisher, Trans. ASM, 47, 451 (1955).

35. A.H. Cottrell and B.A. Bilby, Proc. Roy. Soc., A62, 49 (1949).

36. R. Maddin and N.K. Chen, Progress in Metal Physics, Vol. 5, Pergamon Press, Inc., New York (1954), p. 53.

37. E.N. da C. Andrade and Y.S. Chow, Proc. Roy. Soc., A175, 290 (1940).

38. C.S. Barrett, G. Ansel, and R.F. Mehl, Trans. ASM, 25, 702 (1937).

39. R. Maddin and N.K. Chen, Trans. AIME, 197, 1131 (1953).

40. N.K. Chen and R. Maddin, Trans. AIME, 191, 937 (1951).

41. F.C. Frank and J.F. Nicholas, Phil. Mag., 44, 1213 (1953).

42. J.H. Bechtold and P.G. Shewmon, Trans. ASM, 46, 397 (1954).

43. A. Lawley, "Tensile Behavior of Zone Melted Molybdenum Single Crystals," submitted to Trans. AIME.

44. S. Lever and J.W. Pugh, Trans. AIME, 218, 791 (1960).

45. W.G. Johnston, private communication.

46. W.G. Johnston, "Yield Points and Delay Times in Single Crystals," to be published in J. Appl. Phys.

47. H.G. Sell, "Metallurgy of Tungsten and Tungsten Base Alloys," Progress Rept. dated October 12, 1961 to Air Force under Contract AF-33(616)-6933, Project No. 735101.

48. J.W. Pugh, "Tensile and Creep Properties of Tungsten at Elevated Temperature," ASTM preprint No. 71 (1957).

49. R.P. Carreker and R.W. Guard, Trans. AIME, 206, 178 (1958).

50. J.H. Bechtold, Trans. AIME, 197, 1469 (1953).

51. R.W. Guard, Acta Met., 9, 163 (1961).

52. G.T. Hahn, "A Model for Yielding with Special Reference to the Yield Point Phenomenon of Iron and Related B.C.C. Metals," to be published in Acta Met., 10 (1962).

53. W.G. Johnston and J.J. Gilman, J. Appl. Phys., 30, 129 (1959).

APPENDIX A

RECRYSTALLIZATION CHARACTERISTICS OF COLD-ROLLED TUNGSTEN SINGLE CRYSTALS

H. W. Schadler

INTRODUCTION

In preparation for a study of the effect of purity and grain size on the ductile to brittle transition temperature of polycrystalline tungsten, the recrystallization characteristics of cold-rolled tungsten single crystals produced by electron bombardment floating zone refining were studied. Tungsten single crystals of various orientations were rolled 44, 70, 76, and 85 per cent reduction in area at 450° and 400°C and annealed at temperatures from 600° to 1600°C. The annealed specimens were examined microscopically to determine whether recrystallization had occurred, and the hardness of the samples was measured.

MATERIAL

The tungsten single crystals used for these experiments were grown by electron bombardment floating zone refining. The technique, developed by Calverly, Davis and Lever,[1] has been described in a previous report.[2] The four crystals used in these experiments received two zone-refining passes each and were grown in a vacuum of 10^{-4} mm of Hg. The orientation of the four crystals is shown in Fig. 1 which indicates the plane of rolling (R. P.) and the initial rolling direction (R. D.). Each crystal provided two samples.

PROCEDURE: ROLLING

Several methods of cold-working were tried to determine the most satisfactory technique for deforming single crystals of tungsten uniformly without contaminating the material. Rolling of the crystals at room temperature in air or encased in stainless steel was abandoned early because the crystals failed by cleavage at any reasonable strain rates. Some samples encased in stainless steel were successfully drawn 75 per cent at 500°C, but this technique was abandoned because the casing was difficult to remove. Crystals could be drawn or rolled at 450°C in air, but since it was felt that protection from contamination was essential to maintain the purity of the crystal, the following technique was finally adopted for introducing high plastic strains. The one-eighth-inch diameter crystals were surface ground to a rectangular cross section 0.060 x 0.080 inch and samples about 2 inches long were then encased in stainless steel. The specimens fitted snugly in a blind slot in a stainless block 1 inch wide x 3 inches long x 3/16 inch thick. A second stainless block 1 inch wide x 3 inches long x 3/8 inch thick was welded on top of the first to completely enclose the specimen. To prevent bonding

of the specimen to the casing, the surface of specimen was coated in milk of magnesia. After welding, the assembly was surface ground to a uniform 1/4 inch thickness.

This assembly was rolled at nominal furnace temperatures of 400° to 450°C. The samples were heated for 2 hours before rolling and a 15-minute reheat time was used between passes. Rolling schedules were designed to produce a 10 per cent reduction of actual thickness per pass. It was found that except for total reductions greater than 80 per cent, the specimen and the stainless steel casing were reduced uniformly. Two rolling techniques were used. For the first samples, the rolling direction was along the length of the specimen; compression rolling was used in later experiments to produce a wider sample. For the compression rolling the sample was turned 45° to the rolling direction of the previous pass for each subsequent pass.

The stainless steel casing was removed from the sample by cutting the stainless adjacent to either side of the sample and at each end. The two pieces of stainless then separated, and the sample was removed from the original slotted section by the application of a bending moment perpendicular to the long axis of the specimen.

Table I summarizes the rolling information and for each sample includes the rolling temperature, the per cent reduction in area, the true strain, the as-rolled hardness, and type of rolling. The hardness of the as-grown crystals was between 320 and 340 Vickers. The hardness values reported in Tables I and II are the averages of four readings. The first sample rolled was 200-2, and since no recrystallization was observed after 45 per cent reduction and heating to 1600°C, the remaining specimens were rolled to higher per cent reductions, between 70 and 85 per cent.

PROCEDURE: ANNEALING AND SAMPLE PREPARATION

The recrystallization of the cold-rolled single crystals was carried out by heating one-half-inch lengths of specimen. Samples annealed at temperatures to 1300°C were heated in the evacuated quartz capsules, and samples annealed at 1600°C in flowing pure dry hydrogen were wrapped in tungsten foil to prevent direct contact with the furnace refractories. Heating times of from 15 minutes to 1 1/2 hours were used, and samples were cooled with the furnace over an 8-hour period to 300°C before removal from the furnace. The annealed samples were electropolished in 2 per cent NaOH at 12 volts with respect to a stainless steel cathode and etched in Wolff's[3] reagent for 15 seconds at 45°C. Wolff's reagent is a mixture of two parts of a 25 wt per cent $CuSO_4$ solution with one part reagent grade NH_4OH. The specimens were then examined for signs of recrystallization, and the

Vickers hardness number of the specimens was determined using a 500-gram load and the specimens were examined for signs of recrystallization. A specimen was considered to be completely recrystallized if new grains covered the entire surface; Fig. 2 shows an example of a portion of specimen 191-1 which is completely recrystallized after annealing for one-half hour at 1200°C. A specimen was considered to be partially recrystallized if new grains cover only a portion of the surface. Figure 3 shows two examples of partially recrystallized structures. Figure 3(a) shows a portion of crystal 191-2 annealed for one-half hour at 1000°C, and Fig. 3(b) shows a portion of sample 195-1 annealed for one-quarter hour at 1300°C. Note that the magnification is greater than that in Fig. 3(a) and that the new grains in Fig. 3(b) (arrow) are only about 10 microns in diameter.

RESULTS

The results are presented in Table II and in graphical form in Figs. 4, 5, and 6. Table II summarizes the annealing treatments and the hardness data and indicates whether the specimen recrystallized. Figure 4 shows the change in hardness of the as-rolled crystals as a function of the true strain, defined as the natural logarithm of the ratio of the original to the final cross-sectional area. Although there is considerable scatter, the hardness can be represented as increasing uniformly with strain. The effect of annealing temperature on the room temperature hardness is illustrated in Figs. 5 and 6. The points on Figs. 5 and 6 which have an R next to them indicate completely recrystallized specimens. These data show that unless the hardness is less than 340 Vickers, recrystallization is not complete. Since the grain size of the completely recrystallized specimen is much greater than the size of the hardness impression, the hardness of the recrystallized samples should be the same as an as-grown crystal if no contamination has occurred during annealing. Since there is no appreciable difference in the hardness of the fully recrystallized specimens whether annealed in vacuum or in hydrogen, and since the hardness of the fully recrystallized samples is the same as the hardness of the as-grown crystals, no contamination which affects the hardness has occurred during annealing. On the partially recrystallized specimens, the hardnesses reported are impressions made on unrecrystallized portions of the specimen. It is apparent from Fig. 5 that, for strains below about 70 per cent reduction in area, the recrystallization temperature is a function of the amount of strain. This is illustrated by specimens 200-2 and 200-1 which have the same initial orientation and were reduced 45 and 71 per cent, respectively, at 450°C. Samples from specimen 200-2 did not recrystallize at annealing temperatures to 1600°C while samples from 200-1 recrystallized completely at 1600°C. For strains greater than 70 per cent reduction in area, it is not apparent from the data in Fig. 6 that the recrystallization temperature is a function of the amount of strain. Samples 191-1, 192-1, and 191-2 rolled to 77, 80, and 85 per cent reduction in area, respectively, at 450°C show essentially the same changes of hardness with annealing temperature and complete recrystallization below 1200°C. The only exception is sample 195-2 which was rolled to 75 per cent reduction in area at 400°C

and has not recrystallized after annealing at 1300°C. Since crystals 191 and 192 have very different initial orientations and very similar recrystallization characteristics and, since crystal 195 has an orientation very similar to 192, the difference in recrystallization characteristics of specimen 195-2 is probably not related to any orientation differences. The fact that specimen 195-2 was rolled at a lower temperature does not explain this result either. Since no specimen rolled less than 77 per cent recrystallized below 1600°C and all specimens rolled 77 per cent or more recrystallized between 1200° and 1300°C, these data suggest that there is a critical strain of between 75 and 77 per cent reduction in area for recrystallization at temperatures of 1200° to 1300°C.

The effect of annealing temperature on the grain size of the recrystallized material is illustrated by Figs. 7(a) and (b). The samples shown in Fig. 7 were taken from specimen 191-1 rolled 77 per cent at 450°C. Figure 7(a) shows a sample annealed for one-half hour at 1300°C and Fig. 7(b) shows a sample annealed for 1/4 hour at 1600°C. The grain size is about 0.19 millimeter in both samples. It is apparent from Figs. 7(a) and (b) and from Fig. 7(c), which shows a recrystallized structure in specimen 191-2 rolled to 85 per cent reduction in area and annealed at 1100°C with recrystallized grains 0.08 millimeter in diameter, that it is difficult to obtain a large range of grain sizes by annealing treatments below 1600°C and reductions in area of 85 per cent or less. Higher temperature treatments will probably produce larger grain size, but no samples have been annealed above 1600°C.

CONCLUSIONS

This study has shown that polycrystalline tungsten can be produced from zone-refined single crystals by a suitable combination of cold reduction and annealing. It has further shown that it will be difficult to obtain very fine grained material or a large variation in grain size for heat treatments of samples cold-rolled to less than 85 per cent reduction in area at temperatures below 1600°C.

ACKNOWLEDGMENTS

The work reported in this paper was sponsored by the Office of Naval Research.

The author gratefully acknowledges the assistance of C. L. Kolbe, whose suggestions on the design of the rolling procedure were invaluable.

REFERENCES

1. A. Calverly, M. Davis, and R. Lever, J. Sci. Instr., 34, 142 (1957).

2. H. W. Schadler, "Electron Beam Melting," Metallurgy and Ceramics Research Dept. Memo MC-82.

3. U. E. Wolff, Acta Met., 6, 559 (1958).

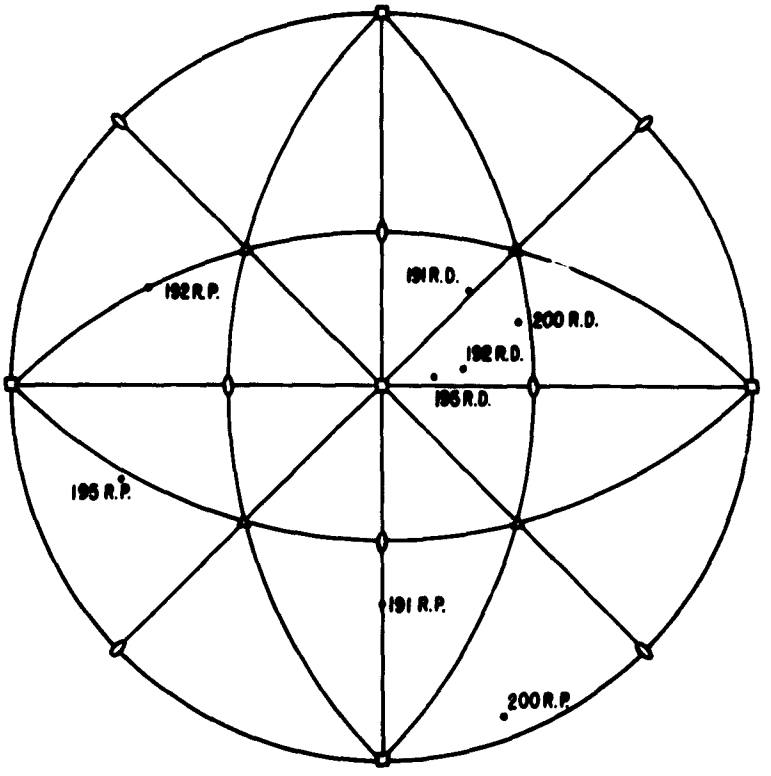

Fig. 1 Orientation of specimens used in cold-working experiments. R.P. indicates rolling plane and R.D. indicates initial rolling direction.

TABLE I

Summary of Rolling Data for Tungsten Single Crystals

Specimen No.	Rolling Temp (°C)	Initial Thickness (in)	Initial Width (in)	Initial Area (10^4 in^2)	Final Thickness (in)	Final Width (in)	Final Area (10^4 in^2)	% Red. in Area	Vickers Hardness No.	True Strain	Type of Rolling
200-1	450	0.0606	0.0856	51.8	0.0137	0.109	14.9	71.2	447*	1.24	Straight
200-2	450	.0604	.0853	51.5	.0280	.102	28.5	44.6	406	0.59	Straight
196-1	450	.0613	.0851	52.1	.0135	.109	14.7	71.8	445	1.27	Compression rolling
196-2	400	.0613	.0847	51.9	.0074	.173	12.8	75.3	510	1.40	Compression rolling
191-1	450	.0633	.0853	54.0	.0078	.160	12.5	76.8	530	1.46	Compression rolling
191-2	450	.0613	.0850	52.0	.0045	.175	7.88	84.8	530	1.88	Compression rolling
192-1	450	.0617	.0847	52.2	.0078	.135	10.5	79.9	507	1.58	Compression rolling
192-2	450	.0598	.0842	50.4	.0073	.156	11.4	77.4		1.49	Compression rolling

*Hardness of as-grown crystals was between 320 and 340 Vickers.

TABLE II

Summary of Heat Treatment and Hardness Data on Cold-Rolled and Annealed Tungsten Single Crystals

Crystal No.	Reduction in Area	Heat Treatment Temp (°C)	Heat Treatment Time (hr)	Vickers Hardness (500-g load)	Evidence of Recrystallization	Average Grain Size (mm)
200-2	45	--	--	406	--	
		1600	0.5	383	Partial recryst.	--
200-1	71	--	--	447	--	--
		600	1.5	433	No recryst.	--
		800	0.5	393		--
		1000	.5	387		--
		1200	.5	369		--
195-1	72	--	--	445	--	--
		1200	.5	385	Partial recryst.	--
		1300	.25	372		--
		1600	.25	323	Recrystallized	0.137
192-2	75	--	--	510	--	--
		800	1.0	499	No recryst.	--
		1000	0.5	486		--
		1300	.25	440	Partial recryst.	--
		1600	.25	328	Recrystallized	0.221
191-1	77	--	--	530	--	--
		1000	.5	435	No recryst.	--
		1200	.5	325	Recrystallized	.161
		1300	.25	327		.193
		1600	.25	334		.185
192-1	80	--	--	507	--	--
		1200	.5	360	Recrystallized	.145
		1300	.5	348		.151
191-2	85	--	--	530	--	--
		1000	.5	410	Partial recryst.	.076
		1100	.5	335	Recrystallized	.077
		1200	.5	348		
		1300	.25	337		

Fig. 2 Sample from specimen 191-1 rolled to 77 per cent reduction in area and annealed for one-half hour at 1200°C. 75X

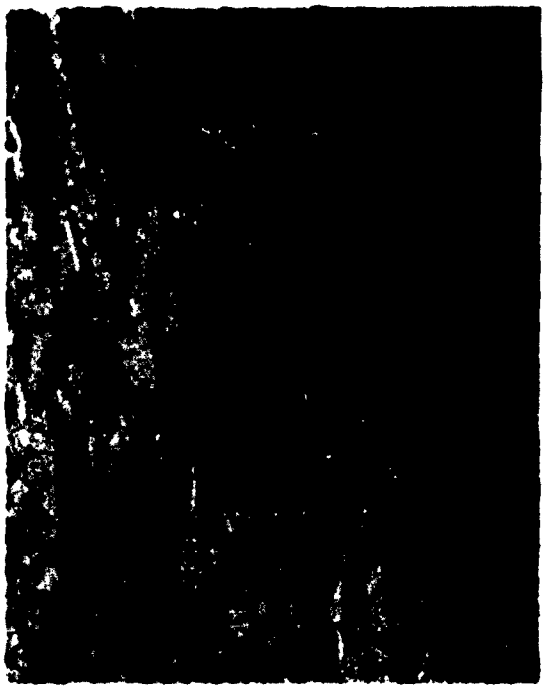

(a) 75X

(b) 250X

Fig. 3 (a) Sample from specimen 191-2 rolled to 85 per cent reduction in area and annealed for one-half hour at 1000°C; (b) Sample from specimen 195-1 rolled to 77 per cent reduction in area and annealed for one-quarter hour at 1300°C.

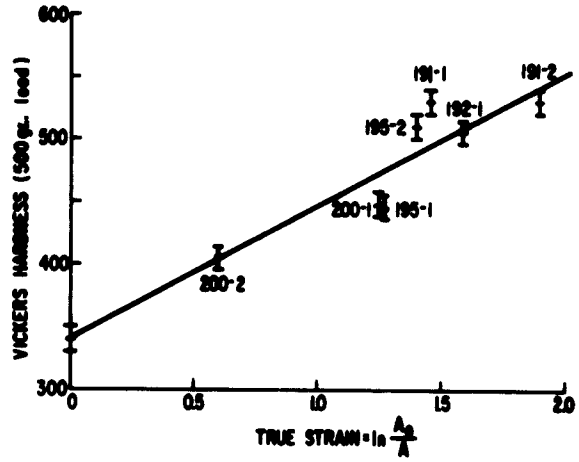

Fig. 4 Vickers hardness of single crystals as a function of true strain.

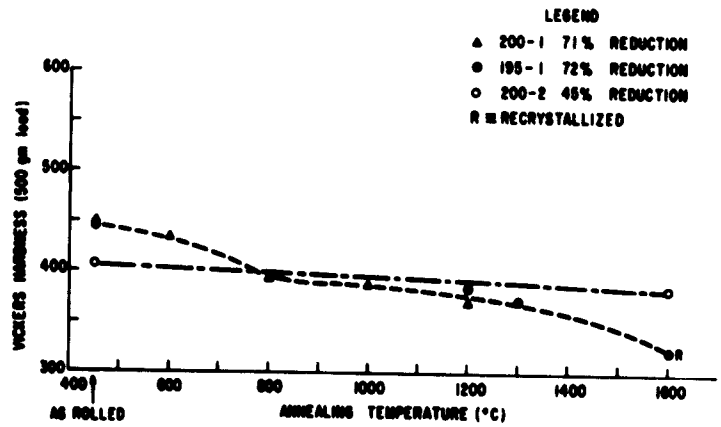

Fig. 5 Effect of annealing temperature on the hardness of specimens Nos. 200-1, 200-2, and 195-1.

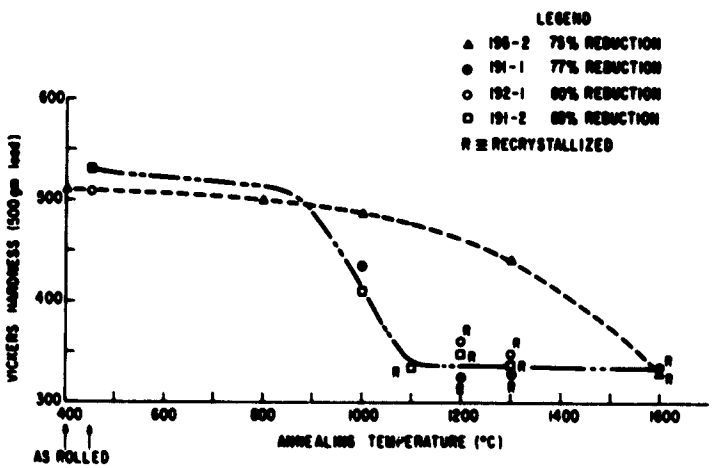

Fig. 6 Effect of annealing temperature on the hardness of specimens Nos. 195-2, 191-1, 192-1, 191-2.

(a) 40X

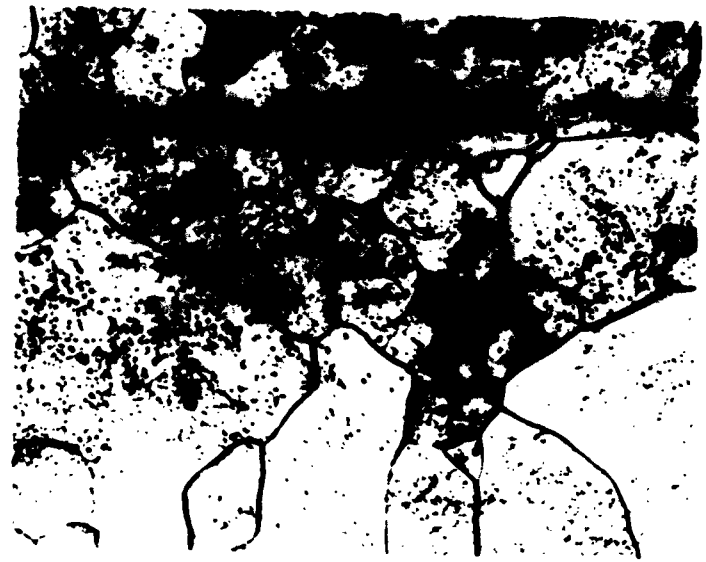

(b) 75X

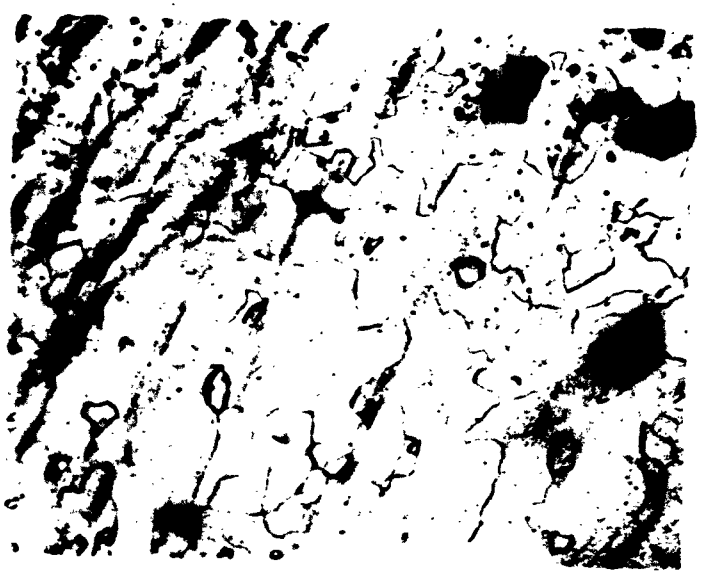

(c) 75X

Fig. 7 Sample from specimen 191-1 rolled to 77 per cent reduction in area and annealed: (a) for one-half hour at 1300°C; (b) for one-quarter hour at 1600°C; (c) for one-half hour at 1100°C.

APPENDIX B

IDENTIFICATION OF DEFORMATION TWINS IN A MOLYBDENUM-35 PER CENT RHENIUM ALLOY

H. W. Schadler and A. Lawley*

INTRODUCTION

Twinning has long been recognized as a possible mode of deformation in crystalline solids and has been studied in a wide variety of crystals.[1] Recently, deformation markings which have the topographical characteristics of twins have been seen in tungsten[2] and the body-centered cubic alloys of tungsten and molybdenum with rhenium.[3-7] These markings have been identified as twins because: (1) they are visible after polishing and etching;[2, 3] (2) their formation is accompanied by an audible click and a drop in load;[4] and (3) the habit plane is $\{112\}$, the plane which has been identified as the twinning plane for several body-centered cubic metals.[1] However, there has been no published evidence for the specific determination of the twinning direction in rhenium alloys of tungsten and molybdenum, because usually the deformation twins were not broad enough to be detected with a conventional x-ray beam. Consequently, $[11\bar{1}]$ is inferred as the twinning direction since the latter must lie in a plane of symmetry perpendicular to the twinning plane (112).

As Sims and Jaffee[3] and Lawley and Maddin[4] have shown, the addition of rhenium to molybdenum and tungsten increases the ductility of the alloy over that of the pure metal, but twinning is much more profuse in these alloys than in the pure elements, particularly at Mo-35 per cent Re† and W-30 per cent Re. Since twinning is often associated with brittle fracture in iron[8] and the silicon-irons,[9] direct experimental proof that the deformation markings in tungsten and molybdenum alloys of rhenium are twins seemed to be needed.

Using the Laue back-reflection technique with a microfocus x-ray tube, the deformation markings in a Mo-35 per cent Re alloy are shown to be deformation twins. The twins have a $\{112\}$ habit plane and the twinning direction is $\langle 11\bar{1}\rangle$.

---

*University of Pennsylvania.

†All compositions quoted are in atomic per cent.

EXPERIMENTAL TECHNIQUE

The molybdenum-35 per cent rhenium specimen used was taken from a 0.060-inch zone-refined single crystal deformed 6 per cent in tension at 78°K. The Laue back-reflection technique, with a film to specimen distance of 2 cm, and white radiation from a copper target were used. The x-ray beam was 25μ in diameter and the exposure time was about 60 hours.

EXPERIMENTAL RESULTS

The deformation markings formed in molybdenum-35 per cent rhenium deformed in tension at 78°K are shown in Fig. 1. The orientation of the original single crystal (hereafter referred to as matrix) is indicated by the indexed points in Fig. 2. Three different sets of twins were identified on the sample, and the three traces, identified as AA, BB, CC, and the corresponding poles, identified by the open circles marked P_A, P_B, and P_C, are also indicated on Fig. 2. The experimental points used for the trace analysis are represented as small crosses. The largest and most numerous markings were formed on the (211) plane identified by the pole P_A, and these were the ones subjected to x-ray analysis. If the markings are in fact deformation twins and $[\bar{1}11]$ is the twinning direction, then the resulting orientation of the twin with respect to the matrix would be as represented by the solid symmetry symbols in Fig. 2.

Figure 2 was used as a guide in analyzing the Laue back-reflection pattern shown in Fig. 3. If the Laue pattern contains poles belonging both to the matrix and to the twinned material (as is the case), then the symmetry evident in Fig. 2 can be used to identify the poles in Fig. 3. The pole closest to the center of the stereographic projection is the (011) pole of the matrix.

About the (011) pole of Fig. 2 the matrix has twofold symmetry, both east-west and north-south. The twin, however, has only twofold symmetry, east-west. Therefore, the poles representing the twinned orientation would show only east-west symmetry. Figure 3 is a tracing of the back-reflection pattern in which the individual poles have been identified and divided into the categories given below the figure. Within the region outlined by the zone traces marked II-013-II-(114)-A, etc., the symmetry of almost all the Laue spots can be checked. Spots having twofold symmetry both north-south and east-west and hence originating from the matrix material are represented as dots. Those spots having twofold symmetry east-west only and identifiable as originating from the deformation markings are represented by the open squares. The other representations are identified in the key below Fig. 3. As a guide in analyzing this pattern the Laue reflections originating from the matrix are indexed in the same sense as the indexing on the stereographic projection in Fig. 2. The Laue reflections from the lattice of the deformation markings are identified as to type by the numbers contained in parenthesis.

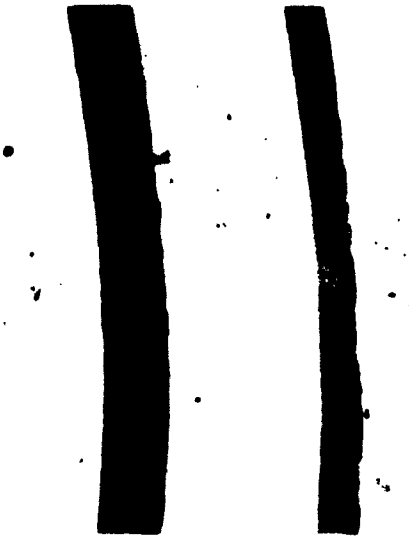

Fig. 1 Deformation markings formed in Mo-35 per cent Re alloy deformed 6 per cent in tension at 78°K. 500X

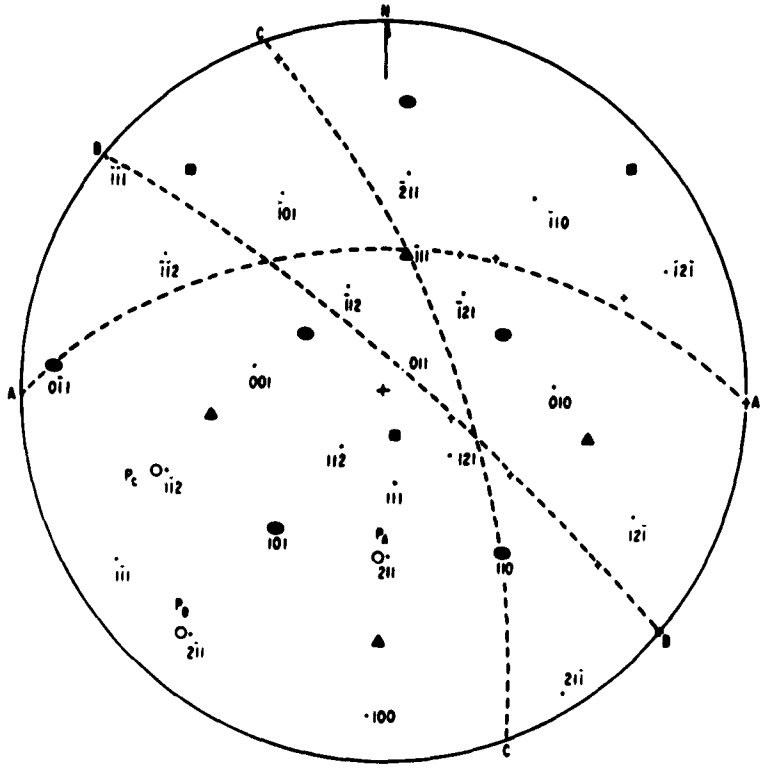

Fig. 2 Stereographic projection indicating orientation of the single crystal matrix (indexed poles) the traces of the deformation markings (dotted lines), and the orientation of the deformation twin (solid symmetry figures) which would result from twinning on the (211) plane in the [$\bar{1}$11] direction.

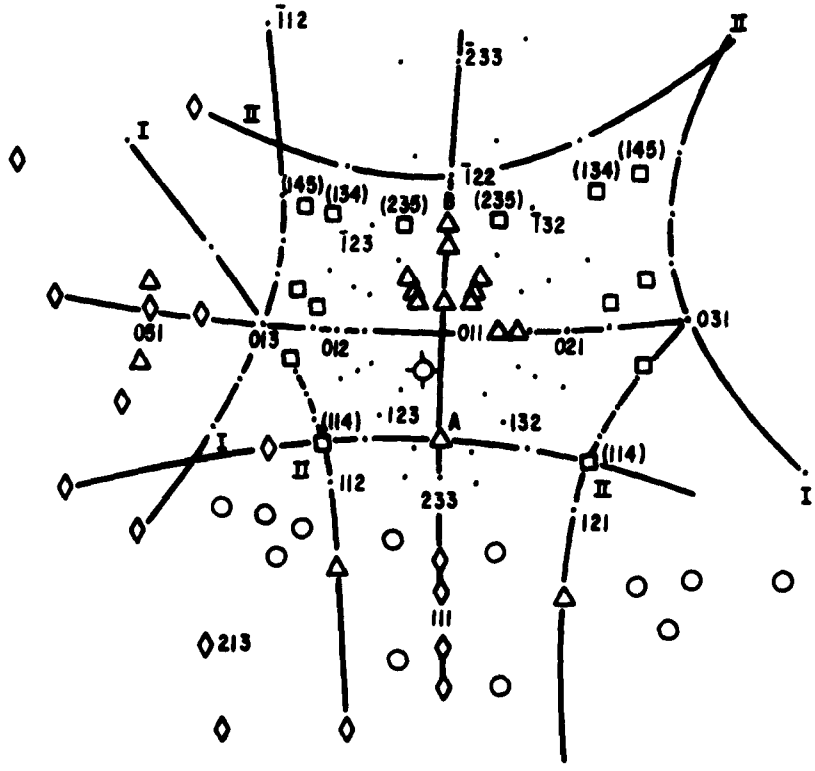

- SYMMETRY: NORTH-SOUTH AND EAST-WEST-MATRIX
- ◊ TEST FOR SYMMETRY NOT POSSIBLE
- O SYMMETRY: EAST-WEST ONLY - TEST FOR NORTH-SOUTH SYMMETRY NOT POSSIBLE
- □ SYMMETRY: EAST-WEST ONLY - IDENTIFIABLE AS TWIN MATERIAL
- △ EXCLUSIVE IDENTIFICATION NOT POSSIBLE OR NOT MADE
- A 122 MATRIX OR (100) TWIN
- B 255 MATRIX OR (112) TWIN

Fig. 3 Tracing of the Laue back reflection pattern obtained from deformed single crystal. The film to specimen distance is 2 cm.

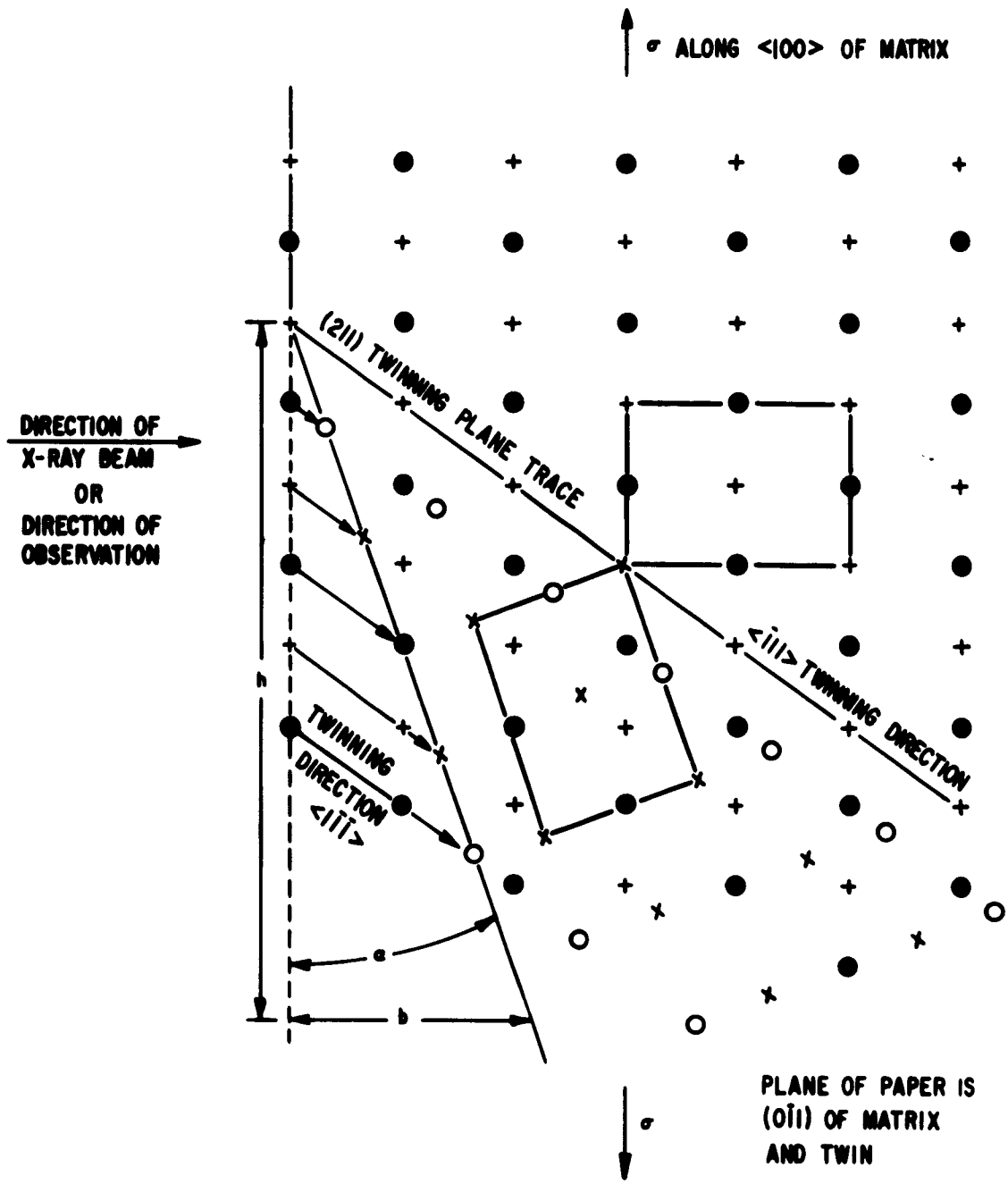

Fig. 4 Schematic representation of atomic positions before and after twinning. Circles are in the plane of the paper and x and + are in the plane immediately above (or below) the paper.

● and + refer to matrix
O and x refer to twin lattice.

The Laue reflections represented as open squares were used to determine the orientation of the deformation markings, and the result is identical with the orientation of the twin indicated on Fig. 2. Thus this back-reflection picture constitutes proof that the deformation markings in this molybdenum-35 per cent rhenium sample are in fact twins with a $\{211\}$ habit plane and a $\langle 11\bar{1} \rangle$ shear direction.

In addition to the x-ray analysis an attempt was made to measure twinning shear directly on the surface of the sample. Figure 4 shows a schematic representation of the original and final positions of the atoms for the matrix and twin orientation which Figs. 2 and 3 indicate. The angle of the twinning shear can be calculated if the distances b and h are measured. The calibrated fine adjustment of the microscope was used to measure b, and an eyepiece micrometer was used to measure h. The two widest twins present on the sample were measured. The values of the angle α calculated from these measurements were 14 degrees and 16 degrees. The theoretical value of α is 19° 28'. The agreement is good considering the inaccuracies, but can be considered only secondary evidence.

CONCLUSIONS

X-ray evidence has shown that in a molybdenum-35 per cent rhenium alloy which was deformed at 78°K, deformation twins form on $\{112\}$ planes by shear in the $\langle 11\bar{1} \rangle$ direction which lies in the twinning plane. Since the deformation markings formed at room temperature in Mo-35 per cent Re form with the same audible click and drop in load as the twins formed at 78°K and, since these markings form on $\{112\}$ planes, they are assumed to be twins also.

ACKNOWLEDGMENTS

The authors are grateful to W.B. Fleck and L.M. Osika for their patient effort in obtaining the x-ray patterns. This work was supported in part by the Office of Naval Research.

REFERENCES

1. E.O. Hall, Twinning and Diffusionless Transformation in Metals, Butterworth Scientific Publications, London (1954).

2. H.W. Schadler, Trans. AIME, 218, 649 (1960).

3. C.T. Sims and R.I. Jaffee, Trans. ASM, 52, 929 (1960).

4. A. Lawley and R. Maddin, to be published.

5. C. Feng, Trans. AIME, 218, 192 (1960).

6. J.M. Dickinson and L.S. Richardson, Trans. ASM, 51, 1055 (1959).

7. J.M. Dickinson and L.S. Richardson, Trans. ASM, 51, 758 (1959).

8. J.R. Low Jr., International Conference on the Atomic Mechanisms of Fracture, Swampscott, Mass., (1959), John Wiley and Sons., New York (1959), p. 114.

9. D. Hull, Acta Met., 8, 11 (1960).

DISTRIBUTION LIST

	No. of Copies
Chief of Naval Research Department of the Navy Washington 25, D. C. Attention: Code 423	(2)
Commanding Officer Office of Naval Research Branch Office 346 Broadway New York 13, New York	(1)
Commanding Officer Office of Naval Research Branch Office 495 Summer Street Boston 10, Massachusetts	(1)
Commanding Officer Office of Naval Research Branch Office 86 E. Randolph Street Chicago 1, Illinois	(1)
Commanding Officer Office of Naval Research Branch Office 1030 E. Green Street Pasadena 1, California	(1)
Commanding Officer Office of Naval Research Branch Office 1000 Geary Street San Francisco 9, California	(1)
Assistant Naval Attache for Research Office of Naval Research Branch Office, London Navy 100, Box 39 F.P.O., N.Y., N.Y.	(5)
Director U.S. Naval Research Laboratory Washington 25, D.C. Attention: Technical Information Officer, Code 2000 Code 2020 Code 6200 Code 6300 Code 6100	(6) (1) (1) (2) (1)
Chief, Bureau of Naval Weapons Department of the Navy Washington 25, D.C. Attention: Code RRMA Code RREN-6	 (1) (1)
Commanding Officer U.S. Naval Air Material Center Philadelphia, Pennsylvania Attention: Aeronautical Materials Laboratory	(1)
Superintendent U.S. Naval Weapons Factory Washington 25, D.C. Attention: Code 720	(1)
Commanding Officer U.S. Naval Ordnance Laboratory White Oaks, Maryland	(1)
Commanding Officer U.S. Naval Proving Ground Dahlgren, Virginia Attention: Laboratory Division	(1)
Chief, Bureau of Ships Department of the Navy Washington 25, D.C. Attention: Code 330 Code 337L Code 343	 (1) (1) (1)

	No. of Copies
Commanding Officer U.S. Naval Engineering Experiment Station Annapolis, Maryland Attention: Metals Laboratory	(1)
Materials Laboratory New York Naval Shipyard Brooklyn 1, New York Attention: Code 907	(1)
Chief, Bureau of Yards and Docks Department of the Navy Washington 25, D.C. Attention: Research and Standards Division	(1)
Commanding Officer David Taylor Model Basin Washington 7, D.C.	(1)
Post Graduate School U.S. Naval Academy Monterey, California Attention: Dept. of Metallurgy	(1)
Office of Technical Services Department of Commerce Washington 25, D.C.	(1)
Commanding Officer U.S. Naval Ordnance Test Station Inyokern, California	(1)
Armed Services Technical Information Agency (ASTIA) Documents Service Center Arlington Hall Station Arlington, Va.	(5)
Commanding Officer Watertown Arsenal Watertown, Massachusetts Attention: Ordnance Materials Research Office Laboratory Div.	(1) (1)
Commanding Officer Office of Ordnance Research Box CM, Duke Station Duke University Durham, North Carolina Attention: Metallurgy Division	(1)
Commander Wright Air Development Center Wright-Patterson Air Force Base Dayton, Ohio Attention: Aeronautical Research Lab. (WCRRH) Aeronautical Research Lab. (WCRRL) Materials Laboratory (WCRTL)	(1) (1)
U.S. Air Force ARDC Office of Scientific Research Washington 25, D.C. Attention: Solid State Division (SRQB)	(1)
National Bureau of Standards Washington 25, D.C. Attention: Metallurgy Div. Mineral Products Div.	(1) (1)
National Aeronautics Space Administration Lewis Flight Propulsion Lab. Cleveland, Ohio Attention: Materials and Thermodynamics Div.	(1)

	No. of Copies
U.S. Atomic Energy Commission Washington 25, D.C. Attention: Technical Library	(1)
U.S. Atomic Energy Commission Washington 25, D.C. Attention: Metals and Materials Branch, Div. of Research	(1)
Eng. Develop. Branch, Div. of Reactor Develop.	(1)
Argonne National Lab. P.O. Box 299 Lemont, Illinois Attention: H.D. Young, Librarian	(1)
Brookhaven National Lab. Technical Information Div. Upton, Long Island, N.Y. Attention: Research Library	(1)
Union Carbide Nuclear Co. Oak Ridge National Lab. P.O. Box P Oak Ridge, Tennessee Attention: Metallurgy Div.	(1)
Solid State Physics Div.	(1)
Laboratory Records Dept.	(1)
Los Alamos Scientific Lab. P.O. Box 1663 Los Alamos, New Mexico Attention: Report Librarian	(1)
General Electric Company P.O. Box 100 Richland, Washington Attention: Technical Information Division	(1)
Iowa State College P.O. Box 14A, Station A Ames, Iowa Attention: F.H. Spedding	(1)
Knolls Atomic Power Lab. P.O. Box 1072 Schenectady, New York Attention: Document Librarian	(1)
U.S. Atomic Energy Commission New York Operations Office 70 Columbus Avenue New York 23, New York Attention: Document Custodian	(1)
Sandia Corporation Sandia Base Albuquerque, New Mexico Attention: Library	(1)
U.S. Atomic Energy Commission Technical Information Service Extension P.O. Box 62 Oak Ridge, Tennessee Attention: Reference Branch	(1)
University of California Radiation Laboratory Information Division Room 128, Building 50 Berkeley, California Attention: R.K. Wakerling	(1)

	No. of Copies
Bettis Plant U.S. Atomic Energy Commission Bettis Field P.O. Box 1468 Pittsburgh 30, Pa. Attention: Mrs. Virginia Sternberg, Librarian	(1)
Commanding Officer and Director U.S. Naval Civil Engineering Laboratory Port Hueneme, California	(1)
Commanding Officer U.S. Naval Ordnance Underwater Station Newport, Rhode Island	(1)
U.S. Bureau of Mines Washington 25, D.C. Attention: Dr. E.T. Hayes	(1)
Defense Metals Information Center Battelle Memorial Institute 505 King Avenue Columbus, Ohio	(2)
Solid State Devices Branch Evans Signal Laboratory U.S. Army Signal Engineering Laboratories c/o Senior Navy Liaison Officer U.S. Navy Electronic Office Fort Monmouth, New Jersey	(1)
U.S. Bureau of Mines P.O. Drawer B Boulder City, Nevada Attention: Electro-Metallurgical Division	(1)
Commanding General U.S. Army Ordnance Arsenal, Frankford Philadelphia 37, Pa. Attention: Mr. Harold Markus ORDBA-1320, 64-4	(1)

Dr. M. Semchyshen
Climax Molybdenum Company
14410 Woodrow Wilson
Detroit 38, Michigan

Dr. J.R. Low, Jr.
General Electric Company
Research Laboratory
P.O. Box 1088
Schenectady, New York

Dr. H.W. Schadler
General Electric Company
Research Laboratory
P.O. Box 1088
Schenectady, New York

Dr. R.I. Jaffee
Battelle Memorial Institute
505 King Avenue
Columbus 1, Ohio

Dr. A.N. Lord
General Electric Company
Research Laboratory
P.O. Box 1088
Schenectady, New York

Dr. C. Lundin
Denver Research Institute
Metallurgy Department
Denver, Colorado

Dr. J. Nachman
Denver Research Institute
Metallurgy Department
Denver, Colorado

Prof. F. Seitz
Department of Physics
University of Illinois
Urbana, Illinois

Prof. T.A. Read
Department of Mining and Met. Engrg.
University of Illinois
Urbana, Illinois

Prof. H. Brooks
Dean Graduate School of Applied Science
Harvard University
Cambridge, Massachusetts